Chlor-Alkali Membrane Cell Process:

Study and Characterization

Dissertation

to obtain the Doctor's degree in

Chemical and Biological Engineering

by University of Porto

Supervisors

Adélio Miguel Magalhães Mendes (FEUP)

Fernão Domingos de Montenegro Baptista Malheiro de Magalhães (FEUP)

Paulo Alexandre Pereira Araújo (CUF-Químicos Industriais)

by

Ana Catarina de Bastos Vidal Dias

LEPAE – Laboratory of Engineering Processes, Environment and Engineering

Chemical Engineering Department

Faculty of Engineering - University of Porto

CUF – Químicos Industriais

Acknowledgments

First of all, I am grateful to Portuguese Foundation for Science and Technology (FCT) for my Ph.D. grant (SFRH/BDE/15558/2005) and to CUF-Químicos Industriais for providing financial support.

I would like to thank Professor Adélio Mendes for giving me the opportunity to carry out this thesis and for his support and to my co-supervisor Professor Fernão Magalhães. I am very grateful to Eng. Francisco Sotto Mayor for accepting me as a Ph.D. student at CUF-QI as for the three months of fruitful discussions. I would like to express my gratitude to Doctor Paulo Araújo for the chance to continue this work, and for his support. I am also grateful to CUF-QI and LEPAE/FEUP for providing me the necessary conditions to develop my work.

I wish to thank Professor Matthias Wessling for receiving me at Membrane Technology Group (MTG), University of Twente, the Netherlands, and to Doctor Jörg Balster for his guidance during my three months internship.

I am greatly indebted to Doctor Lúcia Brandão, who got involved in my impedance adventures. I have really appreciated her help and motivation.

It was a great pleasure for me to perform my thesis at CUF-QI. On the way many people accompanied me giving me practical and theoretical support and bringing me forward in my professional and personal

development. I would like to express my special thanks to Andrew Parker for being always ready for explaining me all my questions, to colleague Alejandro Ribeiro for helping me with the building up of the experimental setup, to my fellow workers Ana Tavares, Alberto Caires, Paula Costa, Rui Andrade, Teresa Marques and Vitor Pinto, for their friendship and advice and to the production Engineers Pedro Costa and António Sousa for their availability to discuss and clarify some doubts. Thankful words are also directed to Maria José Pereira for her help during the experimental tests. Maintenance personnel are also acknowledged for their active help during the experimental setup building up and for sharing their knowledge with me. I also wish to thank Eng. Mário Jorge Pinho, Eng. António Mesquita de Sousa and Eng. David Lopes for their comments and help for this investigation.

I would also like to acknowledge the helpful discussion with Professor Christopher Brett from University of Coimbra, Portugal.

Finally, I would like to thank César Águia for his support, motivation, patience and for listening me in the most turbulent moments. I am also very grateful to my family for their trust and help. Special thanks for my grandparents who lived this journey as intensively as I.

“Nothing in life is to be feared. It is only to be understood.”

Marie Curie

Abstract

The chlor-alkali industry is one of the most energy intensive electrochemical processes in the world. Moreover, the electrical energy consumption is the major fraction of the total producing cost. Therefore, high-energy efficiency processes are crucial for this type of industry. Despite being a mature technology, the knowledge about the chlor-alkali membrane process is dominated by three membrane suppliers and there are few studies reported in the scientific journals. The need for developing independent know-how on this technology was the major motivation of this thesis that also serves the interests of CUF-QI, the most important Portuguese chlor-alkali company.

Two experimental setups were designed, built and tested: an experimental setup for characterizing cation exchange membranes and an electrochemical membrane reactor for studying the membrane cell process. The former unit was built to determine one of the most important properties of ion-exchange membranes, the permselectivity. Concerning this unit and the electrochemical membrane reactor, it was found good agreement between experimental data and reference values. The electrochemical reactor was used to identify the most important parameters of the chlor-alkali membrane process (current density, feed flow rate, brine and caustic concentrations, and temperature) and to investigate their effect on the cell performance. It was

also studied *in situ* the hydrogen evolution reaction (HER) kinetics using cathodes of solid and mesh nickel plates.

The ohmic resistances of the membrane reactor were determined *in situ* by electrochemical impedance spectroscopy (EIS); this technique revealed to be a powerful tool for the characterization of the electrochemical process and namely the cathode and membrane. The hydrogen evolution reaction at commercial nickel cathodes were also investigated *in situ* by EIS. The anode overpotential was assumed to be negligible in comparison to the cathode overpotential and therefore used as a reference electrode; this assumption was validated experimentally. The kinetic properties of solid and mesh nickel cathodes were studied at 75 ºC. The effect of the electrode shape on overpotential and on impedance spectra was addressed. The experimental observation of a second semicircle on the impedance spectra of the mesh electrode was attributed to ac penetration through the mesh structure. Potential-current density curves (*k-factor*) were obtained and compared to the ones computed using the kinetic data.

Significant energy savings can be achieved by choosing the most adequate membrane and by replacing the membrane in the right moment. The average total process cost per ton of chlorine was calculated monthly for three electrolyzers each using a set of a different type membrane. From this

data a benchmarking methodology was developed and the performance of the three different types of membranes reported.

Sumário

A indústria cloro-álcalis é uma das indústrias electroquímicas com maior consumo de energia, sendo que este representa a maior parte dos custos totais de produção. Desta forma, é essencial neste tipo de indústria operar com elevados níveis de eficiência energética. Apesar da tecnologia de células de membrana ter surgido nos anos 80, a informação científica disponível é dominada pelos grandes fornecedores industriais que mantêm limitado o acesso a esse conhecimento. A necessidade de desenvolver conhecimento estratégico sobre a tecnologia de células de membrana, foi a grande motivação desta tese. A investigação nesta área também permitirá aumentar o poder negocial da CUF-QI.

Foram projectadas e construídas duas unidades experimentais: uma unidade para a caracterização da membrana de permuta catiónica e uma unidade experimental de electrólise por células de membrana. A unidade de caracterização de membranas foi construída com o intuito de determinar a selectividade das membranas. O reactor electroquímico de membrana (electrolizador) foi utilizado para identificar os parâmetros críticos de operação (densidade de corrente, caudal de alimentação, concentrações de soda cáustica e salmoura e temperatura) e o seu efeito no desempenho do processo. A cinética da reacção de produção de hidrogénio em cátodos de níquel foi também investigada *in situ* nesta unidade experimental. As

instalações experimentais foram descritas detalhadamente e os dados experimentais comparados com valores de referência. Verificou-se que os valores obtidos estavam de acordo com os valores de referência para este tipo de processo.

A contribuição dos vários componentes da resistência óhmica que constituem a célula de membrana foi investigada *in situ* utilizando a espectroscopia de impedância electroquímica. Esta técnica revelou ser uma ferramenta poderosa na caracterização electroquímica do processo de células de membrana.

A espectroscopia de impedância foi também utilizada *in situ* para o estudo da cinética da reacção de produção de hidrogénio em cátodos de níquel comerciais. O sobrepotencial do ânodo foi considerado desprezável em relação ao sobrepotencial do cátodo e como tal foi usado como eléctrodo de referência. As propriedades cinéticas da reacção de produção de hidrogénio em cátodos sólidos e de rede a 75 ºC foram discutidas. A observação experimental de um segundo semicírculo no espectro de impedância obtido para os eléctrodos de rede, foi atribuído à penetração do sinal CA na rede do eléctrodo. Obtiveram-se curvas de polarização (densidade de corrente - potencial) que foram comparadas com as calculadas utilizando os parâmetros cinéticos.

A escolha adequada das membranas e a sua substituição atempada são aspectos essenciais para minimizar os custos de energia. A média mensal dos custos totais de operação por tonelada de cloro foi estimada para cada electrolizador. Com estes dados desenvolveu-se uma metodologia de benchmarking e avaliou-se o desempenho de três tipos diferentes de membranas.

Sommaire

L'industrie de chlore-alcalis reste parmi les industries chimiques les plus consommatrices d’énergie, ce qui représente une fraction importante du coût total de production. Par conséquent, l’efficacité énergétique est cruciale pour ce type d'industrie. En dépit d'être une technologie mûre, les connaissances sur les procédés chlore-alcalis basée dans la technologie de membrane est dominée par trois fournisseurs de membrane et il y a peu d'études rapportées dans les journaux scientifiques. Le besoin de développer savoir-faire indépendant sur cette technologie était la motivation à la base de cette thèse qui est par ailleurs en accord avec la stratégie de CUF-QI, la compagnie de chlore-alcali portugaise la plus importante.

Deux installations expérimentales ont été conçues, mises en œuvre et utilisées pour des testes: une installation expérimentale pour caractériser des membranes d'échange cationique et un réacteur électrochimique (électrolyseur) de membrane pour étudier le procédé des cellules de membrane. L’installation de caractérisation a été construite afin de déterminer l'une des propriétés les plus importantes des membranes d’échange d'ions, la permsélectivité. En ce qui concerne les résultats obtenu avec cette installation de caractérisation et ceux avec le réacteur électrochimique à membrane, un bon accord avec les valeurs de référence a été trouvé. Le réacteur électrochimique a été utilisé pour identifier les

paramètres les plus importants des procédés chlore-alcalis basée dans la technologie de membrane (densité de courant, débit d'alimentation, concentrations de saumure et de soude, et température) et pour étudier leur effet sur la performance des électrolyseurs. Il a également été étudié *in situ* la cinétique de la réaction de dégagement d'hydrogène (HER) en utilisant des cathodes constitué par des plaques de nickel solide ou en maille.

Les résistances ohmiques du réacteur à membrane ont été déterminés in situ par spectroscopie d'impédance électrochimique (SIE); cette technique s'est révélé être un outil puissant pour la caractérisation du procédé électrochimique et notamment la cathode et la membrane. La réaction de dégagement d'hydrogène à cathodes de nickel commerciaux a également été étudiée in situ par l'EIS.

La surtension anodique a été considéré négligeable par rapport à la surtension de la cathode et donc utilisé comme une électrode de référence; cette hypothèse a été validée expérimentalement. Les propriétés cinétiques des cathodes de nickel constitué par des plaques solides ou par des mailles ont été étudiées à 75 ºC. Les effets de la forme des électrodes sur les surtensions et sur les spectres d'impédance ont été discutés. L'observation expérimentale d'un deuxième demi-cercle sur les spectres d'impédance de l'électrode de mailles a été attribuée à la pénétration du courant alternatif à travers la structure en maille de l’électrode. Les courbes de densité de

potentiel de courant (facteur k) ont été obtenues et comparées à celles calculées en utilisant les données cinétiques.

Des économies d'énergie significatives peuvent être réalisées en choisissant la membrane la plus adéquate et en remplaçant la membrane au bon moment. Le coût total moyen par tonne de chlore a été calculé mensuellement pour trois électrolyseurs, chacun utilisant un ensemble d'un type différent de membrane. De ces données une méthodologie d'évaluation a été développée et la performance des trois types différents de membranes a été rapportée.

Table of Contents

List of Figure Captions

Figure 4.4 – Nyquist and bode plots (figures a) and b) respectively) for HER on the solid and mesh nickel electrodes measured at 25 A m^{-2}. Dots – experimental data; lines – fittings of the equivalent circuits.

Figure 4.5 - Nyquist plots for HER on the solid nickel electrode measured at current densities between a) 25 A m^{-2} and 300 A m^{-2}; b) 400 A m^{-2} and 700 A m^{-2} and c) 800 A m^{-2} and $1.00x10^{3}$ A m^{-2}. Dots – experimental data; lines – fittings of the equivalent circuits.

Figure 4.6 – Randles equivalent electrical circuit.

Figure 4.7 – Nyquist plots for HER on the mesh nickel electrode measured at current densities between a) 25 A m^{-2} and 300 A m^{-2} and b) 400 A m^{-2} and 800 A m^{-2}. Dots – experimental data; lines – fittings of the equivalent circuits.

Figure 4.8 – Equivalent circuit used to fit the impedance data obtained for the cathode mesh electrode.

Figure 4.9 - SEM image of the surface of the cathode mesh electrode.

Figure 4.10 – Charge transfer resistance as a function of the applied overpotential, for HER on nickel electrodes (solid and mesh).

Figure 4.11 – Double layer capacitance as a function of the applied overpotential for HER on nickel electrodes (solid and mesh).

Figure 4.12 – Inverse of charge transfer resistance obtained from impedance data as a function of overpotential for the HER on nickel cathodes.

Figure 5.6 – Dimensionless chlorine current efficiency ($\xi^{*}_{Cl_2}$) as a function of months online (MOL) – lines were introduced for improving the readability.

Figure 5.7 – Dimensionless specific energy consumption per ton of chlorine (corrected for 5 kA·m^{-2}, 32 % NaOH and 90 ºC) for each electrolyzer as a function of months online (MOL) - lines were introduced for improving the readability.

Figure 5.8 – Dimensionless average maintenance costs per month of operation for each electrolyzer.

Figure 5.9 – Dimensionless average energy cost per ton of chlorine produced for membranes M_1, M_2, M_3 as a function of months online (MOL).

Figure 5.10 –Dimensionless total process costs per ton of chlorine as a function of months online (MOL): a) complete plot and b) zoom in for the last months of operation. - lines were introduced for improving readability.

Figure 5.11 – Dimensionless average total process costs per ton of chlorine as a function of months online (MOL) for membranes M_1 and M_3.

List of Table Captions

Table 4.1 – Estimated parameters for solid (12 mm gap) and mesh electrodes (5.5 mm gap).

Table 4.2 – Tafel slopes (b), exchange current densities (j_0) and charge transfer coefficients (α) of HER at nickel solid and mesh nickel cathodes determined from the polarization curves.

Table 4.3 – Parameters *Q* and *S* obtained directly from the polarization curve for $j < 1$ kA m^{-2} (*Q-factor* method) (Table 1) and calculated from the kinetic data in Table 4.2.

Table 4.4 – Charge transfer resistance and double layer capacitance of the cathode (solid electrode) obtained by fitting the experimental results to the equivalent circuit.

Table 4.5 – Charge transfer resistance and double layer capacitance of the cathode (mesh electrode) obtained by fitting experimental results.

Table 4.6 – Tafel slopes, exchange current densities and charge transfer coefficients of HER at nickel solid and mesh nickel cathodes determined from the EIS analysis.

Table 5.1 – Dimensionless slope of the polarization curve (k^*) for each type of membrane at the beginning of operation (month 0).

Chapter 1 – Introduction

1.1. Chlor-alkali process

The chlor-alkali industry is one of the major electrochemical processes producing mainly chlorine and sodium hydroxide (caustic soda). Chlorine and sodium hydroxide are among the most produced chemicals in the world. They are used in the manufacturing of a variety of intermediates in the chemical (e.g. polymers, pulp and paper), pharmaceutical (85 % of medicines use chlorine) and crop protection industries [1,2].

There are three different processes for the manufacture of chlorine and sodium hydroxide from saturated sodium chloride solutions (brine): mercury, diaphragm and membrane cell. Diaphragm cell was the first chlor-alkali technology developed to produce chlorine and sodium hydroxide [3-5]. It was invented in 1851 by Charles Watt and the first commercial cell was built in 1888. Few years later (1892), Hamilton and Castner developed the mercury cell process [3,4]. During approximately 100 years these two technologies were used to produce chlorine and sodium hydroxide all over the world. From mid-1950s efforts were made to replace the asbestos used as a separator on the diaphragm cell by a polymer membrane [3,4]. Although, serious problems were found concerning the short life-time of the membrane [3,4]. The erosion of the carbon anodes was also an issue in the membrane

cell process. In the early 1960's, the increasing concern about the toxicological effects of asbestos and mercury used in the mercury cell led to the study and development of alternative solutions [3-5]. The development of metal anodes in the early 1970's revolutionized the chlor alkali industry and foster the research to develop a suitable membrane-cell technology. In 1970, 30 % of the world production of chlorine and sodium hydroxide was by diaphragm cells and 70 % using mercury cells [3,4]. The first commercial membrane cell plant was commissioned in 1975 in Japan, which was the first country producing chlorine and sodium hydroxide using a membrane cell technology [3,4]. Fifteen years later, the membrane cell technology represented 15 % of the world production of chlorine and sodium hydroxide. Since then, many developments have made the membrane cell process more economical and environmentally safe [3,4]. The membrane cell technology accounted for 35 % of world's capacity in 2002 whereas the diaphragm process was the most used representing 41 % [4]. In 2003, the chlorine production using the membrane technology exceeded the chlorine produced from diaphragm process and became the technology with the major world chlorine production capacity (40 %) [4]. The worldwide fraction of chlorine produced by membrane cells is expected to be 55 % in 2010 [2]. In 2008, the world chlorine production capacity was 62.8 million metric tons, distributed as shown in Figure 1.1 [2].

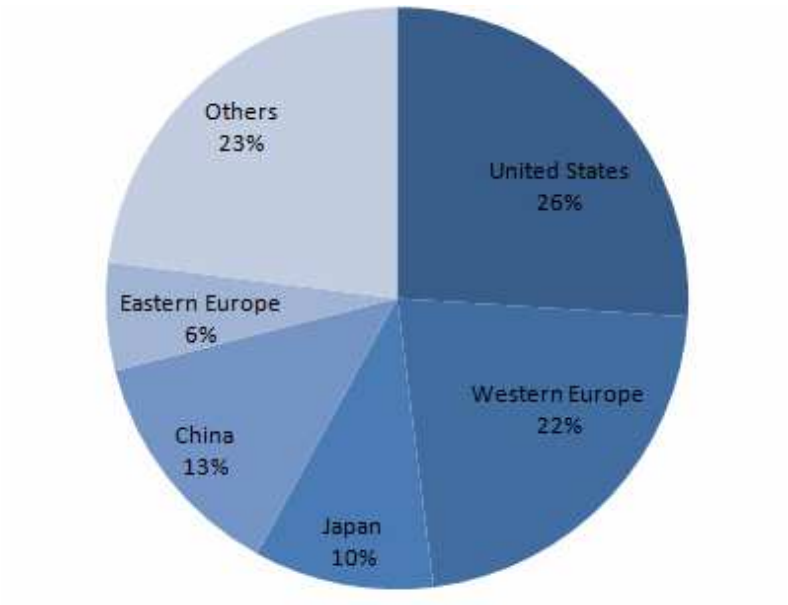

Figure 1.1 - Geographic distribution of the worldwide chlorine production in 2008 [2].

The chlor-alkali process involves the electrolysis of sodium chloride solution (brine) producing chlorine at the anode and sodium hydroxide (caustic soda) at the cathode, via the overall reaction [3-5]:

$$2\,NaCl + 2\,H_2O \rightarrow 2\,NaOH + Cl_2 + H_2 \qquad (1.1)$$

To prevent the mixing of anolyte and catholyte a separator is used between the compartments. In the diaphragm cell a permeable diaphragm, usually made of asbestos fibers, is used to separate the anode from the cathode compartments. A weak caustic (30 %) stream contaminated with sodium chloride is produced by this technology [3-5]. On the other hand, a mercury cell produces a strong high purity caustic solution (50 %). A

mercury cell is divided in two units: the electrolyzer and the secondary electrochemical reactor (often called decomposer), Figure 1.2.

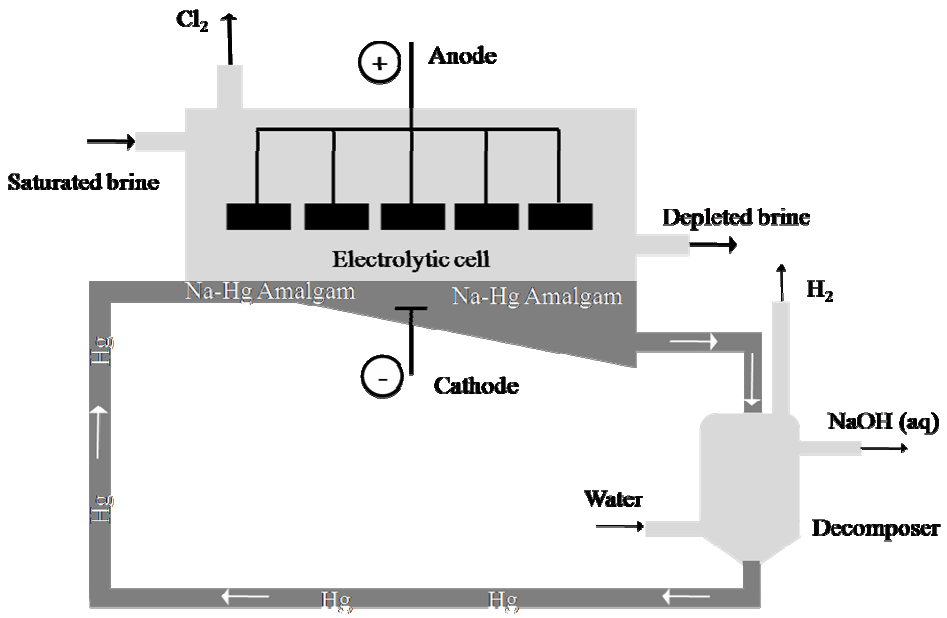

Figure 1.2 – Schematic representation of a chlor alkali mercury cell [3-5].

In the electrolyzer chlorine is produced at the anode and sodium amalgam forms at the cathode. Then, the sodium amalgam goes to a secondary electrochemical reactor where water is used to decompose the sodium amalgam into sodium hydroxide and mercury producing hydrogen. [4]. Moreover, water is reduced at the cathode and the sodium amalgam decomposed at the anode. The chlorine and sodium hydroxide produced via the mercury-cell are contaminated with trace amounts of mercury. The membrane cell process appeared as an alternative to the diaphragm and

mercury cells. It is very similar to a diaphragm cell but the permeable diaphragm is replaced by a permselective ion-exchange membrane.

CUF – Químicos Industriais is a chemical company operating in the fields of the organic and inorganic (chlor-alkali) intermediates to the chemical and pharmaceutical industries. CUF-QI is nowadays focused on the production of key raw materials (aniline, chlorine and caustic soda) for the production of MDI (methylene diphenyl diisocyanate) that is an intermediate to the polyurethane industry. Additionally, other products as hydrochloric acid, sodium hypochlorite, hydrogen, nitric acid, mononitrobenzene, sulphanylic acid and ciclohexylamine are also been produced.

CUF-QI is the third major chlorine producer in Iberian Peninsula [1]. Since 1959 CUF-QI has been producing chlorine and caustic soda by mercury cells. In 1992, the first membrane cell electrolyzers were installed and recently, in 2002, the mercury cell technology was entirely converted to the most modern membrane cells. The present thesis aimed developing knowledge on membrane cell technology and implementing characterization tools and operating procedures targeting the reduction of costs. Furthermore, it allows developing strategic knowledge at CUF to improve its autonomy and negotiation ability with suppliers.

1.2. Chlor-alkali membrane process

The membrane cell technology has several advantages compared to the other processes: high energy efficient, high purity of caustic and smaller environmental impact [3-5]. However, high brine quality is required to avoid membrane fouling. A membrane cell consists of two compartments divided by an ion-exchange membrane as can be seen schematically in Figure 1.3.

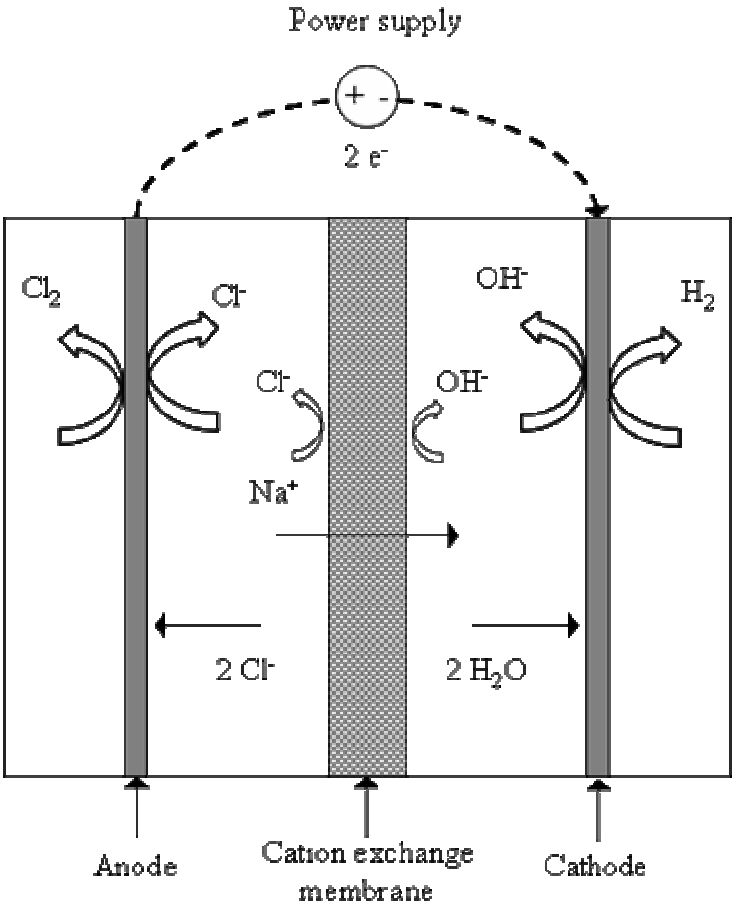

Figure 1.3 – Schematic representation of a chlor-alkali membrane cell.

A saturated sodium chloride solution is fed to the anode where the chloride ions are oxidized to chlorine. The sodium ions migrate through the membrane to the cathode compartment and combine with the hydroxyl ions produced from the water reduction at the cathode where hydrogen is also produced. The reactions evolved in this process are the following [3-5]:

At the anode:

$$2\,Cl^- \rightarrow Cl_2 + 2\,e^- \tag{1.2}$$

At the cathode:

$$2\,H_2O + 2\,e^- \rightarrow H_2 + 2\,OH^- \tag{1.3}$$

1.2.1. Thermodynamics

The electrochemical reactions can proceed spontaneously or can be driven by an electric potential. Electrochemical cells in which the electrode reactions take place spontaneously (ΔG < 0) are called galvanic cells. On the other hand, an electrochemical cell where a chemical reaction is driven by a power supply is termed electrolytic cell (ΔG > 0). The Gibbs free energy (ΔG) of an electrochemical reaction at constant temperature and pressure is given by [6]:

$$\Delta G = -nFE^0 \tag{1.4}$$

where n is the number of moles of electrons transferred, F the Faraday's constant (the charge required to drive a mole of electrons) and E^0 is the

standard electrode potential. ΔG is the minimum electrical work that must be supplied to an electrolytic cell to drive the electrochemical reactions. The standard electrode potential values can be easily found in the literature and the standard potential of a given electrochemical cell can be calculated by combining the potentials of the two half reactions (oxidation and reduction). The equilibrium electrode potentials ($E_{0,a}$ and $E_{0,c}$) corrected for the electrolytes concentration, temperature and pressure are given by equation (1) and (2) [4,7].

$$E_{0,a} = E_a^0 + \left(\frac{dE_a{}^0}{dT}\right)_T (T-25) + \frac{1}{2}\left(\frac{d^2E_a{}^0}{dT^2}\right)_T (T-25)^2 + \frac{2.303RT}{F}\log\left[\frac{p_{Cl_2}{}^{1/2}}{[NaCl]}\right] \tag{1.5}$$

$$\mathrm{E}_{0,c} = E_c^0 + \left(\frac{dE_c{}^0}{dT}\right)_T (T-25) + \frac{1}{2}\left(\frac{d^2E_c{}^0}{dT^2}\right)_T (T-25)^2 + \frac{2.303RT}{2F}\log\left[\frac{a_{H_2O}^2}{p_{H_2}a_{OH^-}{}^2}\right] \tag{1.6}$$

where E_a^0 and E_c^0 are the anode and cathode standard electrode potentials (25 ºC and with reactants and products at unit activity), T the cell temperature, R the ideal gas constant, p_{Cl_2} and p_{H_2} refers to the partial pressure of chlorine and hydrogen, [NaCl] is the concentration of the sodium chloride solution and $a_{H_2O}^2$ and $a_{OH^-}{}^2$ the activity of water and hydroxyl ions [4]. Table 1.1 shows the anode and cathode electrode potentials for normal

operating conditions in a chlor-alkali membrane cell. These conditions are: 90 °C, 1 bar, 3.5 M of NaCl and 10 M of NaOH.

Table 1.1 – Equilibrium electrode potentials of the half electrochemical reactions taking place in a typical chlor-alkali membrane cell [4].

	Reaction	E_0/V
Anode	$Cl_2(g) + 2e^- \rightarrow 2Cl^-(aq)$	1.23
Cathode	$2H_2O(l) + 2e^- \rightarrow H_2(g) + 2OH^-(aq)$	-0.99
Overall	$2NaCl(aq) + 2H_2O(l) \rightarrow 2NaOH(aq) + Cl_2(g) + H_2(g)$	-2.23

1.2.2. Kinetics

An electrochemical reaction comprises the transfer of electrons between an electronically conducting electrode and an ionically conducting electrolyte. The rate of electrons transfer through this boundary phase is limited by an activation barrier that depends on the reaction mechanism. Furthermore, the reaction mechanism determines the rate of the electrochemical reaction. Since the activation barrier (electron energy at the Fermi level) depends on the potential of the cell, the kinetics of electrochemical reactions can be controlled by the applied potential. Current is directly related to the rate of electrochemical reactions and is related to the activation overpotential by the well known Butler-Volmer equation [6-8]:

$$j = j_0\left\{\exp\left(\frac{-\alpha\eta F}{RT}\right) - \exp\left(\frac{(1-\alpha)\eta F}{RT}\right)\right\} \quad (1.7)$$

where η is the activation overpotential, j_0 is the exchange current density and α is the transfer coefficient. The activation overpotential of an electrochemical reaction is the difference between the applied potential (E) and the equilibrium cell potential (E_0). This is related to the difference between the Fermi energy of the metal and the free energy of the electron in the redox system (electrolyte). At the equilibrium between the metal and the surrounding electrolyte these two levels of energy are equal and the resulting current density is known as exchange current density. When a potential difference is applied to the cell, the potential of the metal electrodes are changed relative to the electrolytes. The magnitude of the activation overpotential and then the rate of the electrochemical reaction is essentially determined by the interaction between the excess charge on the metal and the ions on the electrolyte [6-8]. Two limiting cases of Butler-Volmer equation (1.7) can be identified [6-8]: for small (< 5 mV) overpotentials the Butler-Volmer equation can be fitted to a linear relation:

$$j = j_0\left(\frac{-\alpha\eta F}{RT}\right) \quad (1.8)$$

while for high overpotentials (> 200 mV) the Butler-Volmer equation is well described by the Tafel equation:

$$\eta = k\{\ln(j_0) - \ln(j)\} \quad (1.9)$$

where $k = \left(-\frac{RT}{\alpha F} \right)$ and is defined as the Tafel slope.

Electrocatalysis studies the factors affecting the activation barrier and how the rate of an electrochemical reaction can be improved. The electrocatalytic activity of the metals is strongly correlated with the electron structure of their atoms, which in turn determines the adsorption behavior of the species on their surface [6-8]. A good electrocatalyst is characterized by a high value of exchange current density. The so-called volcano plot relates the bond energy between the metal and the adsorbed species (e.g. hydrogen) with the exchange current density, Figure 1.4.

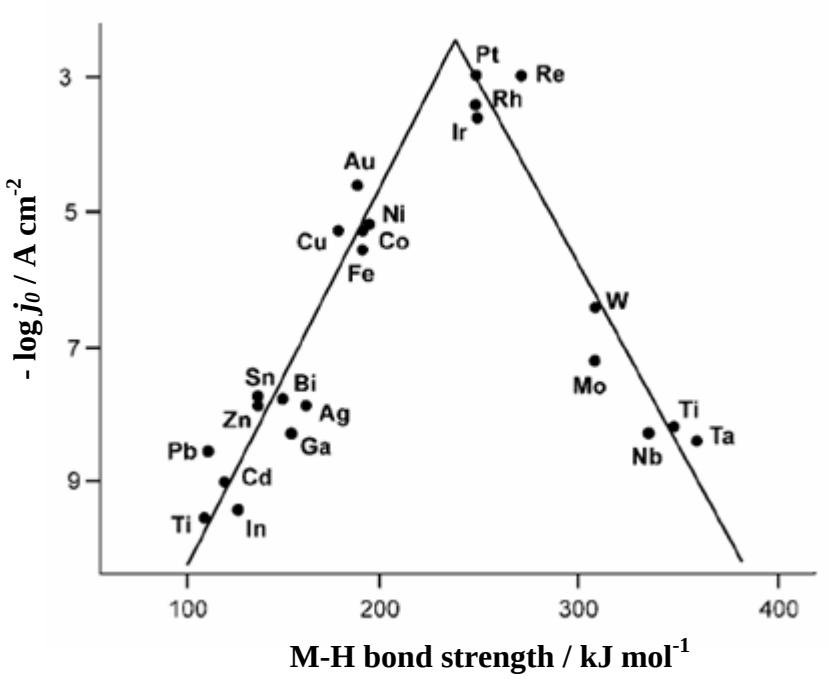

Figure 1.4 – Volcano plot for the hydrogen evolution reaction (HER) (adapted from [4]).

Maximum exchange current densities (j_0) are achieved for Pt-group metals and intermediate values are found for the transition metals such as Cu, Au, Ag, Fe, Cu and Ni. The selection of the proper electrode material is a determinant factor for electrochemical reaction rate.

One of the most important problems in chlorine production is the occurrence of a side reaction producing oxygen at the anode. The standard reversible potential of the electrochemical oxidation of water (equation (1.11)) is lower than the chlorine standard potential, being then thermodynamically favorable:

$$2Cl^- \rightarrow Cl_2 + 2e^- \qquad (E^0 = -1.36\ V) \qquad (1.10)$$

$$2H_2O \rightarrow 4H^+ + O_2 + 2e^- \qquad (E^0 = -1.23\ V) \qquad (1.11)$$

Due to the kinetics and reaction mechanism of the oxygen evolution reaction, low exchange current densities are obtained at noble metals and the exchange current densities for the chlorine evolution reaction are usually greater [4,6-8]. This way, the chlorine evolution reaction is predominant at intermediate and high current densities. To minimize the oxygen production, high chloride concentrations should be kept in the anode surface and the pH maintained in the optimum range of 2-5. In practice, saturated brine solutions are fed to the anode compartment to assure high coverage of chloride ions at the surface of the electrode. The main requirements for the anode material are: electrochemical stability against oxidation and chemical attack by NaCl,

HCl, Cl_2, HOCl, ClO_3^- and O_2, high electrical conductivity and high electrocatalytic activity for the chlorine reaction (high exchange current density) [4,6-8]. The cathode material must have high corrosion resistance in concentrated alkaline solutions, high stability at open circuit conditions and exhibit high electrocatalytic activity towards hydrogen evolution [4,6-8].

1.2.3. Charge and mass transport

Charge transport in aqueous electrolytes

In an electrochemical system charges are present as electrons and ions. The electrons (negatively charged) are transported through the external circuit from the electrode where they are produced (anode) to the electrode where they are consumed (cathode). The accumulation/depletion of ions on the electrode surfaces creates a potential and a concentration gradient that drives the ion transport through the electrolytes. There are three major driving forces for charge transport: electrical potential gradient ($\frac{dE}{dx}$), concentration gradient ($\frac{dc}{dx}$) and pressure gradient ($\frac{dp}{dx}$) [4,7]. Table 1.2 summarizes these transport processes.

Table 1.2 – Summary of transport processes to charge transport (adapted from [7]).

Transport Process	Driving force	Coupling coefficient	Equation
Conduction J_m	$\frac{dE}{dx}$	Conductivity σ	$J = \frac{\sigma}{\lvert z_i \rvert F}\frac{dE}{dx}$
Diffusion J_d	$\frac{dc}{dx}$	Diffusivity D	$J = -D\frac{dc}{dx}$
Convection J_c	$\frac{dp}{dx}$	Viscosity μ	$J = \frac{G_c}{\mu}\frac{dp}{dx}$

While in metal electrodes only an electrical potential gradient drives the electron charge transport, the motion of ions through electrolyte solutions can be driven by any of the transport mechanisms present in Table 1.2. In a membrane cell process the most relevant driving force to the charge transport is the electrical potential gradient (electric field) generated by the depletion of anions/accumulation of cations and accumulation of electrons on the anode surface and the depletion of cations/accumulation of anions and depletion of electrons on the cathode surface. Moreover, positively charged ions (cations) are transported from the anode to the cathode compartment. Conductivity measures the ability of a material to conduct electric current and is affected

by the material properties and by the temperature. Conductivity is related to the resistance of a conductor by the following equation:

$$R_c = \frac{\ell}{\sigma A} \tag{1.12}$$

where R_c is the conductor resistance, σ is the conductor conductivity, ℓ is the length of the conductor and A is the cross-sectional area of the current flow. As shown in Table 1.2, charge transport due to an electric field (J_m) increases as the potential gradient increases. Ohm's law relates the potential (E) applied to the cell with the rate of electric charge flow:

$$E = R\, j \tag{1.13}$$

where j is the charge flux (current density) through the cell.

The presence of gas bubbles in the electrolytes greatly affects the electrolyte conductivity and consequently the cell potential. The effect of bubbles on electrolyte resistivity is given by the Bruggemann equation [4, 9]:

$$\frac{\rho}{\rho_0} = (1-\varepsilon)^{-\frac{3}{2}} \tag{1.14}$$

where ρ is the resistivity (inverse of conductivity: $\frac{1}{\sigma}$) of the electrolytes, ρ_0 is the resistivity of pure electrolyte (free of gas bubbles) and ε is the gas void fraction.

Charge and mass transport through the ion-exchange membrane

Ion-exchange membranes are classified by their function as a separator; cation-exchange membranes, that contain fixed negatively charged ions, are used in the electrolysis process to prevent the anion transport from the cathode compartment to the anode compartment [10]. The fixed ions of the membrane are in equilibrium with the mobile ions (referred to as counter-ions) whereas the ions that carry the same charge as the fixed charge (referred to as co-ions) are more or less efficiently excluded from the membrane matrix – Donnan exclusion effect - as illustrated in Figure 1.5.

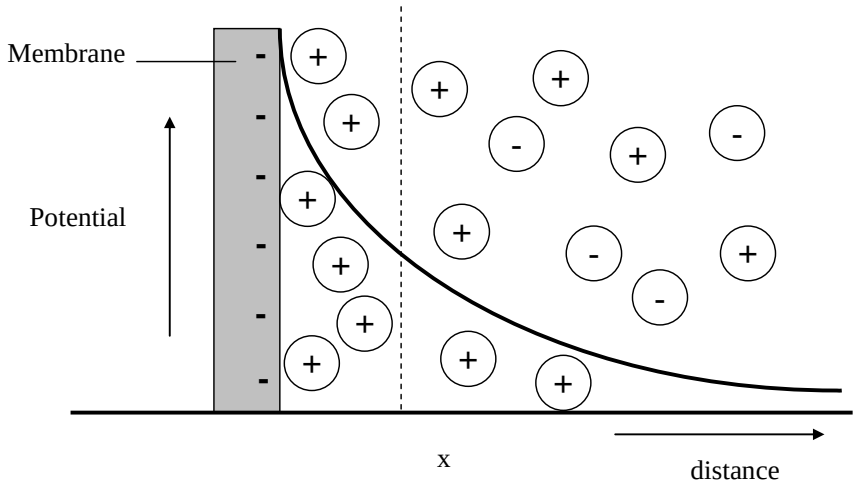

Figure 1.5 – Illustrative scheme of Donnan exclusion effect [11].

The most important characteristics of an ion-exchange membrane are: high permselectivity for the counter-ions (exclusion of co-ions), high ionic conductivity, good mechanical, form and chemical stability [10]. The ion

permselectivity of an ion-exchange membrane is related to its ability to reject co-ions. Due to the Donnan exclusion effect the permselectivity is affected by the electrolyte concentration of the surrounding solution and by the ion-exchange capacity of the membrane. An ideal permselective membrane should totally exclude co-ions from the membrane matrix. The ionic conductivity of the membrane also depends on the concentration of the electrolyte solution which affects the swelling of the membrane (membrane water content). Furthermore, the mobility of the ions through the membrane matrix depends strongly on the water content of the membrane, on the interaction between the mobile and fixed ions (that depends on the valence, size and extent of hydration of the ions) and on the temperature. Water content increases the free volume inside the membrane matrix improving the ability of ions to move across the polymer [4,10]. The nature of the membrane polymer, the nature and concentration of the ion-exchange groups and counter-ions and the degree of cross-linking of the polymer determines the membrane water content. Moreover, membrane water content affects not only the membrane selectivity and conductivity but also its dimensional stability (i.e. dimensional changes between wet and dry states of the membrane) [10]. Additionally, the ion-exchange membranes used in the chlor-alkali industry must have low permeability to hydrogen, chlorine and

oxygen to prevent the hazardous mixture of these gases and to allow high gas purity production [4].

The water transport across the ion-exchange membrane is due to osmosis and electroosmosis. While the osmotic water transport through the membrane is the result of different transport rates of water and salts through the membrane under the effect concentration gradients, the electroosmosis is the water transported under the influence of an electric field. Moreover, the electroosmotic water transport results from the water molecules carried across the ion-exchange membrane in the hydration shell of the ions. The membrane water content is greatly affected by the water transported across the membrane [4,10].

Mass transport

Transport of the reactants from the bulk of the solution to the electrode surface and the removal of products from the surface are inherent steps in electrochemical reactions. When these steps are slow and or the electric field very high, the mass transport at the surface of the electrodes become rate controlling and adversely affects the rate of the electrochemical reaction; in the limit we may reach $c_R^* \to 0$ and $c_p^* \to 0$ (equation 1.7). This phenomenon is called concentration polarization and is often neglected

in the electrolysis process because the raw materials are supplied in excess and no limitations to the mass transport are normally found.

1.2.4. Electrochemical characterization techniques

In electrochemical systems there are three fundamental variables: current, potential and time. The relationship between current and potential, *j*-*E* curves, gives information about the overall performance of the system. When a current is applied to the electrochemical cell an activation overpotential is needed for the reaction to proceed in a given direction. The electric field that results from the polarization of the electrodes drives the ion transport through the electrolytes and membrane whereas the electrons are transported across an external circuit. This way, the output cell potential is the sum of all these contributions (thermodynamics, reaction kinetics, charge and mass transport) and is given by the following equation [4,7]:

$$E = E_{0,a} - E_{0,c} + \eta_a - \eta_c + \eta_{ohmic} \tag{1.15}$$

where $E_{0,a}$ and $E_{0,c}$ are the thermodynamic potential of anode and cathode reactions, η_a and η_c are the anodic and cathodic activation overpotentials, and η_{ohmic} is the ohmic resistance to the charge transport through the electrolytes and the membrane. Substituting and rearranging equations that describe the activation overpotential (1.8) and the ohmic resistances (1.12) the following equation is obtained [4]:

$$E = E^* + (k_a - k_c)\log(j) + (R_{ele} + R_m)j \tag{1.16}$$

where

$$E^* = E_{0,a} - E_{0,c} - k_a \log(j_{0,a}) + k_c \log(j_{0,c}) \tag{1.17}$$

Subscripts *a* and *b* refers to the anode and to the cathode, respectively.

The current-density potential curve provides an overall evaluation of the membrane cell performance. Although, a more sophisticated technique is required to accurately study the different interfaces present in the cell: metal/solution interface and membrane/solution interface [7]. The electrochemical impedance spectroscopy (EIS) allows the differentiation between the different components of an electrochemical membrane reactor. Similarly to the electrical resistance, the impedance of an electrochemical system measures the ability of a system to influence the electrical current flux. While the electrical resistance is time and frequency independent, impedance varies with these two parameters and is defined as [7]:

$$Z = \frac{E(t)}{j(t)} \tag{1.18}$$

where E (t) and j (t) are the potential and current density at time t, respectively. A small sinusoidal perturbation (e.g. $E(t) = E_0 \cos(wt)$) is applied to the potential or to the current and the system response monitored. Usually, the impedance of a system is represented in *Nyquis*t and *Bode* plots and gives detailed information about the electrochemical processes.

Energy consumption is the major factor affecting the chlor-alkali production cost. Therefore, it is the most import feature of the process performance. The energy consumption calculation requires knowledge about the potential and current efficiency and is given by [4]:

$$P_c = \frac{1}{E_q}\frac{E}{\xi_{NaOH}} \tag{1.19}$$

where E_q is the electrochemical equivalent of caustic soda, ξ_{NaOH} is the caustic soda current efficiency and E the potential across the electrolyzer. The caustic soda current efficiency is obtained from the ratio of the total caustic soda produced by the amount of caustic soda that is expected to produce. The Faraday's law of electrolysis gives the expected amount of caustic soda produced when a given amount of current is applied to the cell (current) over a certain period of time (t) [6]. This is given by:

$$m_{NaOH} = E_q \frac{It}{F} \tag{1.20}$$

where I is the applied current and t is the time.

1.3. State of the art of the chlor-alkali membrane process

In the last 30 years many improvements were made in the chlor-alkali industry. There are two main milestones that revolutionized this process, the development of metal anodes and the changeover of the old diaphragm and mercury technologies to membrane cells [3]. Nowadays, the membrane cell

process is the most used in the world [1,2]. The complete conversion to the membrane technology is expected in the next years due to the mandatory deadline (2020) to phase out the mercury cells in Europe [1]. CUF-QI converted the old mercury cells to the state of the art membrane cell technology already in 2002. At that time, the newly developed Azec-B1 electrolyzers from Asahi Glass were installed and represented 75 % of the total chlorine production capacity of the company. These electrolyzers have a narrow gap between membrane and electrodes. DSA® anodes and Raney nickel cathodes are currently used as electrodes. Different types of membranes have been tested.

1.3.1. Electrodes

Anode

The primarily materials used in the chlor-alkali industry as anodes were platinum, magnetite and carbon. Platinum was expensive and magnetite had poor conductivity leading to really low current densities (0.4 kA m^{-2}). The graphite anodes were widely used from the 1900s to the late 1960s. However, their short life (6-24 months), the products contamination with chlorinated hydrocarbons and their negative effect on the cell performance led to the replacement of the graphite anodes by coated metal anodes. Many mixed oxide coatings were tested without success until the discovery of titanium

anodes coated with a layer of the mixed dioxides of titanium and ruthenium in 1965 by Henry Beer. A few years later these anodes were commercialized by DeNora under the trade name of Dimensionally Stable Anodes (DSA®) [3-5].

The DSA® anodes have very high electrocatalytic activity and selectivity towards anodic chlorine evolution, exhibiting then low overpotential. These electrodes are also very stable during a long period of time; their expected lifetime is 8 years. While titanium dioxide is catalytically inactive but gives stability to the coating, the ruthenium dioxide exhibits high exchange current densities for the chlorine reaction [4,6,8]. When the ruthenium dioxide content is higher than 30 % the obtained Tafel slopes are in the range of 40-60 mV. However, with extend usage the anode can deactivate and can achieve Tafel slopes of 300-400 mV (at this point the anode is considered deactivated) [13]. The deactivation mechanism has been investigated by several authors. It is known that for ruthenium dioxide (RuO_2) contents below 20 wt. % the chlorine overpotential increases significantly [13-16]. Generally, the anode deactivation mechanism is attributed to the consumption of RuO_2 and/or to the formation of an insulating TiO_2 layer at the titanium/coating interface [13-16]. The blockage of the electrode surface by impurities can also give rise to the loss of active sites. The addition of iridium dioxide (IrO2) to the DSA® anode coatings is a

common procedure as it prevents the Ru corrosion; as a result higher anode durability can be achieved. The anolyte pH has an important effect on the reaction rate of the water oxidation reaction and on the lifetime of the anode. At high anolyte pH, the water oxidation reaction is favored (pH > 5) and the dissolution of the coating is more likely to occur (pH >12). Low pH (< 2) can lead to titanium dissolution [4,8].

Alternative anode compositions have been investigated and the most promising are: titanium substrate coated with a mixture of platinum and iridium, cobalt spinels, palladium oxide based coatings and platinates [4, 17, 18].

Cathode

Carbon steel cathodes had been used in diaphragm cell since 1910. After the development and commercialization of the ion-exchange membranes, carbon steel cathodes were replaced by stainless steel and nickel cathodes in the membrane cells [3-5]. In the early 90's the nickel cathodes come into general use due to their excellent corrosion resistance in the chlor-alkali cells, i.e. high stability in high concentration sodium hydroxide solutions. Another important concern on the choice of the cathode material is its resistance against oxidation (corrosion) by chlorine-based chemical species that can be reduced in the anode during shutdowns [3-5]. The improvement of the membrane cell performance made the energy savings a

crucial issue to the investigation of new high performance materials. As nickel is not the most suitable material in terms of electrocatalytic activity for the hydrogen reaction (HER), high surface nickel based cathodes were investigated and developed; i.e. metals with higher electrocatalytic activity for the HER (see Figure 1.4) were incorporated in a nickel substrates. Several techniques have been investigated for the preparation and characterization of nickel type coatings doped with different elements (e.g. Cr, Co, Ti, W, Mo and Fe) [19,20]. An activation overpotential of c.a. 500 mV is expected for the hydrogen evolution reaction (HER) at smooth nickel surfaces while 200 mV can be attained with Ni-Al type Raney nickel cathodes [4]. Significant energy savings, above 10 %, arise from using cathodes with lower overpotential.

1.3.2. Membranes

The first generation of commercial membranes (1975) was able to directly produce sodium hydroxide solutions of 2-40 wt. %. They were made from fluoropolymers functionalized with sulfonic groups. However, the current efficiencies were low being the highest efficiency (85 %) attained for concentrations in the range 10-15 wt. % NaOH [4]. These membranes were relatively thick with heavy reinforcement cloths and the electrode gap was 9 mm. Due to these membrane characteristics the typical operating potentials

were high (3.8 to 4.0 V at 2.5 kA m^{-2}) that combined with low current efficiency give a DC energy consumption of 3300 kWh ton^{-1} of caustic soda [3]. Additionally, the current efficiency decline was quite fast due to impurities precipitation in the membrane structure. Later on, the development of a laminated membrane structure with two different functional groups revolutionized the chlor-alkali membrane cell process by improving the current efficiency and reducing the operating potential.

Nowadays, the commercially available membranes in the chlor-alkali industry are bilayer membranes with a polymeric matrix made of tetrafluoroethylene. Sulfonic and carboxylic groups are used as fixed ionic groups on the anode and cathode side of the membrane, respectively (Figure 1.6).

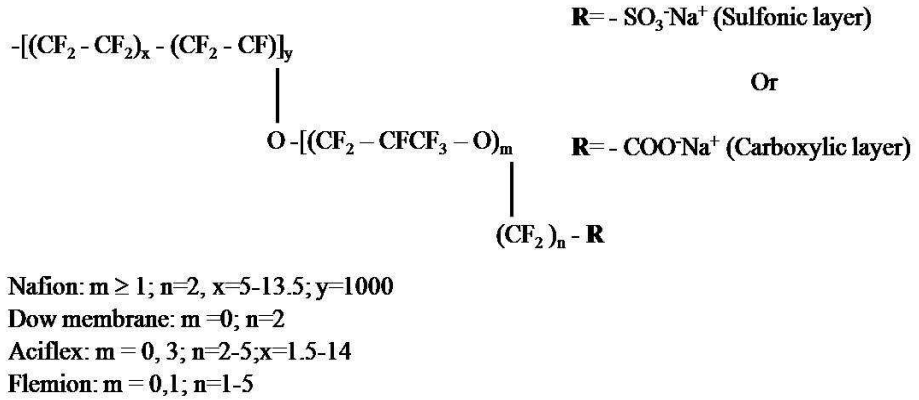

Figure 1.6 – Illustrative scheme of the structure of different commercial membranes [4].

The use of different ionic groups, as illustrated in Figure 1.6, has significant effects on the permselectivity and conductivity of each layer. Furthermore, the sulfonic groups are excellent proton conductors while the carboxylic groups are highly permselective to cations due to their lower water content [10]. The mechanical properties of the membranes (tensile and tear strength) are greatly improved by reinforcements; a PTFE woven cloth is used to reinforce the membrane structure to prevent damage or tearing of the membrane. There are different types of cloths to reinforce the membranes and in some cases sacrificial fibers are also used. More and thinner fibers increase mechanical strength besides providing low voltage and high current efficiency [4,19]. To prevent the adherence of bubbles to the membrane surface, the membranes surfaces are made hydrophilic [4,10]. The typical structure of a commercial ion-exchange membrane is shown in Figure 1.7.

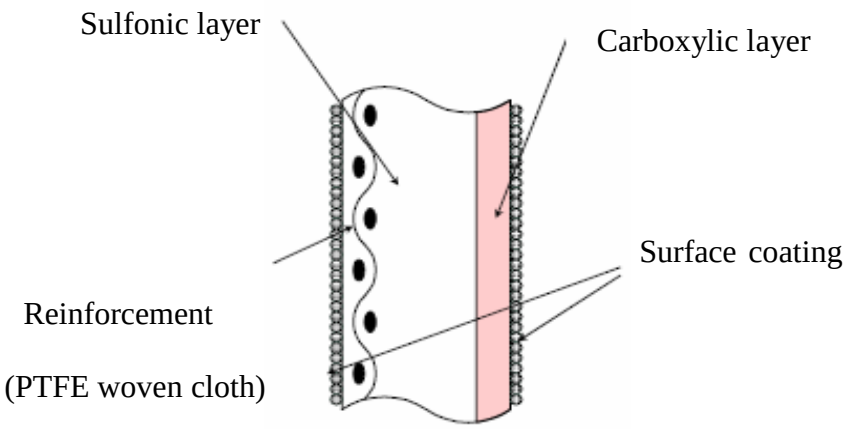

Figure 1.7 – Schematic representation of a commercial ion-exchange membrane (adapted from [22]).

There are three main manufacturers of ion-exchange membranes to the chlor-alkali industry: DuPont (USA), Asahi Glass (Japan) and Asahi Kasei (Japan). The differences between suppliers are related to the modifications made on the polymer and on the functional groups, the type of reinforcement used and other chemical and mechanical details. The membranes commercially available for the chlor-alkali industry can be divided in two classes regarding their characteristics: high performance and high mechanical strength membranes. Low resistance membranes are more adequate to narrow gap electrolyzers due to their low voltage. On the other hand, high strength membranes are used in more robust electrolyzers where the main requirement is high physical strength. Today, membranes operate at higher current densities with current efficiencies of about 97 % producing a caustic soda stream of 32 wt. %. The typical DC energy consumption values are as low as 2100 kWh/ton of caustic soda [4].

1.3.3. Electrolyzers

A commercial membrane plant has several individual membrane cells, called elements, which are combined to form an electrolyzer. The electrolyzers can be classified in two categories with respect to their electrode configuration: monopolar and bipolar [3,4]. Monopolar electrolyzers are connected in series and the individual cells in parallel,

forming an electrolyzer with high current and low voltage. On the other hand, the bipolar electrolyzers are connected in parallel and the single elements in series. This results in a low current and high voltage electrolyzer. The main differences between these two arrangements are related to the capital cost of the cells and the electrical supply system (rectifiers and transformers) [3,4]. Nowadays, there are five suppliers of membrane cell electrolyzers (monopolar and bipolar): Asahi Kasei (Japan), Chlorine Engineers (Japan), Eltech (USA), Uhde (Germany) and Ineos Chlor (UK). Currently, the bipolar technology is the most popular due to the trend of higher current density operation [4].

1.4. Motivation and Outline

The present thesis aims to study the chlor-alkali membrane cell technology, which is the process used by CUF-QI. Despite being a mature technology little information can be found in the literature about this process. Furthermore, there are only three main manufacturers of the cation exchange membranes and a few suppliers for electrolyzers. These suppliers dominate the knowledge of this technology. The process performance has a great impact on the energy consumption that is the major cost factor in the production cost; this way, it is desirable to operate at high performance. The need for further know-how to continuously improve the process performance

and the negotiation ability of CUF-QI were the major motivations for this research work.

The main questions that this thesis addresses are:

- Which factors affect the most the cell performance and what is the contribution of each of them?
- How can we do the characterization of each component of the cell?
- What are the strategies for decreasing the operating costs of the process?

The first part of this work is focused on the development of the experimental setups needed for the research work: a unit to characterize the membrane permselectivity and an experimental chlor-alkali membrane cell. This was a rather great challenge because information on this subject is scarce [22-24]. **Chapter 2** describes the experimental setups developed and their performance.

After optimizing the experimental electrochemical membrane reactor, the effect of the operating parameters (current density, feed flow rate, brine and caustic concentration and temperature) on the overall performance was studied and reported in **Chapter 3**. The electrochemical impedance spectroscopy (EIS) was used to characterize *in situ* the ohmic resistances of the cell.

Following the characterization of the ohmic resistances of the cell, the EIS was used to study the hydrogen evolution reaction (HER) on nickel cathodes. Solid and mesh electrodes were investigated and the kinetic parameters of HER obtained. This is discussed in **Chapter 4**.

Chapter 5 presents a benchmarking methodology of three different types of ion exchange membranes. This also allows deciding the best moment for membrane replacement. The methodology is based on the average cost history of the chlorine produced. The performance of three different membranes operating at CUF-QI industrial plant were assessed and compared.

Finally, **Chapter 6** presents the conclusions of this work and suggests future developments and lines of work.

1.5. References

[1]– www.eurochlor.org/, accessed in May 2010.

[2]– worldchlorine.com/, accessed in May 2010.

[3]– T. Navin, "Membrane Cell Technology - State of the art industry", Eltech Systems Corporation, 2002.

[4]– T. F. O'Brien, T. V. Bommaraju, and F. Hine, in *Handbook of Chlor-Alkali Technology*, Springer, New York, Volume I and V, 2005.

[5] - P. Schmittinger, *Chlorine-Principles and Industrial Practice*, 1st edition, Wiley-VCH (2000).

[6]– C.H. Hamann, A. Hamnett, W. Vielstich, in *Electrochemistry*, 2nd edition, Chapter 4 and 5, Wiley-VCH (2007).

[7]– R. O' Hayre, Suk- Won Cha, W. Colella and F. B. Prinz, in *Fuel Cell Fundamentals*, Wiley, New York (2006).

[8]– V.S. Bagotsky, in *Fundamentals of Electrochemistry*, 2nd edition, Chapter 15, 17 and 26, Wiley Interscience, New Jersey (2006).

[9]– Ph. Mandin, J. Hamburger, S. Bessou, G. Picard, *Electrochimica Acta*, **51** (2005) 1140-1156.

[10]– H. Strathmann, in *Ion-Exchange Membrane Separation Processes*, Chapter 3, Membrane Science and Technology Series, 9, Hungary (2004).

[11]– M. Mulder, *Basic Principles of Membrane Technology*, Chapter 5, Kluwer Academic Publishers,2nd edition, Netherlands (1997).

[12]– J. Krol, *Monopolar and Bipolar Ion Exchange Membranes- Mass Transport Limitations*, PhD thesis, University of Twente, Netherlands, 1997.

[13]– B.V. Tilak, V.I. Birss, J. Wang, C.-P. Chen and S.K. Rangarajan, *J. Electrochem. Soc.*, **148** (9), D112-D120 (2001).

[14]– L.K. Xu, J.D. Scantlebury, *Corrosion Science*, **45**, 2729 (2003).

[15]– A.S. Pilla, E. O. Cobo, M. M.E. Duarte, D.R. Salinas, *J. Applied Electrochemistry*, **27**, 1283 (1997).

[16]– T. Loucka, *J. Applied Electrochemistry*, **7**, 211 (1977).

[17]– B. Conway and G. Ping, *J. Chem. Soc. Faraday Trans.*, **86** (6), 923 (1990).

[18]– M. Santana and L. Faria, *Electrochimica Acta*, **51** (17), 3578 (2006).

[19]– A.C.D. Angelo, *International Journal of Hydrogen Energy*, **32** 542 (2007).

[20]– R. Theobald, "Mechanical aspects of membrane operation", Paper presented at the Eltech Seminar, October, Cleveland, Ohio (2000).

[21]– Technical information, "Characteristics of Flemion Membranes", Asahi Glass Co., Ltd (Flemion Seminar 2002).

[22]– T. Mirzazadeh, F. Mohammadi, M. Soltanieh and E. Joudaki, *Chem. Eng. J.*, **140**, 157 (2008).

[23]–A.A. Jalali, F. Mohammadi and S.N. Ashrafizadeh, *Desalination*, **237** 126 (2009).

[24]–N.S. Kaveh, F. Mohammadi and S.N. Ashrafizadeh, *Chem. Eng. J.*, **147**, 161 (2009).

Chapter 2- Chlor-alkali membrane cell – laboratorial setups

2.1. Abstract

The experimental setups build and used in the present work for studying the chlor-alkali process are described and characterized. It was build an experimental setup for characterizing the permselectivity of cation exchange membranes and an electrochemical membrane reactor for studying the brine electrolysis process. The experimental procedure for operating with the electrolysis setup is described in detail. The performance of this setup was assessed and compared whenever possible with bibliographic results. It was concluded that the experimental setups performed as planned.

2.2. Introduction

The chlor-alkali membrane cell process is a well-known technology for producing chlorine and sodium hydroxide. Despite being a mature a technology, the cation exchange membranes and the electrodes used are still very sensitive to damage and deactivation. Moreover, the overall energy efficiency of the electrochemical process is around 70 %.

The ion exchange membranes are a key component of these cells and are classified by their function as a separator; cation exchange membranes that contain fixed negatively charged ions are used in the electrolysis process to prevent the anion transport from the cathode to the anode compartment. The most important characteristics of an ion exchange membrane are: high permselectivity to the counter-ions (exclusion of co-ions), high ionic conductivity, good mechanical, dimensional and chemical stability [1-3]. Different procedures and techniques can be applied to determine relevant properties of the ion-exchange membranes. Nagarale et al. [2] described the methodologies used for the characterization of these membranes and their applications. The ionic transport in Nafion® membranes in concentrated solutions were investigated by a radiotracer- weight method [3]. The radiotracer method was also used to measure the permselectivities of some chlor-alkali membranes [4]. Other studies concerning the transport properties through the membrane [6-8], the impact of different operating parameters on

the cell performance [9-12] and the electrodes kinetics [13-17] were also reported.

In order to increase the understanding of the chlor-alkali process and to improve the membrane cell performance an experimental setup facility is needed. The reported studies on this subject are rather scarce [9-12]. Mirzazadeh et al. [9] have described a laboratorial setup for zero-gap oxygen-depolarized chlor-alkali cell that used a modified commercial micro-flow cell. The effects of various operating parameters on the cell potential and current efficiency were studied in a laboratorial chlor-alkali membrane cell [10]. In this work, a micro-flow cell was also used for experimental design. A similar investigation but using a different technique was performed by N. Kaveh et al. [11] in a divided filter press type cell (ElectroCell, Sweden). All these setups found in the literature are equipped with filter press type membrane cells from ElectroCell that allows the use of a variety of cell designs.

In the present work the most important membrane characterization methods were implemented and an experimental device was developed to measure the permselectivity of membranes. In order to study the components of a membrane cell unit (electrochemical membrane reactor) and to produce insights for improving the overall performance of the industrial process an experimental setup was built up. Herein, we are describing the developed

experimental setup that comprises the membrane cell, feeding and temperature control systems, outlet system and power supply and data acquisition system. The performance of this setup was assessed and the experimental results obtained compared to the literature and with reference values.

2.3. Experimental

Two experimental setups were developed; an experimental setup to perform the membrane characterization and a chlor-alkali membrane cell to study and optimize the process.

2.3.1. Membrane characterization

The membrane permselectivity was obtained by a static membrane potential method [1-4]. This method is based on the determination of the potential gradient between two compartments of different electrolyte concentrations separated by the membrane. The experimental setup used to determine the membrane permselectivity is shown schematically in Figures 2.1 and 2.2. This setup was made of Plexiglass (250 x 170 x 250 mm) and comprises two cylindrical cells (150 mm of diameter) connected by a diffusion element (used to place the membrane) with an inside diameter of 50 mm. Two stirrers are used to homogenize the solutions up to the membrane

surface. The feeding system consists of two peristaltic pumps (Watson Marlow model 323 S) that supply the sodium chloride solutions of different concentrations to the cell compartments.

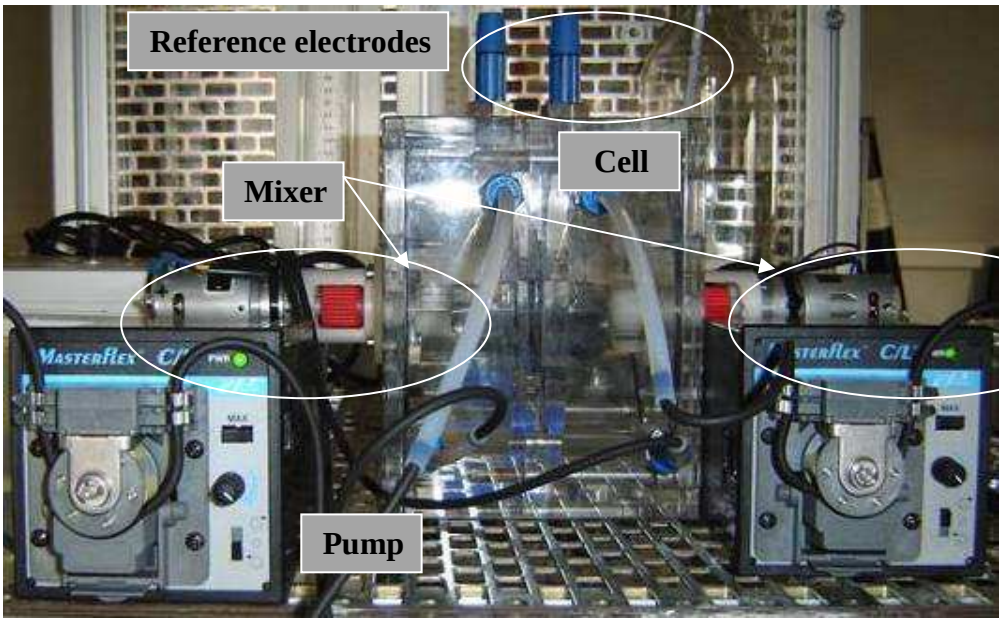

Figure 2.1 – Picture illustrating the unit used to obtain the permselectivity of membranes.

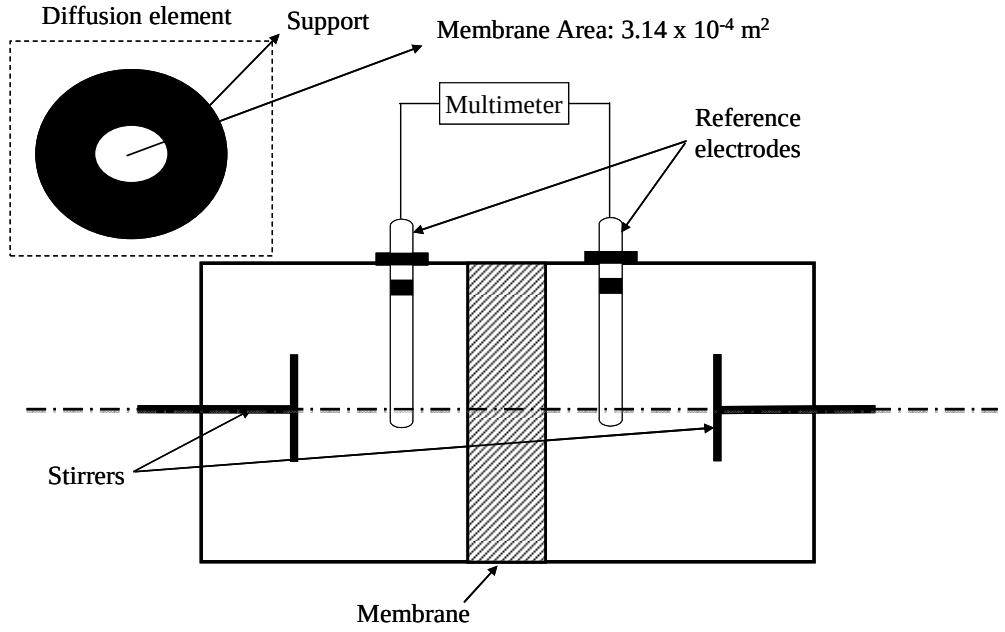

Figure 2.2 – Schematic representation of the unit used to measure the permselectivity of membranes.

Prior to the permselectivity determination, the ion exchange membrane was equilibrated in a sodium chloride solution of 0.1 M over night. Then the membrane was installed in the experimental setup. The cell chambers were filled with sodium chloride at different concentrations (i.e. 0.1 M and 0.5 M) and the stirrers turned on. The potential gradient between the two electrolyte solutions were measured with two calomel electrodes (KCl solution - 3 M) after the steady state being achieved - normally after 20 minutes.

The permselectivity of an ion-exchange membrane was then determined by the ratio between the electric charges transported by the

counter-ions and the total electric current carried by the membrane. In the present work, where a cation exchange membrane was used, the sodium ions are the counter-ions and the chloride ions the co-ions. The permselectivity can be obtained by the following equation (2.1):

$$\psi_m = \frac{\varphi_{m,measured}}{\varphi_{m,sp}} \times 100 \tag{2.1}$$

$$\varphi_{m,sp} = \frac{RT}{F} \ln\left(\frac{a_i^1}{a_i^2}\right) \tag{2.2}$$

where ψ_m is the membrane permselectivity, $\varphi_{m,measured}$ is the measured potential difference and $\varphi_{m,sp}$ is the membrane potential of a strictly permselective ion exchange membrane. R is the gas constant, T is the absolute temperature, F is the Faraday constant and a_i the activity of the salt solution where 1 and 2 refer to the solutions separated by the membrane [1].

This unit was used to determine the permselectivity of membranes used in this work. In order to validate the good performance of this unit the permselectivity of a well known fresh membrane (A) was determined and compared with the corresponding values obtained in a well known laboratory in membrane characterization – Membrane Technology Group, Twente. A permselectivity of 93.6 % was obtained for this membrane, which agrees with the values obtained at MTG of 93.6 %.

Additionally, this setup was used to measure the permselectivity of the same membrane after 100 hours of operation and of a blistered membrane from the industrial plant of CUF-QI. The permselectivity of the sulfonic layer of these membranes was also obtained and compared with the ones obtained for the carboxylic layer, Table 2.1.

Table 2.1 – Permselectivity of membrane A under different conditions: fresh membrane, membrane with 100 hours of operation and a blistered membrane.

	Ψ_m / %	
Membrane	**Sulfonic layer**	**Carboxylic layer**
Fresh	84.7	93.6
100 hours of operation	84.6	93.4
Blistered	67.3	78.3

As expected, the permselectivity of the carboxylic layer is higher than the selectivity of the sulfonic layer; the water content in the carboxylic layer is lower than in the sulfonic one and therefore has high permselectivity [18]. After 100 hours of operation in the laboratorial setup the permselectivity is practically the same as for the fresh membrane. However, a significant permselectivity decline is observed for the blistered membrane. Blistering is a form of mechanical damage that delaminate the membranes between layers

and can lead to a performance decline. SEM images of the carboxylic layer of the blistered membrane were obtained, Figure 2.3.

Figure 2.3 – View of the blistered carboxylic layer of membrane A (40 x).

As can be seen in Figure 2.3, the membrane matrix is severely damaged being disrupted in some points. This justifies the loss of permselectivity of the membrane.

2.3.2. Experimental setup of the Chlor-alkali Membrane cell

The schematic representation of the membrane cell setup that was developed is shown in Figure 2.4. This setup can be divided in 4 subsections: membrane cell, feeding and temperature control systems, outlet system and power supply and data acquisition system. All fittings and tubing are in PFA to avoid corrosion from the sodium chloride and sodium hydroxide solutions and chlorine.

Membrane cell

A filter press type membrane cell from *ElectroCell Europe A/S*, Denmark (ElectroMP-cell, monopolar) with two compartments was used (Figure 2.5). The cell uses PVDF (a polymer of vinylidene fluoride) frame sets and EPDM (ethylene propylene diene monomer) gaskets; all components are pressed together using stainless steel end plates. The compartments were separated by an ion exchange membrane with an effective surface area of 1.00×10^{-2} m^2. A DSA® (dimensionally stable anode) anode made of titanium coated with titanium, ruthenium and iridium oxides was used in the anode compartment and a nickel electrode was used in the cathode.

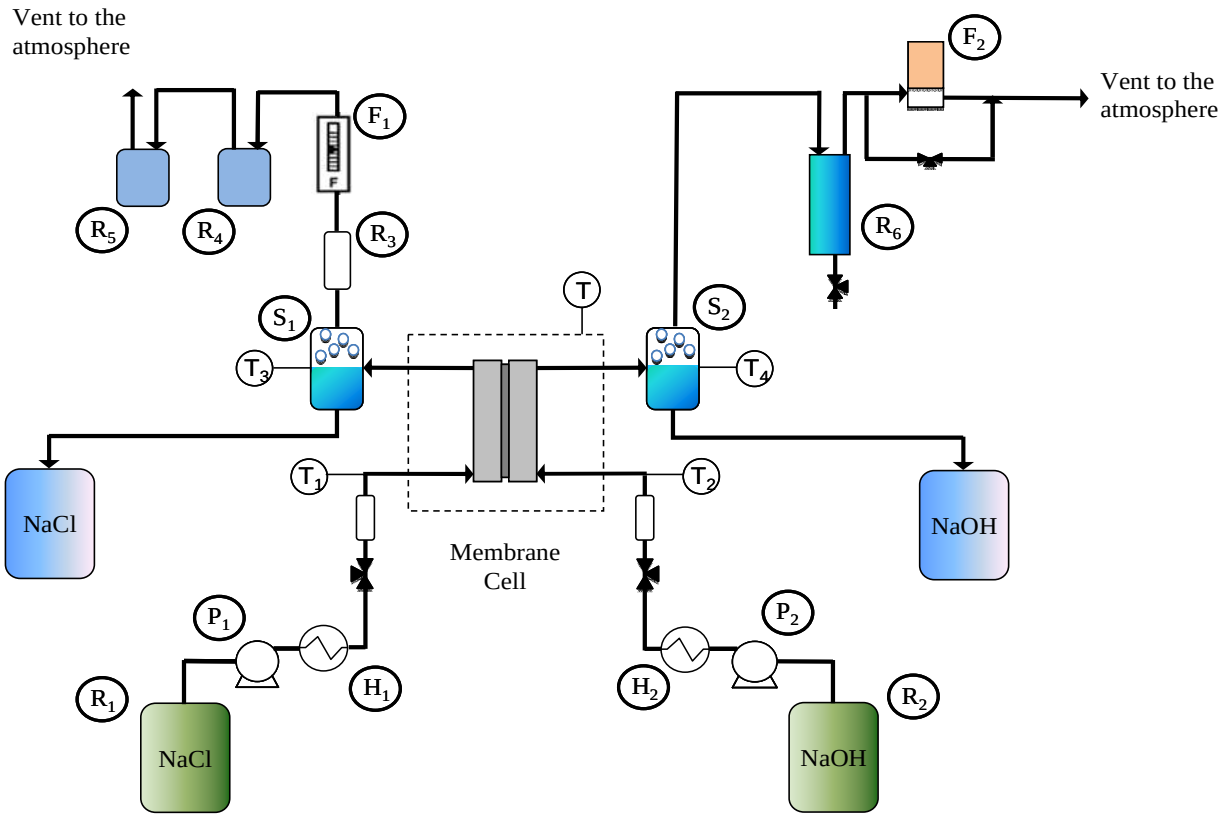

Figure 2.4 – Schematic representation of the membrane cell setup.

R_1 – NaCl feeding tank

R_2 - NaOH feeding tank

P_1 – NaCl pump

P_2 – NaOH pump

H_1 – NaCl heat exchanger

H_2 – NaOH heat exchanger

A_1, A_2- Air traps

S_1 – Anolyte separator

S_2 – Catholyte separator

R_3 – Chlorine cooling column

R_4 – Absorption tank 1

R_5 - Absorption tank 2

R_6 – Hydrogen cooling column

R_7 – NaCl waste container

R_8 – NaOH waste container

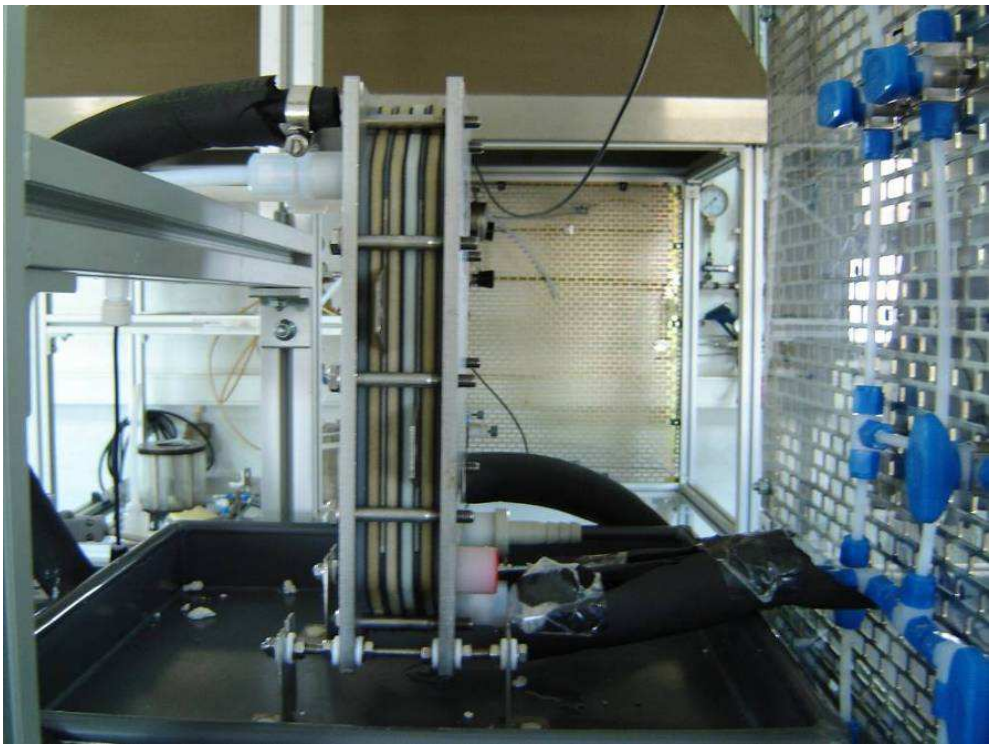

Figure 2.5 –View of the commercial laboratorial membrane cell.

The cell has a versatile design that allows several combinations of elements and flow patterns. Two types of electrodes were tested in the membrane cell: solid and mesh electrodes. The electrode-membrane gap was 6.0 mm for the solid electrodes and 2.75 mm for the mesh electrodes (Figure 2.6). A lower gap between electrodes allowed a significative reduction of the cell ohmic resistance and higher current densities were obtained for the same cell potential.

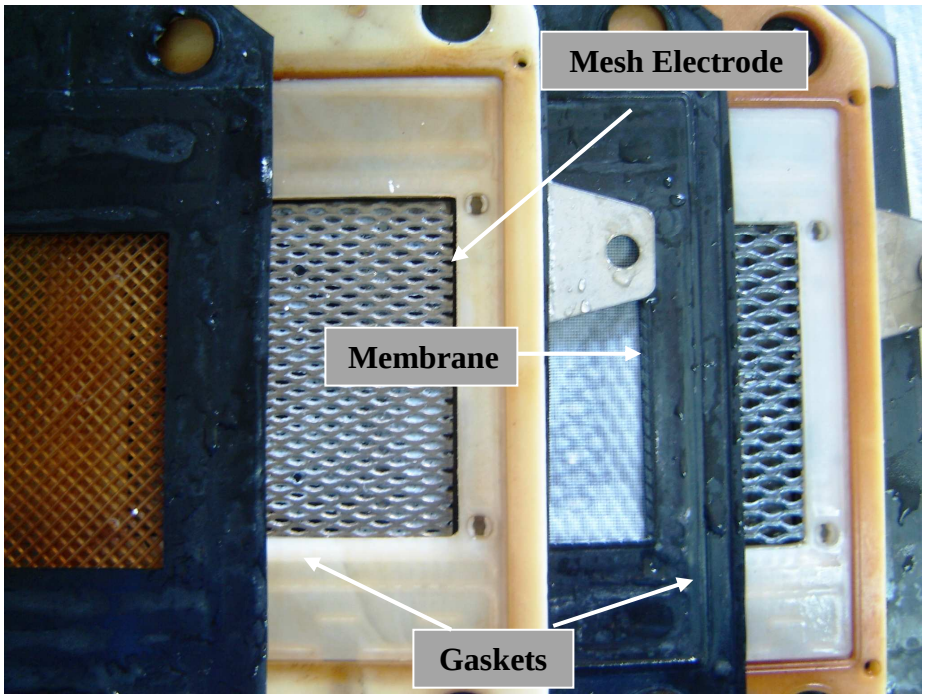

Figure 2.6 – View of the different components of the membrane cell using mesh electrodes.

Membranes with different characteristics and from different suppliers were used in this work. Membrane types A, B, C and D are defined as high performance membranes due to their low operating potential [18-20]. On the other hand, membrane types E and F are defined as high strength membranes. Table 2.2 shows the main characteristics of these membranes [18-20].

Table 2.2 – Characteristics of the membranes used.

Membrane	Cell potential	Tensile strength kg cm^{-1}	Manufacturer	Reinforcement
A*	-50 mV	4.5	A	Cloth with sacrificial fibers
B*	-50 mV	4.5	A	Cloth with sacrificial fibers
C*	-40 mV	6.3	A	Stronger cloth without sacrificial fibers
D**	2.95 V	4.0	B	Cloth with sacrificial fibers
E**	3.20 V	7.5	B	Cloth without sacrificial fibers
F**	3.23 V	7.5	B	Cloth without sacrificial fibers

*Conditions: The cell potential is compared with a reference membrane at 4 kA m^{-2} [19-21].

** Conditions: 0 mm gap, DSA anode, Activated cathode, 32 wt.% NaOH, 200 g L^{-1} anolyte, 90 ºC, 4 kA m^{-2} [19-21].

Type B membrane has the same structure as type A but it has a new carboxylic polymer that makes the membrane more resistant against impurities and operating upsets (i.e. blisters). Type C membrane is made from the same polymer as type B but it is reinforced with a stronger cloth without sacrificial fibers. This way, type C membrane has higher mechanical strength and also higher potential than type A. Type D and F membranes have the same type of reinforcement but they are made from a different type

of polymer. The polymer used for in type E and D membranes is the some whereas an improved reinforcement structure is used for type E [18-20].

Feeding and temperature control system

Two tanks (R_1 and R_2) are used to store the electrolytic solutions to be fed to the cell; NaCl is fed from tank R_1, whereas NaOH from tank R_2. The electrolytes that are fed to the membrane cell should have high purity to avoid precipitation in the membrane inner structure. The recommended amount of impurities in the feed brine given by the membrane suppliers is shown in appendix B The electrolytes are made circulating in separate hydraulic circuits by a double-headed peristaltic pump (Watson Marlow 323 S) (P_1 and P_2). The feed flow rates ranged from 50 to 250 mL min^{-1} corresponding to flow velocities in the cell from 5 to 25 mm min^{-1}. A tracer experiment showed that within this velocity range there is a uniform concentration distribution of the electrolyte solutions over the membrane surface.

The operating temperature has a great impact on the cell potential and so the temperature control is an important issue. The inlet and outlet temperatures are monitored by four thermocouples (T_1, T_2, T_3, T_4) that are connected to a data acquisition board. To keep the cell warm, a thermostatic bath (Huber model CC1) was used for circulating hot water in the outer

compartments of the cell. Beyond that, the electrolytes were heated up to 90 ºC by means of two shell and tube heat exchangers (Figure 2.7). As the electrolytes used are aggressive to the common construction materials, the sodium chloride heat exchanger was made of titanium and the sodium hydroxide heat exchanger was made of nickel tubes. The electrolytes inlet and outlet headers of the heat exchangers were made of PTFE. The shell side of the heat exchanger has baffles to promote the flow through the shell and minimize dead volumes. Hot water was circulated through the shell side from a thermostatic bath (HAAKE model HK-P1-W26).

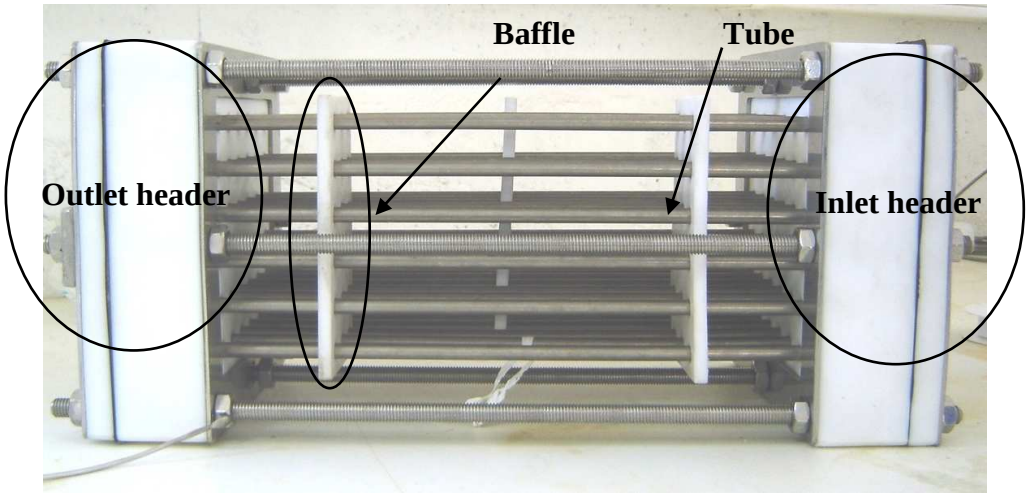

Figure 2.7 – Shell and tube heat exchanger used for heating the electrolyte solutions.

At room temperature there is air dissolved in the solutions that is released after heating up. Two air traps (A_1 and A_2) were then used to remove bubbles from the solutions before the inlet of the membrane cell – Figure 2.8.

Figure 2.8 – Air trap placed before the membrane cell inlet.

Outlet system

The chlorine gas coming out from the anode chamber was saturated with water vapour at 80-90 ºC. The chlorine gas produced was separated from the anolyte solution in a gas-liquid separator unit (S_1) (Figure 2.9) and dehydrated with the help of a cooling column working at around 15 °C (R_3),

and the flowrate measured using a rotameter (with Teflon body and glass float) (F_1). Dehydration of the chlorine is very important to avoid condensation and flow blockage at the rotameter. The chlorine gas produced was then absorbed in a 6.6 M sodium hydroxide solution (R_4); this concentration avoids NaCl precipitation. For safety reasons this tank (R_4) was connected to a second tank (R_5) containing also a 6.6 M sodium hydroxide solution.

Figure 2.9 – Gas-liquid separator.

Similarly to the anolyte, the hydrogen produced in the cathode chamber was saturated with water vapor at 80 - 90 ºC and was separated from the sodium hydroxide in a gas-liquid separator (S_2). The sodium hydroxide solution went to the waste container (R_8) while the hydrogen was cooled in a jacketed stainless-steel column (R_6). A flowmeter (F_2) (Bronkhorst Hi-Tec F-101, 1 L min^{-1}, ±1 % full scale) was used to measure the hydrogen flow rate that was then vented to the atmosphere.

Power supply and data acquisition system

A power supply from SwitchKraft with a maximum output of 6V / 100 A DC was used. The electrochemical characterization of the membrane reactor was made using an electrochemical workstation from Zanher Elektrik with a frequency range from 10 μHz to 3 MHz (IM6ex) with a power potentiostat with a maximum output of ± 5 V / ± 40 A from Zanher Elektrik (PP240).

The experimental setup was controlled using a computer equipped with an acquisition board. A Labview program was developed to control and monitor the inlet and outlet temperatures, the hydrogen flow rate, the current applied to the cell and the potential output.

2.4. Assessment of the Chlor-alkali Membrane cell unit

Membranes should be handled carefully to prevent physical damage (punctures, creases or scratches) [18]. Prior to assemble a membrane in the electrochemical cell, it must be pre-conditioned to prevent improper membrane dimensional changes during start-up that can lead to physical damages (wrinkling or stretching). The membrane dimensional changes are related to the membrane properties, water content (hydration), temperature and composition of the contacting solutions [1, 18]. Due to osmotic effects, the equilibrium between the membrane and the electrolyte solutions is greatly affected by the electrolyte solutions concentration. The swelling of a membrane not only affects its dimensional stability but also its mechanical properties, ionic selectivity and conductivity [1, 18]. The membrane hydration changes during the start-up of the membrane cell due to temperature and electrolyte concentration changes. To avoid the formation of membrane wrinkles that can cause tentering during operation, a proper membrane pre-treatment must be done. As the carboxylic layer sorbs less water than the sulfonic layer [1, 18], the sodium hydroxide concentration affects more the membrane water content than the sodium chloride solution. This way, the sodium hydroxide concentration has a more pronounced effect on the degree of membrane hydration and consequently on the dimensions of the membrane.

Several tests were performed at different sodium hydroxide concentrations and temperatures to evaluate the dimensional changes of the membranes. The membrane swells with temperature (thermal expansion) and contracts with electrolyte concentration (the hydration level of the membrane decreases).

Figure 2.10 shows schematically the dimensional changes that should occur during the start-up of the experimental membrane cell when equipped with type A membrane, obtained experimentally ex-situ.

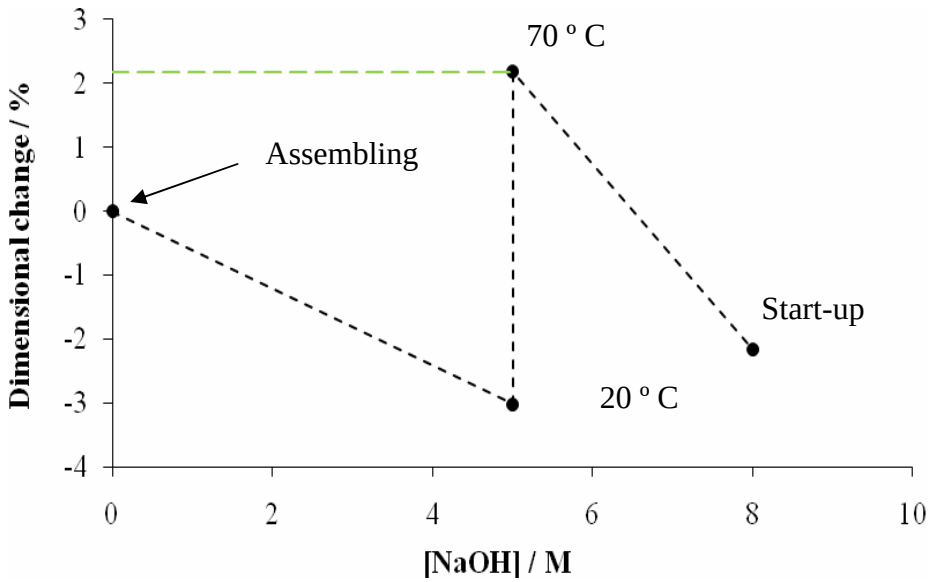

Figure 2.10 – *Ex-situ* membrane dimensional changes during the start-up of a membrane cell for type A membrane.

Figure 2.10 shows that the membrane should contract around 3 % when the electrolyte is fed to the cell and should expand 5 % due to the temperature

rise. Membrane wrinkling occurs if the membrane expands more than the initial dimensions (assembling dimensions). Thus, to prevent wrinkling the membrane must be expanded prior to be assembled to compensate the start-up thermal expansion. The membrane should be pre-conditioned in contact with a 0.5 M solution of sodium hydroxide for at least 4 hours. The membrane must be assembled flat in the cell and with the correct face orientation (i.e. with the cathode side facing the cathode). The complete membrane cell assembling procedure and operation is complex and it is described in appendix C

As one of the main objectives of this work was to develop an experimental setup to contribute to optimize the operation of an industrial plant, some tests were performed to validate the results obtained in the experimental setup and compared to the corresponding ones found in the literature. For that, the profile of the most relevant variables was assessed: temperature, hydrogen flow rate and the relationship between current and potential (polarization curves). The temperature profile has a great impact on the cell potential mainly because the electrolyte conductivity increases with temperature rise. However, at temperatures higher than 90 ºC the amount of water vapor increases tremendously and the membrane stability decreases. It is usually recommended to operate in the range 80 - 90 ºC. The anolyte and catholyte temperatures must be similar in both compartments to avoid

thermal shocks on the membrane. An example of the outlet temperature history (anolyte and catholyte) obtained for this setup is shown in Figure 2.11.

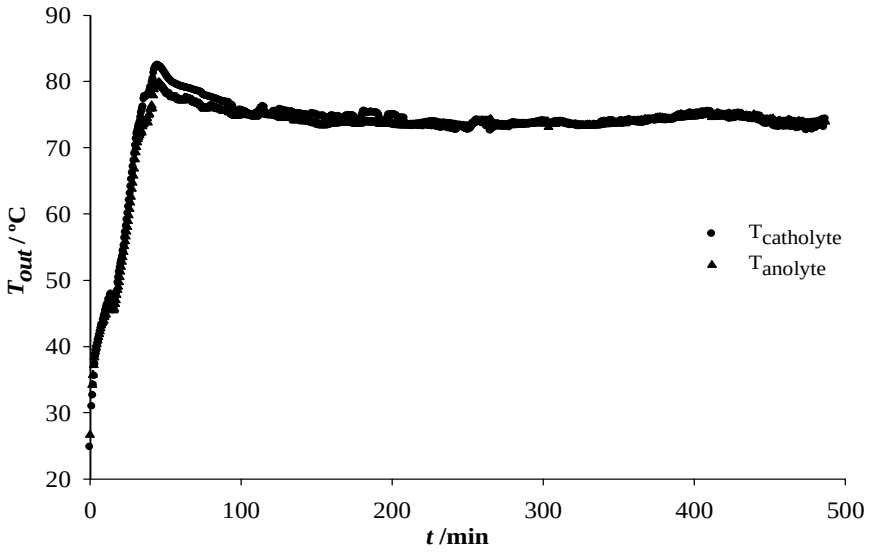

Figure 2.11 – Outlet (anolyte and catholyte) temperature history.

As shown in Figure 2.11, the desired temperature profile was achieved and the anolyte and catholyte temperatures are close to each other.

The hydrogen gas flowrate as a function of current density is shown in Figure 2.12. For reference, it is also shown the thermodynamic hydrogen flow rate.

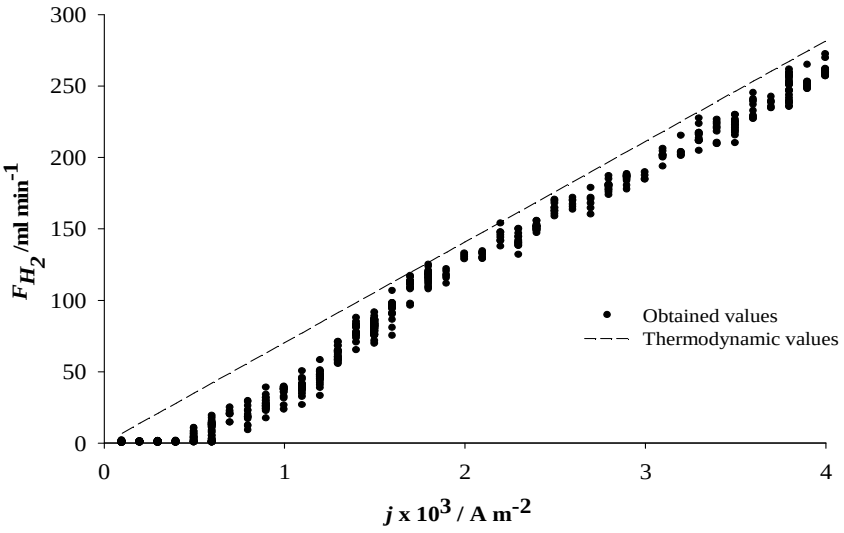

Figure 2.12 – Hydrogen gas flow rate as a function of current density; the thermodynamic hydrogen flow rate based on the applied current was added as a reference.

Figure 2.12 shows some hydrogen gas flow rate variations that must be related to pressure fluctuations. The hydrogen current efficiency can be determined from the ratio of the obtained values by the thermodynamic values calculated from the Faraday's law of electrolysis. The obtained current efficiency is around 90 % for higher current densities. However, higher values were expected. The differences between the obtained hydrogen flow rate and the thermodynamic values should be related to the hydrogen flowrate measuring system. This system was made by a hot-wire mass flow meter (Bronkhorst Hi-Tec F-101, see section 2.2) that uses the heat

conductivity of fluids to determine mass flow. This makes the hydrogen gas flow rate very sensitive to humidity and other contaminants.

Finally, to evaluate the overall performance of the membrane cell, polarization curves for three different membranes were obtained, Figure 2.13.

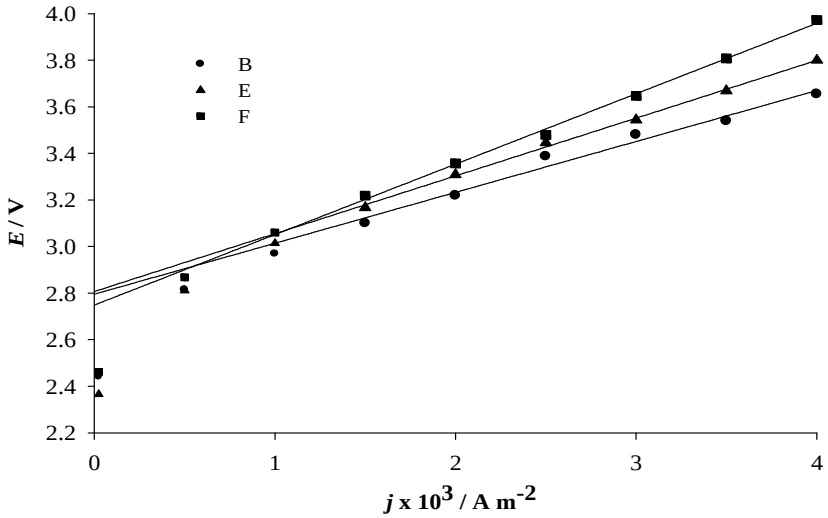

Figure 2.13 – Polarization curves for type B, E and F membranes.

Two regions can be distinguished in Figure 2.13; a logarithmic and a linear region. A curvilinear part of the polarization curve is observed in the lower current density region where the electrode kinetics is dominant whereas a linear region is observed over the current density range of 1.5 - 5 kA m^{-2} where the so called *k-factor* method applies. The *k-factor* method is widely used in the chlor-alkali industry to characterize the overall performance of

the process. The relationship between potential and current density is given by:

$$E = k \times j + E_0 \quad (2.3)$$

where k is associated to ohmic resistances and E_0 is related to the electrode overpotential [19]. Equation (2.3) was fitted to the linear region of the polarization curves of type B, E and F membranes (Figure 2.13) and the slope (k) and interception (E_0) values obtained are shown in Table 2.3.

Table 2.3 – Slope (k) and interception (E_0) of the polarization curve, and corrected slope for zero gap cell and reference values from the suppliers, for type B, E and F membranes.

Membrane Type	k **V kA^{-1} m^2**	E_0 **V**	$k_{corrected}$ **V kA^{-1} m^2**	$k_{suppliers}$ **V kA^{-1} m^2**
F8020	0.191	2.765	0.132	0.130
NE-2100	0.256	2.659	0.197	0.210
N2020	0.282	2.712	0.224	0.220

The slope of the polarization curves (k) obtained are higher than the values given by the suppliers due to the higher membrane-electrode gap (2.75 mm) of the experiemental setup. As a rule, the reported values are obtained for a zero gap cell. To estimate the slope of the polarization curve that would be obtained in a zero gap cell ($k_{\text{corrected}}$) the electrolytes resistance should be

subtracted. The corrected values of *k* for zero gap are in agreement with the values given by the suppliers – Table 2.3, and with the ones found in the industrial plant at CUF-QI.

The interception values of the polarization curves given in Table 2.3 are in agreement with the expected ones found in the literature for a nickel cathode and a DSA® anode [18]. Additionally, comparing the slope *k* it can be observed that type B membrane performes better (lower slope) than type E and F membranes. This was expected since type B membrane is high performance while type E and F are high strenght membranes, as shown in Table 2.2.

The ion exchange membrane is a key component in the electrolysis membrane cell as it normally determines the energy consumption of the process. This way, the membrane conductivity measurement is of great importance. The true ohmic resistance of the membrane cell can be obtained by electrochemical impedance spectrosocopy (EIS) at high frequency. The membrane resistance can then be obtained by substracting the electrolytes resistance, Table 2.4. The membrane conductivity (σ_m) is then computed using the following equation [1-3]:

$$\sigma_m = \frac{\ell}{R_{ohm} A} \tag{2.4}$$

where ℓ is the membrane thickeness, R_{ohm} is the ohmic resistance and A the effective area of the membrane.

Table 2.4 – Ohmic resistance of the membrane cell and conductivity of type B, E and F membranes.

Membrane Type	R_{ohm} **Ω cm^2**	σ_m **S cm^{-1}**
B	2.37	0.043
E	2.64	0.029
F	3.05	0.02

The values obtained are in agreement with the ones found in the literature [1, 3]. Table 2.4 shows that the membrane with the highest conductivity is type B membrane and the one with the lowest conductivity is type F. This is in agreement with the data given by the suppliers, Table 2.2, where type F is the most robust membrane (highest strength).

The experimental setup allows the simulation of common problems occurring in industrial plants. As an example, it was possible to reproduce the formation of blistered membranes in the experimental setup. The de-lamination (separation) between sulfonic and carboxylic layers is denominated blistering, Figures 2.14 and 2.15. Blistering is a form of mechanical damage of the membrane, commonly occurred in the chlor-alkali industry, that can ultimately lead to a performance decline and/or to the

formation of holes in the membrane which reduce its selectivity and allows hydrogen and chlorine to mix, which is potentially dangerous.

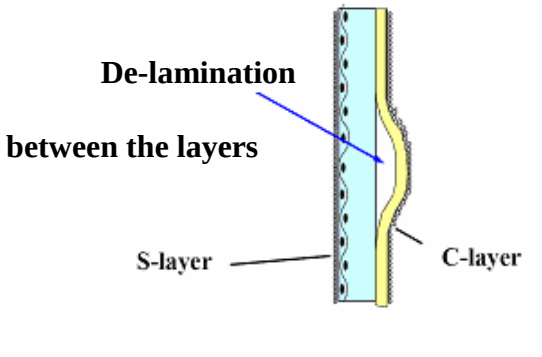

Figure 2.14 – Blister schematic representation (adapted from [21]).

Figure 2.15 – View of a blistered membrane.

There are many reasons that can lead to formation of blisters in the membrane such as reverse water transport during shutdown, too low temperature, too high caustic or brine concentration, excessive local current density, backward installation of the membrane, impurities precipitation and so on [17]. It was possible to reproduce in the lab the formation of blisters in the membrane. The interruption of brine feed flow before the start-up, cause the brine concentration to increase resulting in salt precipitation inside the membrane. When the feed flow is re-established and the temperature increases the salt dissolves creating voids that became filled with water. When the cell is heated from room temperature to the operating temperature, the partial pressure of the water vapour increases originating blisters. The tie-up of exchange sites increases the membrane resistance as it can be seen in Figure 2.16. These are results obtained with the developed experimental setup. The ohmic resistance of the cell is constant during the start-up (< 1.5 kA m^{-2}) increasing afterwards. The electrical resistance increases at the blisters spots causing the current density to increase at the other locations and then accelerating the degradation of the whole membrane.

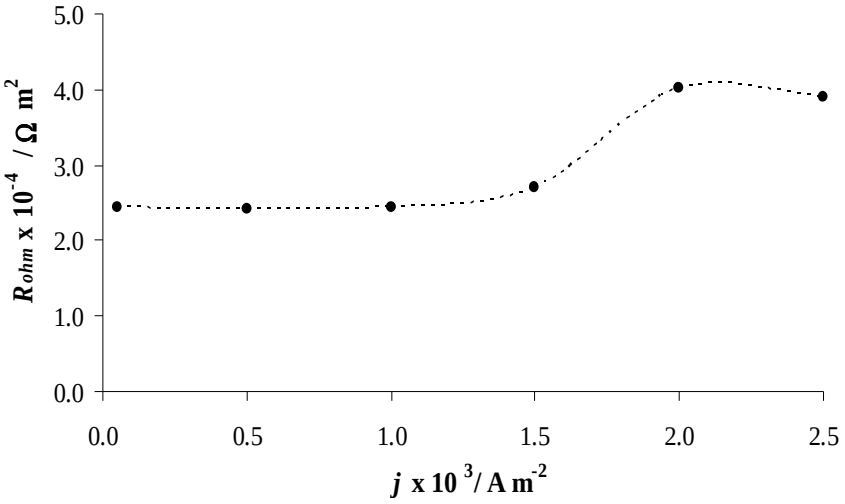

Figure 2.16 – Cell ohmic resistance (R_{ohm}) as a function of current density.

The polarization curve of a blistered membrane was compared with one without blisters, Figure 2.17.

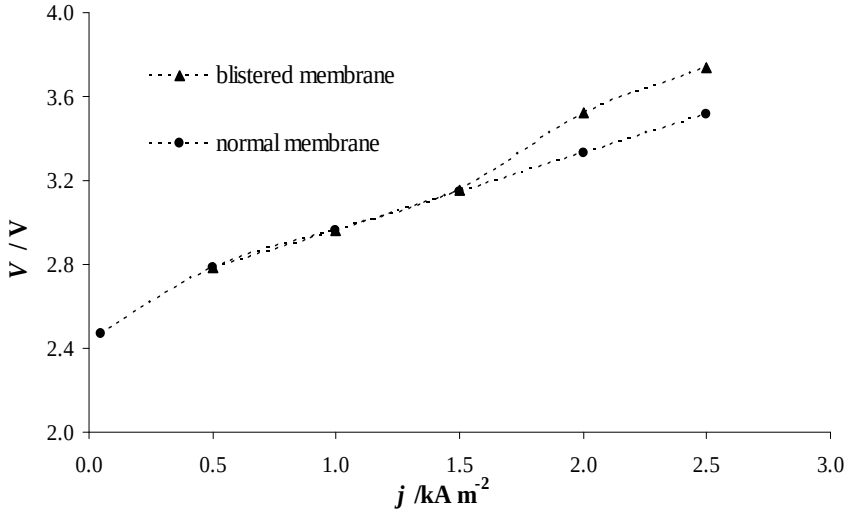

Figure 2.17 – Polarization curve for membranes with and without blisters - lines were introduced to improve readibility.

An abrupt potential rise at 2.0 kA m^{-2} is observed in Figure 2.17.

2.5. Conclusions

Two experimental setups were developed and tested: an experimental setup to measure the membrane permselectivity and a chlor-alkali membrane cell setup (electrochemical membrane reactor). The results obtained with the former experimental setup were compared to the ones obtained in a well-known laboratory. It was found good agreement between these results.

A detailed description of the chlor-alkali membrane cell setup was presented. The membrane dimensional changes between assembling and start-up were investigated and it was concluded that prior to installation the membrane must be pre-treated to prevent the formation of wrinkles.

The performance of the experimental setup was assessed by comparing some critical parameters (cell temperature, hydrogen gas flow rate, current-density potential curve and membrane conductivity) with reference values given by the suppliers. It was concluded that the temperature in both anode and cathode chambers can be controlled accurately. The hydrogen flow rate read was below the expected value. This should be related to the presence of contaminants in the hydrogen stream. This malfunction should be addressed and solved in a near future. The current-density potential curve parameters (k and E_0) showed to be in agreement with the values given by the suppliers and

with the ones obtained in the industrial plant. The membrane conductivities were also in agreement with the literature values.

It was possible to reproduce one of the most important damages occurring in the chlor-alkali industry – the membrane blistering. The presence of blisters on the membrane structure causes the ohmic resistance to increase.

2.6. References

[1] – H. Strathmann, in *Ion-Exchange Membrane Separation Processes*, Chapter 3, Membrane Science and Technology Series, 9, Hungary (2004).

[2] – J. Krol, *Monopolar and Bipolar Ion Exchange Membranes- Mass Transport Limitations*, PhD thesis, University of Twente, Netherlands, 1997.

[3] – T. Sata, *in Ion Exchange Membranes – preparation, characterization, modification and application*, RS•C, United Kingdom (2004).

[4] – R. Nagarale, G. Gohil and V. Shahi, *Advances in Colloid and Interface Science*, **119**, 97 (2006).

[5] – H. Yeager, B. O'Dell and Z. Twardowski, *J. Electrochem. Soc.*, **129**, 85 (1982).

[6] – A. Adam, Gronowski and H. Yeager, *J. Electrochem. Soc.*, **138**, No. 9, (1991).

[7] – S.Sang, H. Huang and Q. Wu, *Colloids and Surfaces A: Physicochem. Eng. Aspects* **315**, 98 (2008).

[8] – H. Yeager and B. Kipling, *J. Electrochem. Soc.*, **127**, No. 2, (1980).

[9] – T. Mirzazadeh, F. Mohammadi, M. Soltanieh and E. Joudaki, *Chem. Eng. J.*, **140**, 157 (2008).

[10] – A.A. Jalali, F. Mohammadi and S.N. Ashrafizadeh, *Desalination*, **237** 126 (2009).

[11] – N.S. Kaveh, F. Mohammadi and S.N. Ashrafizadeh, *Chem. Eng. J.*, **147**, 161 (2009).

[12] – A.C. Dias, M. J. Pereira, L. Brandão, P. Araújo, A. Mendes, *J. Electrochem. Soc.*, **157** (5), E75 (2010).

[13] –Y. Ogata, H. Hori, M. Yasuda, and F. Hine, *J. Electrochem. Soc.*, **135** (1), 76-83 (1988).

[14] – N. Krstajic, M. Popovic, B. Grgur, M. Vojnovic, D. Sepa, *J. Electroanal. Chem.*, **512,** 16-26 (2001).

[15] – C. Hitz, A. Lasia, *J. Electroanal. Chem.*, **500**, 213-222 (2001).

[16] – F. Hine, M. Yasuda and T. Yoshida, *J. Electrochem. Soc.*, **124** (4), 500 (1977).

[17] – Z.Yi, C. Kangning, W. Wei, J. Wang and S. Lee, *Ceramics International*, **33**, 1087(2007).

[18] – T. F. O'Brien, T.V. Bommaraju and F.Hine, in *Handbook of Chlor-Alkali Technology – Volume I*, chapter 4, Springer, New York (2005).

[19] – R. Theobald, Paper presented at the Eltech Seminar, October, Cleveland, Ohio (2000).

[20] – Technical information, Introduction of Flemion Membranes, Asahi Glass Co., Ltd (Flemion Seminar 2002).

[21] – "Characteristics of Flemion Membrane (2) Membrane Durability (Wrinkle, Blister)", Technical information Flemion Seminar, Asahi Glass Co., Ltd (2002).

[22] – "Prevention of blisters in Chloralkali membranes", Technical Information Bulletin 91-09, DuPont Company.

Appendix A

Membrane characterization

Ion exchange capacity

The ion exchange capacity of a membrane is a measure of the number of fixed charges per unit weight of dry polymer. The ion exchange capacity is determined by titration of the exchanged ions in the membrane. Firstly, the ion exchange membranes are equilibrated in a 1 M HCl solution for 24 hours to bring the membrane to the proton form (H^+). Then the membranes are rinsed with deionized water to remove the sorbed acid and immersed in a 2 M NaCl solution to exchange the protons with the sodium ions. This procedure is repeated two more times to guarantee the complete exchange of ions. Finally, the resulting solutions are titrated with a 1 M NaOH solution. The ion exchange capacity (IEC) can then be computed by:

$$IEC = \frac{a \times b}{W_{dry}} \tag{A1}$$

where *a* is the burette reading of base, *b* the concentration of base and *w* is the weight of the dried membrane. The ion exchange capacity is usually expressed in mili-moles per gram of dry membrane as the fixed charges of these membranes are monovalent. The ion-exchange capacity of ion exchange membranes ranges between 1 and 3 mmol g^{-1} [1]. The experimental data considers a uniform distribution of the ions through the polymer matrix.

The obtained values are between 0.01 and 0.04 mmol g^{-1} that are two small compared with the ones found in the literature [1].

References

[1] - H. Strathmann, in *Ion-Exchange Membrane Separation Processes*, Chapter 3, Membrane Science and Technology Series, 9, Hungary (2004).

Appendix B

Electrolytes specifications

Table B1 – Specifications of the sodium chloride solutions.

pH	NaCl ($g\ L^{-1}$)	$NaClO_3$ ($g\ L^{-1}$)	Fe ($mg\ L^{-1}$)	SO_4^{2-} ($g\ L^{-1}$)	Mg ppb	Ca ppb	Sr ppb	Ba ppb	Al ppb	Mn ppb	Ni ppb	SiO_2 ppm
10	290-310	<14	< 0.4	< 6	< 3	<5	< 1	< 2	< 69	< 20	< 65	< 5

Table B2 – Specifications of the sodium hydroxide solutions.

NaOH (wt.%)	Fe (ppb)
29-31	< 0.12

Appendix C

Experimental procedure

To preserve the physical, mechanical and chemical integrity of the membrane, the operating conditions must be kept within the specified range. Three operating stages can be defined for the chlor-alkali membrane cell, namely start-up, normal operation and shutdown. In each of these stages the electrolytes concentration and temperature must be adjusted according to the diagram presented in Figure C1.

After the assembly of the cell, the electrolytes are fed to the cell and the temperature is increased slowly at the same rate for both compartments to avoid thermal shocks on the membranes. As the outlet temperature reaches 50 ºC, a constant potential of 2.2 V can be applied to the cell (potentiostatic mode) until the equilibrium is attained, which normally happens after 30 min. A minimum temperature of 75 ºC is required to start increasing the current. Anolyte pH must be measured during the start-up to check for membrane damage (excess alkalinity) that can lead to anode coating damage and to the mixture of hydrogen and chlorine that is potentially hazardous. The operating conditions such as temperature, catholyte and anolyte concentration and current density must be adjusted according to the diagram shown in Figure C1.

The current density-potential curves are obtained under galvanostatic mode at normal operating conditions; a given current is applied and the potential response measured. The current is increased by 1 A steps and kept constant in each step for at least 5 min allowing the steady state to be attained. An outlet temperature between 80 - 90 ºC is desirable during normal operation.

For the cell shutdown the current is reduced step by step until it reaches a current lower than 1 kA m^{-2}. At this point, a potential of 2.2 V must be applied to the cell to prevent the galvanic corrosion of the electrodes (reverse current flow). A large amount of chlorine-based chemical species (chlorine gas, chlorate and hypochlorous acid) are available for reduction at the anode while hydrogen gas is available for oxidation at the cathode. Due to a higher solubility of chlorine gas in the anolyte in comparison to hydrogen gas in the catholyte, after the hydrogen gas is depleted due to oxidation, the chlorine reduction continues with a corresponding oxidation (corrosion) of the cathode coating. The chemical species that result from the corrosion of the electrodes may precipitate in the membrane surface and cause damage. This way, the chlorine species must be removed from the cell by the continuous flow of the electrolytes. Furthermore, this procedure is also important to keep the membrane immobilized in the proper position avoiding membrane damage. To decrease the diffusion rate of the species evolved in

the electrolysis from the anolyte to the catholyte, the cell temperature should be reduced. When the temperature reaches 40 ºC, the feed pumps can be stopped and the potentiostat turned off. The cell can then be drained and flushed with nitrogen to purge the chlorine gas to the absorption vessel (R_4 and R_5) and the hydrogen gas to the atmosphere. Distillated water is fed to both compartments to maintain the membrane wet and flat.

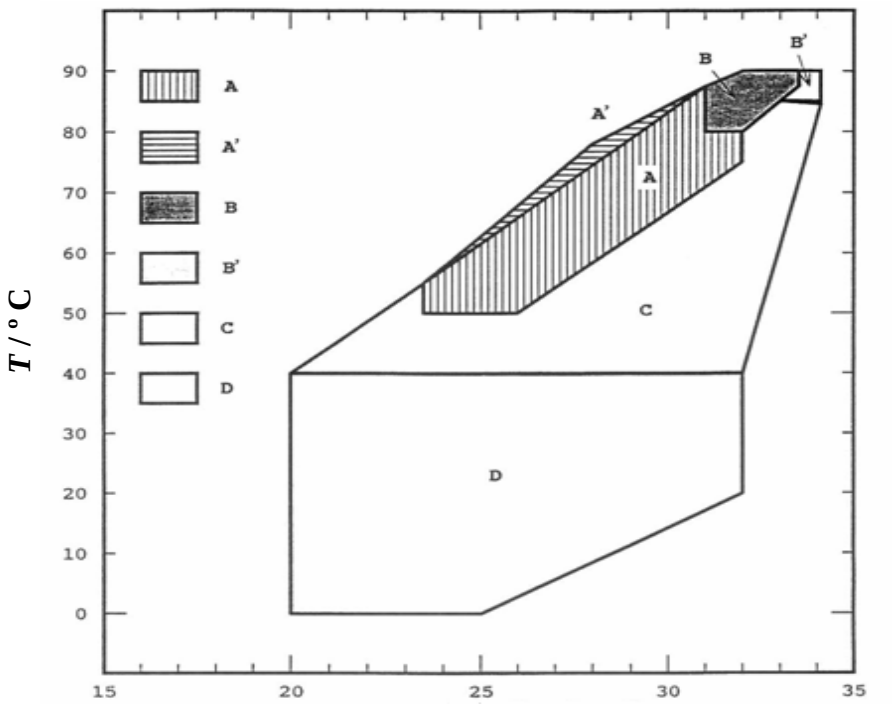

Figure C1 – Specified range of operating temperature and catholyte concentration to keep in each operating stage: A and A' are conditions for start up and transient condition (for a short period of time), respectively; B is the condition for normal operation (3-5 kA m^{-2}); C is the allowable condition for a short term after shutdown and D is the condition for a long term shutdown (>24 h) (adapted from [1]).

References

[1] - T. F. O'Brien, T.V. Bommaraju and F.Hine, in *Handbook of Chlor-Alkali Technology* – Springer, New York (2005).

Chapter 3 - Characterization of the Chlor-Alkali Membrane Process by EIS. Part I- Ohmic resistance[1]

3.1. Abstract

The effect of the operating parameters current density, feed flow rate, brine and caustic concentrations and temperature of a laboratory-scale chlor-alkali membrane cell on its overall performance (power consumption) was studied. Electrochemical impedance spectroscopy (EIS) was used to evaluate *in situ* the ohmic resistances of electrolytes and membrane. The cell temperature and the brine concentration were the most important variables on the cell voltage. The gas bubble evolution had a great effect on the ohmic resistance, especially at the anode side, where the gas void fraction was about 10 %.

---

[1] A.C. Dias, M. J. Pereira, L. Brandão, P. Araújo, A. Mendes, "Characterization of the chlor-alkali membrane process by EIS Part I- Ohmic resistance", *J. Electrochem. Soc*, **157** (5), E75 (2010).

3.2. Introduction

The chlor-alkali process is an electrochemical process that produces chlorine, hydrogen, and caustic soda by the electrolysis of a brine solution. Chlorine is a key raw material in the chemical industry for the production of polymers as particularly poly(vinyl chloride), polyurethanes, and polycarbonate, and as an intermediate in other chemical, pharmaceutical (85 % of medicines use chlorine), and crop protection industries [1]. A recent study reports a yearly production of 62.8 million metric tons worldwide in 2008, where Europe production represents 20 % [2].

The conventional cation-exchange membrane used in the membrane cell process is composed of a thick layer of tetrafluoroethylene functionalized with sulfonic groups at the anode side and a thinner layer of tetrafluoroethylene functionalized with carboxylic groups at the cathode side [3-6]. The sulfonic acid group is an excellent proton conductor. The carboxylic group has a high selectivity to the cations, rejecting the anions (e.g., hydroxyl ions). However, this carboxylic layer shows a lower proton conductivity [5, 6].

The commonly used anode is made of titanium coated with oxides of titanium, ruthenium, and iridium. Moreover, these titanium-ruthenium-iridium oxide anodes exhibit a very high electrocatalytic activity and selectivity towards the anodic chlorine reaction. They are usually termed

dimensionally stable anodes (DSA®) [7] because of their high stability and resistance to degradation. The cathode is normally made of nickel.

Notwithstanding the improvements, there are still some drawbacks in the membrane cell process related to membrane damage due to a variety of reasons, such as (*i*) tears, pinholes, blisters and brine impurity precipitation; (*ii*) electrode deactivation caused by deposition of impurities at the surface, shutdowns and oxygen generation; (*iii*) gas bubble accumulation in the electrolyte and electrodes [8-15]. The presence of dispersed gas bubbles in the electrolyte can have a strong effect on the ionic conductivity of the electrolyte solutions. Moreover, gas bubbles can cover the electrode surface and reduce the active surface area of the electrodes and affect the current and concentration distribution inside the cell [13-16].

Despite being a well-known technology, the reported studies on this subject are rather scarce. The impact of the different operating variables on the performance of the membrane (current efficiency and voltage) was assessed experimentally using black box approaches [17-20]. In turn, the effects of brine impurity precipitation [8-9], and the problems related with membrane cell operation [11, 17-20] were also reported. These studies addressed the importance of high purity brine feed to achieve a longer membrane life.

The overall performance of the chlor-alkali system is usually carried out by performing polarization curves (*I* vs. *E*). To accurately differentiate each component of the cell, electrochemical impedance spectroscopy (EIS) is used. EIS analysis is based on the system's response to a sinusoidal voltage perturbation monitoring the current response (a sinusoidal current perturbation can be used instead). By analyzing the sinusoidal response of the system at several frequencies, the different cell elements can be studied, namely (*i*) the electrochemical reactions at metal/solution interface (electrochemical kinetic reaction mechanism), (*ii*) the resistance to the ionic transport through the membrane and through the electrolyte (ohmic resistances), and (*iii*) the limitations to the mass transport [21-23]. This way, the EIS gives much more insight into the process than the much simpler *I* vs. *E* curves. However, reports concerning the use of this powerful technique on the chlor-alkali process are very scarce, as concluded after a thorough search into major scientific databases. For instance, Antozzi et al. [24] reported the use of EIS for the characterization of the stability of different Pt based cathode electrodes. They concluded that these electrodes showed strong activity and good stability upon polarity inversion studies. Pilla et al. [12] studied different techniques to evaluate the catalytic activity and the residual service life of DSA® by EIS and cyclic voltammetry.

The present study addresses the influence of different operating variables on the cell performance, evaluated in terms of the different ohmic resistances obtained by EIS. Additionally, the optimum operating conditions for the system presented are discussed.

3.3. Experimental

3.3.1. Experimental setup

The scheme of the experimental setup used to characterize the chlor-alkali process is shown in Figure 3.1. The electrolysis cell (EC Electro MP-Cell, ElectroCell, Denmark) is divided into two compartments: the DSA® and the nickel cathode. The compartments are separated by an ion exchange membrane (Flemion 893, Asahi Glass Co.) with an effective area of 0.01 m^2 and 250 µm thickness. The electrode membrane gap for this cell configuration is 6 mm. Before assembling the cell the membrane was soaked in a 0.5 M NaOH solution for 4 h, to avoid dimension changes due to the increase in temperature and concentration. These changes could either cause membrane wrinkling or shrinking during start-up [4, 5].

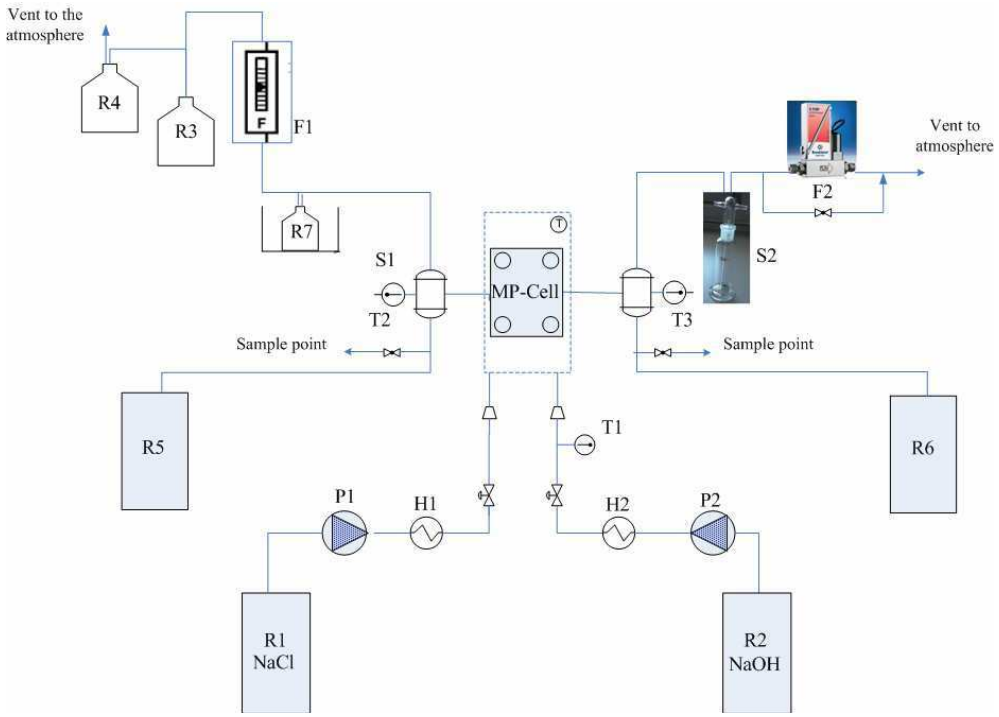

Figure 3.1 – Process flow diagram of the membrane cell setup used in this work: Membrane flow cell (MP Cell); electrolyte vessels (R1, R2); peristaltic pumps (P1, P2); heat exchanger (H1, H2); thermometer (T1); gas-liquid separators (S1, S2);rotameter (F1); flowmeter (F2); vessels for the Cl_2 gas absorption (R3, R4); gas-liquid separator (S1, S2).

The electrolytic solutions fed to the cell were stored in vessels (T1 and T2) and previously heated before entering the cell by using heat exchangers (H1 and H2). The operating cell temperature was monitored by four thermocouples inserted into the inlet and outlet of the anode and cathode. The electrolytes circulate in separate hydraulic circuits using peristaltic pumps

(P1 and P2), at flow rates that assure uniform concentration distribution inside the anode and cathode chambers. At the exit of both cell compartments the gaseous products were separated from the aqueous solutions (S1 and S2), dehydrated with the help of water traps and the fluxes measured using a rotameter in the anolyte circuit and a flowmeter (*Bronkhorst* Hi-Tec F-101, 1 L min^{-1}, ±1 % FS) [full scale (FS)] in the catholyte circuit. A data acquisition system based on Labview software was developed to control and monitor the experimental setup. The electrochemical characterization was made using an electrochemical workstation (*Zahner-elektrik*, IM6eX, PP-240).

3.3.2. Design of experiments

A response surface methodology was employed to obtain the operating conditions that minimize power consumption (output voltage), using the commercial software JMP 7.0 (SAS software). The design considered, for a current density of 1.5 kA m^{-2}, three levels and four factors: feed flow rate (Q), NaCl and NaOH electrolyte concentrations and the operating temperature (T_{out}).

The range of interest used to obtain the response surface is given in Table 3.1 and it was based on preliminary experimental results and on general recommendations of the chlor-alkali industry [4-6].

Table 3.1 – Range of the operating variables.

Operating variable	Lower limit	Upper limit
[NaCl] / g L^{-1}	210	300
[NaOH] / wt.%	26	30
T_{out} / ° C	60	80
Q / mL min^{-1}	40	180

The statistical method recommended performing 19 experiments shown in Table 3.2; every experimental value is the average of at least three runs.

3.3.3. Electrolyte conductivity

The resistance of the anolyte and catholyte were obtained independently by EIS using the laboratory cell without membrane at resting potential. The experiments were performed for brine solutions with concentrations ranging from 210 to 300 g L^{-1}, and for sodium hydroxide solutions ranging from 26 wt.% to 32 wt.%, at different temperatures and at a constant flow rate (50 mL min^{-1}).

Table 3.2 – Operating conditions of the experiments suggested by the design.

Run No.	[NaCl] g L^{-1}	[NaOH] wt.%	T_{out} ° C	Q mL min^{-1}
1	255	30	80	40
2	210	26	70	180
3	255	28	70	110
4	255	26	70	110
5	300	26	80	40
6	300	28	60	40
7	300	26	60	180
8	210	30	60	40
9	255	30	60	180
10	210	26	60	40
11	300	30	70	110
12	255	28	70	110
13	210	28	70	40
14	300	28	80	180
15	210	30	80	180
16	210	28	60	110
17	255	28	70	110
18	210	26	80	110
19	255	28	70	110

3.3.4. EIS analysis

The cell was operated for 30 min at a fixed voltage of 2.2 V. The load was increased by 1 A steps, allowing for the steady state to be reached on each step, which normally happens after 5 min.

To study the effect of each variable by EIS, the voltage and the EIS spectra were obtained for each step. The EIS spectra were recorded at ten

points per decade by superimposing a 10 mV AC signal over the frequency range from 100 kHz to 100 mHz. The overall ohmic resistance was obtained by the interception of the curve at high frequencies with the real axis in the Nyquist diagram [21]. Experimental measurements were performed according to the operating conditions shown in Table 3.3.

Additionally, the same procedure was applied at 65, 75 and 80 ° C ([NaCl] = 300 g L^{-1}; [NaOH] = 28 wt.% and Q = 150 mL min^{-1}) to investigate the effect of temperature on the overall ohmic resistance.

Table 3.3 – Operating conditions of the experiments performed and the results in terms of voltage, ohmic and membrane resistance and average gas void fraction (ϕ).

	No.	j kA m^{-2}	[NaOH] wt. %	[NaCl] g L^{-1}	T_{out} °C	Q mL min^{-1}	E V	R_{ohmic} Ω	$R_{membrane}$ Ω	ϕ
Flow rate	2	1.0	28	300	75	85	3.2220	0.0531	0.0094	0.0861
	3	1.0	28	300	75	110	3.2243	0.0531	0.0094	0.0861
	4	1.5	28	300	75	85	3.5351	0.0552	0.0094	0.1271
	5	1.5	28	300	75	110	3.5311	0.0546	0.0094	0.1159
	6	1.5	28	300	75	150	3.5219	0.0543	0.0094	0.1101
	7	2.0	28	300	75	110	3.8272	0.055	0.0094	0.1232
	8	2.0	28	300	75	150	3.8055	0.0549	0.0094	0.1216
Concentration	4	1.5	28	300	75	110	3.5311	0.0546	0.0094	0.1159
	9	1.5	28	255	75	110	3.5434	0.055	0.0076	0.1159
	10	1.5	28	210	75	110	3.5902	0.0569	0.0065	0.1159
	11	2.0	26	300	75	150	3.7974	0.055	0.0095	0.1216
	12	2.0	28	300	75	150	3.8055	0.0549	0.0094	0.1216
	13	2.0	30	300	75	150	3.8543	0.0567	0.0112	0.1216
	14	2.0	32	300	75	150	3.8942	0.0594	0.0139	0.1216

3.4. Results and discussion

3.4.1. Design of experiments

The experimental design allowed identifying the operating conditions that require minimum cell voltage. The current density was kept constant to simplify the analysis of the ohmic resistances as a function of temperature, feed flow rates and anolyte and catholyte concentrations.

The experimental voltage for the operating conditions given in Table 3.2 was fitted to a second order polynomial:

$$E = \beta_o + \sum_{i}^{4} \beta_i X_i + \sum_{i}^{4} \sum_{j \geq i}^{4} \beta_{ij} X_i X_j \qquad (3.1)$$

where E is the predicted voltage of the electrochemical cell; β_0 is a constant; β_i are the linear coefficients; β_{ii} is the squared coefficient; and with β_{ij} with $i \neq j$ are the cross-product coefficients. X_i are the operating variables considered: temperature, the electrolyte concentrations, and flow rates.

The model parameters were obtained by minimizing the sum of the square differences. An Analysis of Variance (ANOVA) of the model was performed [22]; the coefficient of determination obtained, R^2 = 0.9863, indicates that the model can explain most of the experimental variance. As shown in Figure 3.2, it can be concluded that the model fits quite well the experimental values.

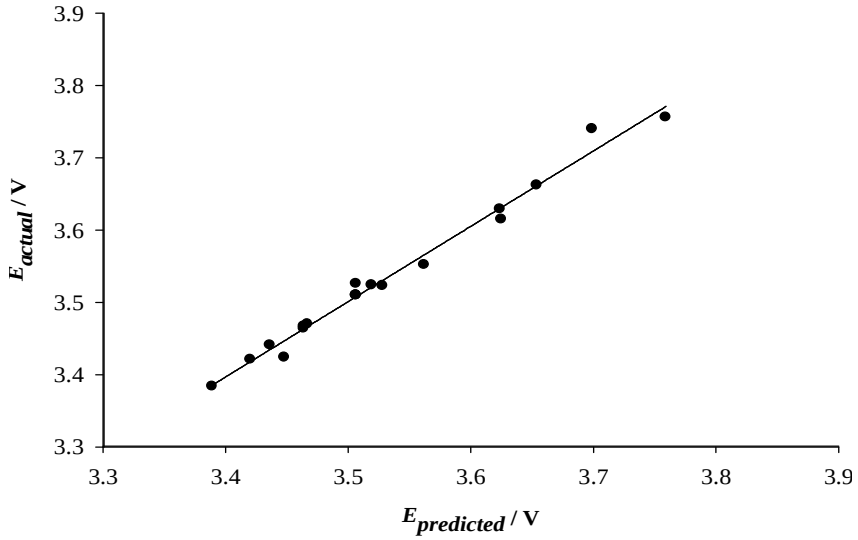

Figure 3.2– Comparison between predicted cell voltage and experimental results (R^2 = 0.9863) in terms of cell voltage.

The parameters should now be assessed for their contribution to the model; parameters with *p*-values smaller than 0.05 indicate that they have a significant effect on the response, [22] while parameters with *p*-values higher than 0.15 should be eliminated from the model. Parameters with *p*-values between 0.05 and 0.15 have a marginal effect on the response and they should be considered in a first stage, before the elimination of parameters with *p*-values higher than 0.15, and eliminated afterward [22]. The final fitting model obtained is:

$$E = 3.506 - 0.052 \cdot [\mathrm{NaCl}] + 0.038 \cdot [\mathrm{NaOH}] - 0.058 \cdot T_{out} - 0.025 \cdot Q - 0.088 \cdot [\mathrm{NaCl}]^2 + 0.036 \cdot [\mathrm{NaCl}] \cdot [\mathrm{NaOH}] - 0.021 \cdot [\mathrm{NaOH}]^2 + 0.010 \cdot [\mathrm{NaOH}] \cdot T_{out} + 0.092 \cdot T_{out}^2 - 0.057 \cdot T_{out} \cdot Q + 0.057 \cdot Q^2 \quad (3.2)$$

Figure 3.3 shows the predicted voltage of the cell for a current density of 1.5 kA m^{-2} as a function of the operating variables.

a)

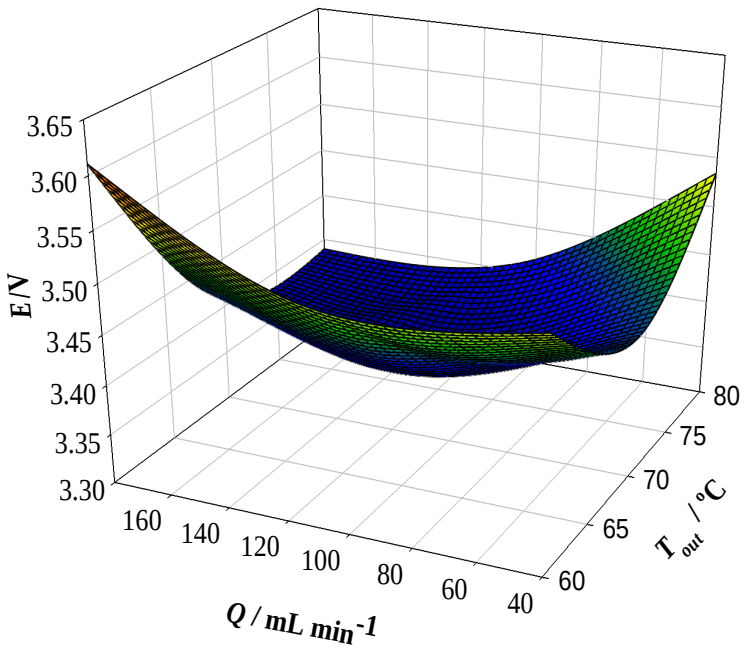

b)

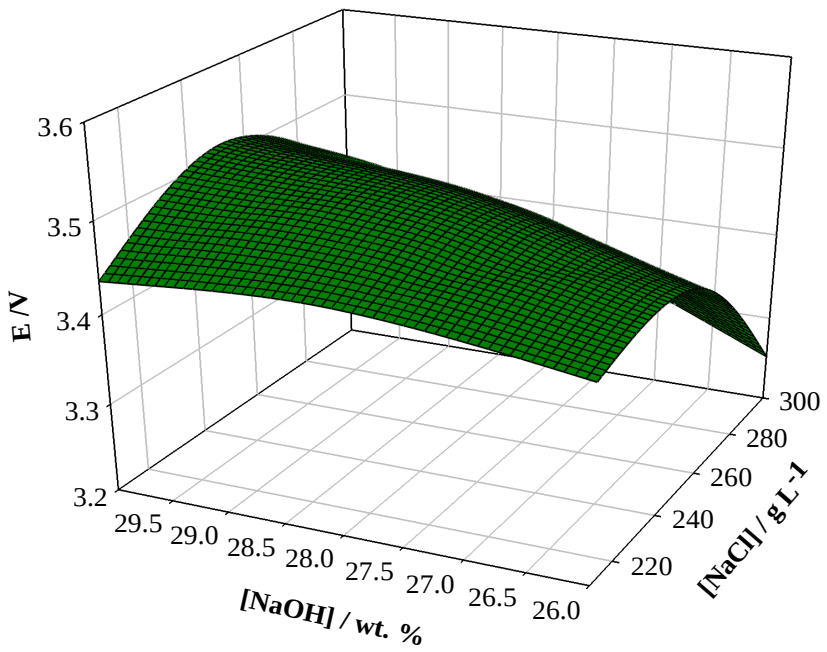

Figure 3.3 – Cell voltage at 1.5 kA m^{-2} and as a function of: a) feed flow rate and temperature of the cell; b) brine (anolyte) and sodium hydroxide (catholyte) concentrations.

From Figure 3.3 it can be concluded that the optimum cell voltage value is observed for higher feed flow rates (150 mL min^{-1}), higher sodium chloride concentrations (300 g L^{-1}), lower sodium hydroxide concentrations (26 wt.%) and higher temperatures (75 ° C). By increasing the feed flow rate the cell voltage decreases due to increasing gas removal from the cell. The gas bubble effect is of great concern in these systems because it affects the

electrical properties of the electrolyte and the membrane, and thus the cell performance [14-16]. The overall cell performance increases significantly as the brine concentration increases – Figure 3.3a shows a slight voltage increase for low anolyte concentrations that should be related to the uncertainty of the interpolating model. This is likely to be due to an increase in electrolyte conductivity. A lower sodium hydroxide concentration has a positive effect on the cell voltage. Presumably this is related with membrane dehydration and a decrease in electrolyte conductivity. Furthermore, the cell performance improved with temperature. This positive contribution should be related to internal kinetic processes, which are normally exponentially temperature dependent, and to the NaCl and NaOH conductivity increase.

3.4.2. Impact of different operating variables on cell ohmic resistance by using EIS

EIS experiments were performed to study separately the effect of each operating variable on electrolytes and membrane resistances. Figure 3.4 shows a typical Nyquist plot of the membrane cell system, obtained for a current density of 0.1 kA m^{-2}, [NaCl] = 300 g L^{-1}, [NaOH] = 28 wt.%, electrolyte flow rates of 150 mL min^{-1} and for T = 75 ° C.

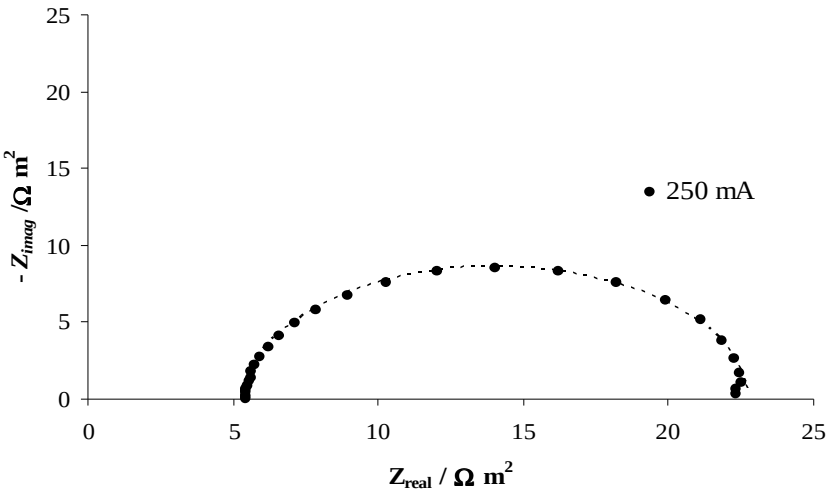

Figure 3.4 - Impedance spectra (Nyquist plot) of the membrane cell.

Bubble effect

The presence of gas bubbles formed at the electrodes' surface, inside the electrolyte chambers, can highly affect the electrolyte resistance [13-15]. The ohmic resistance should be constant for the same electrolyte concentration and temperature, according to Ohm's law [23]. Figure 3.5 shows the overall ohmic resistance (obtained by EIS) as function of the current density from experiments performed at constant operating conditions.

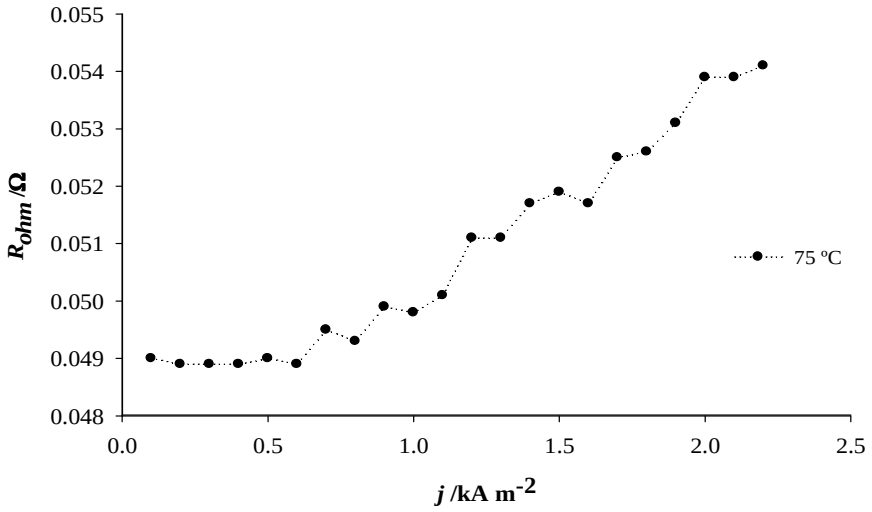

Figure 3.5 - Ohmic resistance as a function of the current density ([NaCl] = 300 g L^{-1}; [NaOH] = 28 wt.% and T=75 °C).

In this figure and for higher current densities, a clear linear trend can be observed, indicating that the bubbles formed are changing the ohmic resistance.

An empirical model was used to estimate the gas void fraction [19, 25]. The main assumptions of the model are the following:

1. Catholyte void fraction is negligible [16].

2. Membrane resistance does not change with void fraction (due to the 6 mm gap between the electrode surface and the membrane [13]);

3. Membrane resistance is determined at low current densities (lower than 0.5 $kA \cdot m^{-2}$) where the bubble effect is negligible on the electrolyte resistance.

The procedure followed for obtaining the gas void fraction (ε) was: (*i*) obtain the overall ohmic resistance, for low current densities, where the bubble effect is negligible, $\rho_{o,overall}$; (*ii*) obtain the electrolyte resistances by removing the membrane from the cell, $\rho_{o,a} + \rho_{o,cl}$, and (*iii*) computing the membrane resistance, ρ_m, for the same operating conditions region by subtracting the resistances of the electrolytes; and (*iv*) determine the overall ohmic resistance for the current density under study, $\rho_{overall}$, and compute the anodic resistance according to:

$$\rho_a = \rho_{overall} - \rho_{o,c} - \rho_m \tag{3.3}$$

The gas void fraction (ε) can now be obtained from [13, 25]:

$$\frac{\rho_a}{\rho_{o,a}} = (1-\varepsilon)^{-3/2} \tag{3.4}$$

Figure 3.6 shows the anolyte void fraction obtained for different current densities at constant operating conditions.

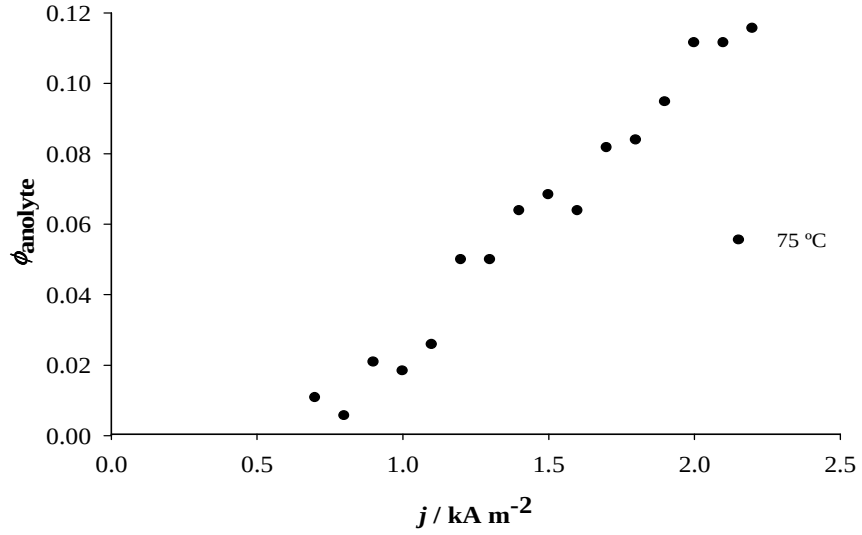

Figure 3.6 - Anolyte void fraction as a function of the current density ([NaCl] =300 g L^{-1}; [NaOH] =28 wt.% and T=75 ° C).

As can be seen, the anolyte void fraction is greatly affected by the current density. This void fraction can reach more than 10 %, indicating that the gas bubbles inside the anode chamber are relevant for the performance of the cell. This can suggest a difficult separation of gas bubbles from the electrolyte solution and an accumulation of gas bubbles on the anode surface.

Flow rate

The circulation of the electrolyte solution through the anode chamber is important to minimize the gas bubble effect. Different studies have shown that for the same current density, increasing the flow rate decreases the

electrolyte resistance due to better gas removal [13, 17-20], and this was also observed in the present work (Table 3.3). Moreover, the present experiments were conducted with solid electrodes, where this phenomenon is more likely to occur [13].

To study the effect of the feed flow rate on the ohmic resistance and hence on the gas void fraction several experiments were performed at 1.0, 1.5 and 2.0 kA m^{-2}. In these experiments, all other operation variables were kept constant. Table 3.3 shows the operating variables and the results obtained for the experiments performed. The influence of flow rate on cell performance was evaluated in terms of the electrolyte resistance only, because the membrane resistance was assumed to be constant (for the same concentrations and temperature) due to the 12 mm cell gap between electrodes (Experimental section). This gap should guarantee that all bubbles formed do not contact the membrane [13] and this way the membrane surface area should not change between experiments.

As observed before (Figure 3.6), as the current density increases the bubble effect is more pronounced. At 1.5 kA m^{-2} the gas void fraction is ca. 11 %, corresponding to an increase in ohmic drop of about 74 mV at the higher chosen flow rate (150 mL min^{-1}). At 2.0 kA m^{-2} the gas void fraction is ca. 12 % meaning an increase in ohmic drop of about 110 mV at the same flow rate.

Anode and cathode electrolyte concentration

The electrochemical cell used has a large gap between the electrodes and the membrane (6 mm). This gap originates a significant ionic resistance, and then the change in ions concentration should deeply affect the total ohmic resistance of the cell.

The anolyte conductivity (without the membrane) was determined at different concentrations and temperatures. Figure 3.7 shows the electrolyte conductivity for different NaCl concentrations and temperatures.

a)

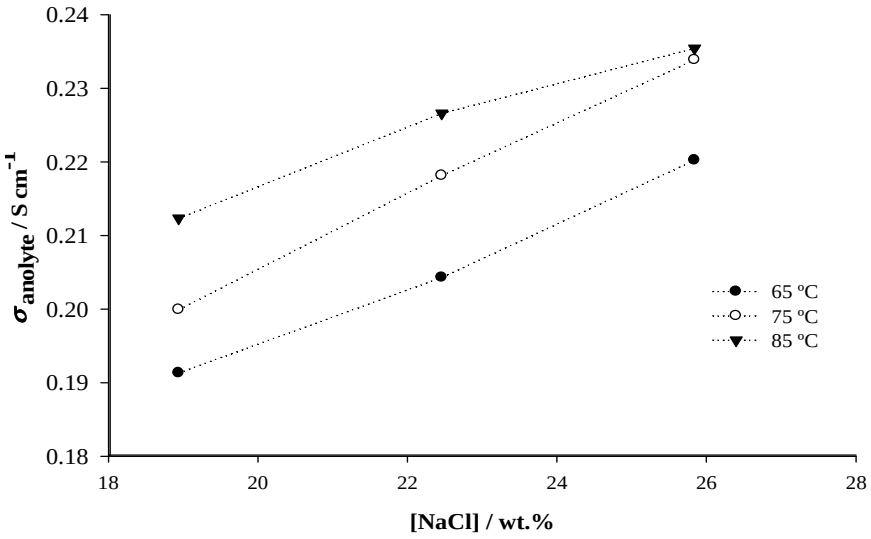

b)

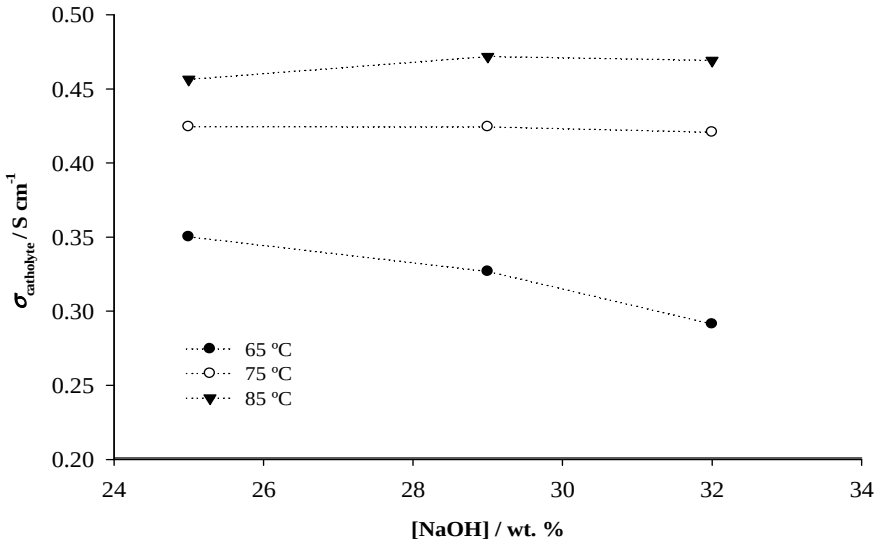

Figure 3.7 - Electrolyte conductivity at different temperatures and brine concentrations: a) anolyte and b) catholyte.

The anolyte conductivity increased with temperature for all the concentrations tested. The values of the NaCl aqueous conductivity obtained were within the same order of magnitude of the ones found elsewhere [26].

The membrane resistance, ρ_m, can be computed as a function of the electrolyte concentration, assuming that the void fraction is independent of the electrolyte concentration and equal to the gas void fraction previously determined. Accordingly, rearranging Eq. (3.3) one obtains:

$$\rho_m = \rho_{overall} - \rho_a - \rho_{o,c} \tag{3.5}$$

Table 3.3 (runs nos. 5 and 9-10) shows the influence of the NaCl concentration on the overall ohmic resistance of the cell, obtained at 1.5 kA m^{-2}, while the other operation variables were kept constant. Figure 3.8 shows the contribution of the electrolytes and of the membrane resistance to the overall resistance as a function of the anolyte concentration.

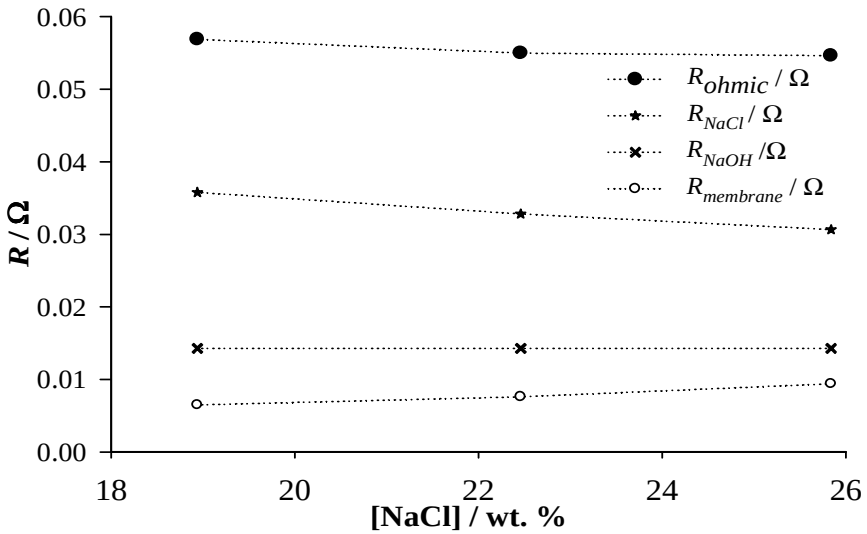

Figure 3.8 – Ohmic resistances (R) as a function of brine concentration.

The lowest overall ohmic resistance is obtained for the highest brine concentration, following the anolyte resistance decrease with concentration (Figure 3.7a). Clearly, that the variation in the overall ohmic resistance with brine concentration is mostly due to the anolyte resistance, where it represents ca. 60 % of the overall ohmic resistance. Increasing the NaCl concentration from 210 to 300 g L^{-1} (from 19 to 26 wt.%), the cell voltage

decreased 59 mV and the overall ohmic resistance decreased 2.3 mΩ (Table 3.3). The membrane resistance increased from 6.5 to 9.4 mΩ (Table 3), or its conductivity decreased ca. 1.7 mS cm^{-1}/ wt. % NaCl, while the anolyte conductivity increased ca. 4 mS cm^{-1}/wt. % NaCl (Figure 3.7a). The membrane conductivity decrease is related with the effect of the anolyte on the water transport through the membrane and the extent of water absorption and therefore on the conductivity and selectivity of the ion-exchange membrane [27]. At lower water content the membrane conductivity can decrease drastically due to the stronger binding effect of the mobile ions by the matrix.

The influence of the catholyte concentration on the ohmic resistance of the cell is shown in Figure 3.9.

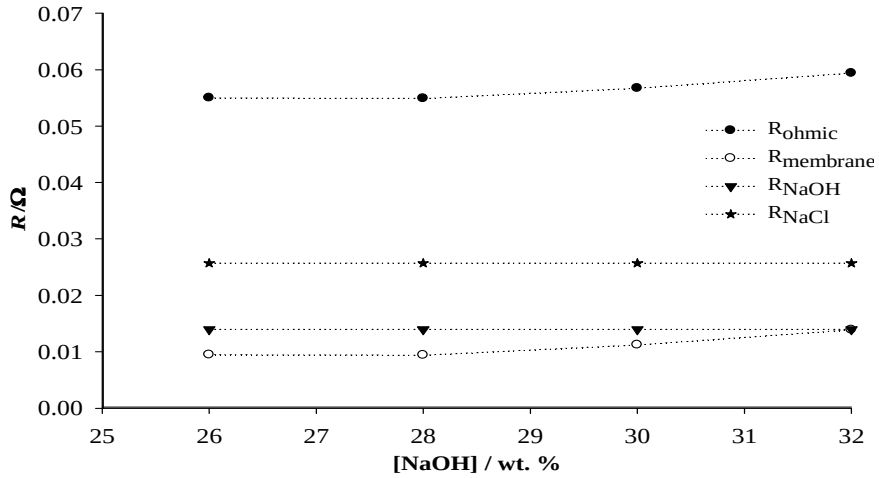

Figure 3.9 – Ohmic resistances (*R*) as a function of caustic concentration.

The experiments were performed at constant current (2.0 kA m^{-2}) and various concentrations of NaOH solutions (Table 3.3, runs nos.11-14). The catholyte conductivity is practically independent of concentration; this way the ohmic resistance increase with the NaOH concentration should reflect the membrane dehydration (Figure 3.9). The water absorption behavior in the membrane is different for the sulfonic (anode side) and the carboxylic (cathode side) layers [27]. Moreover, the carboxylic layer absorbs less water than the sulfonic layer [27], and as a result, the membrane conductivity is more affected by the catholyte concentration (ca. 2.1 mS cm^{-1}/wt. % NaOH compared with 1.7 mS cm^{-1}/wt. % NaCl) than by the anolyte concentration (see above).

Finally, the overall voltage of the electrochemical cell decreases with the anolyte concentration ca. 10 mV/wt. % NaCl and increases with the catholyte concentration ca. 17 mV/wt. % NaOH. In these experiments the membrane conductivity varied in the range 0.02 - 0.04 S cm^{-1}, which is within the conductivity range found elsewhere [23]. Additionally, the experimental voltage of the electrochemical cell as a function of the electrolyte concentrations shows the same trend as the interpolation model.

Temperature

The anolyte and catholyte feed temperatures must be almost the same to avoid thermal shock on the membranes. Three different temperatures (65, 75, and 80 ° C) were studied, as shown in Table 3.4, at the current density of 0.5 kA m^{-2}.

Table 3.4 – Influence of the cell temperature on the conductivity of the membrane and on the electrolytes at a current density of 0.5 kA m^{-2}.

T **°C**	σ_m **S cm^{-1}**	σ_{NaCl} **S cm^{-1}**	σ_{NaOH} **S cm^{-1}**	***E*** ***V***
65	0.0165±5.0 x 10^{-4}	0.222±0.001	0.333±0.001	3.003±0.001
75	0.0263±5.0 x 10^{-4}	0.231±0.001	0.429±0.001	2.923±0.001
80	0.0287±5.0 x 10^{-4}	0.231±0.001	0.429±0.001	2.941±0.001

The voltage of the cell decreased by 8 mV by increasing the temperature from 65 to 75 ° C. The better performance at higher temperatures is related to the decrease in the overall ohmic resistance mainly for two reasons: (*i*) increase in the cation diffusion rate inside the membrane, which is an activated transport, and (*ii*) decrease in the electrolytes and membrane resistance with temperature.

However, the temperature also affects the vapor pressure and the gas solubility. For the same current density, the gas volumetric rate should

increase with temperature due to gas expansion, increase in water vapor pressure, and decrease in chlorine gas solubility. This makes the fraction of the total solution occupied by the gas bubbles (gas void fraction) rise with temperature.

In addition, the membrane stability may decrease due to decarboxylation for temperatures higher than 90 ° C [27]. At industrial scale, physical damage to the membrane (blistering) becomes more likely to occur at temperatures lower than 75 ° C. This is due to localized internal overheating caused by high electrical resistances [27].

3.5. Conclusions

The study of the operating variables of the chlor-alkali membrane process is important to understand and avoid performance decline and the progressive degradation of the membranes. A preliminary study was made to find the optimum range of each operating variable on the overall performance of the electrochemical cell. EIS has been shown to be a powerful technique for obtaining the ohmic resistances of the electrolytes and of the membrane, *in situ*.

The ohmic resistance and cell voltage are strongly affected by the presence of gas bubbles in the electrolyte, especially at the anode side. A

better separation of gas bubbles from the anolyte can be achieved using high feed flow rates. Even though, for a given current density, the brine concentration and the cell temperature have the highest effect on the cell voltage the membrane conductivity is mostly affected by the caustic concentration (2.1 mS cm^{-1} /wt.% NaOH) and by the brine concentration (1.7 mS cm^{-1}/wt.% NaCl). In this study, the large electrode gap originates a high ohmic overvoltage, enhancing the effect of the electrolyte concentration on the electrochemical cell performance. The choice of the operating variables must then be appropriated for the cell configuration (electrode gap, solid, or perforated electrodes) to minimize the power consumption.

3.6. References

[1] - www.eurochlor.org/chlorine-industry-facts-2007, accessed in May 2010.

[2] - worldchlorine.com/, accessed in July 2010.

[3] - T. Navin, "Membrane Cell Technology - State of the art industry", Eltech Systems Corporation, 2002.

[4] - F. Sotto-Mayor, Internal information, Uniteca, S.A., 1999.

[5] - "General Information on Nafion Membrane for electrolysis", Technical Information Bulletin 97-01, Dupont Company (2002).

[6] - T. F. O'Brien, T.V. Bommaraju and F.Hine, in *Handbook of Chlor-Alkali Technology – Volume I*, chapter 4, Springer, New York (2005).

[7] - V.S. Bagotsky, in *Fundamentals of Electrochemistry*, 2nd ed., chapter 17 and 26, Wiley Interscience, New Jersey (2006).

[8] - T. Momose, N. Higuchi, O. Arimoto, and K. Yamaguchi, *Journal of The Electrochemical society* **138** (1991) 735-741.

[9] - Y. Ogata, T. Kojima, S. Uchiyama, M. Yasuda, and F. Hine, *Journal ofThe Electrochemical Society* **136** (1989) 91-95.

[10] - D. Bergner and M. Hartmann, *Journal of Applied Electrochemistry* **24** (1994) 1201-1205.

[11] - D. J. Groszek and J. A. Moomaw, *Modern Chlor-alkali Technology* **4**. (1990) 215.

[12] - A.Pilla, E. O. Cobo, M. M. E. Duarte, D. R. Salinas, *Journal of Applied Electrochemistry* **27** (1997) 1283-1289.

[13] - F. Hine, M. Yasuda, R. Nakamura, T. Noda, *Journal of The Electrochemical Society* **122** (1975) 1185-1190.

[14] - Y. Xiong, L. Jialing, S.Hong, *Journal of Applied Electrochemistry* **22** (1992) 486-490.

[15] - Ph. Mandin, A. Aissa, H.Roustan, J. Hamburger, G. Picard, *Chemical Engineering and Processing* **47** (2008) 1926-1932.

[16] - Y. Noaki, H. Shiroki, Paper presented at The Electrochemical Society Meeting, May 16-21, Honolulu Hawaii (1993).

[17] - T. Mirzazadeh, F. Mohammadi, M. Soltanieh, E. Joudaki, *Chemical Engineering Journal*, **140** (2008) 157-164.

[18] - N. S. Kaveh, S.N. Ashrafizadeh, F. Mohammadi, *Chemical Engineering Research and Design* **86** (2008) 461-472.

[19] - A.A. Jalali, F. Mohammadi, S.N. Ashrafizadeh, *Desalination*, **237** (2009) 126-139.

[20] - N. S. Kaveh, F. Mohammadi,, S.N. Ashrafizadeh, *Chemical Engineering Journal* **147** (2009) 161–172.

[21] - R. O' Hayre, Suk- Won Cha, W. Colella and F. B. Prinz, in *Fuel Cell Fundamentals*, Wiley, New York (2006).

[22] - M. J. Anderson and P. J. Whitcomb, in *RSM simplified*, Productivity press, New York (2005).

[23] - C.H. Hamann, A. Hamnett, W. Vielstich, in *Electrochemistry*, 2nd edition, Wiley-VCH (2007).

[24] - A. Antozzi, C. Bargioni, L. Iacopetti, M. Musiani , L. Vázquez-Gómez, *Electrochimica Acta* **53** (2008) 7410–7416.

[25] - Ph. Mandin, J. Hamburger, S. Bessou, G. Picard, *Electrochimica Acta*, **51** (2005) 1140-1156.

[26] - www.smartmeasurement.com, accessed in July 2009.

[27] - H. Strathmann, in *Ion- exchange membrane separation processes*, Membrane Science and Technology series, 9 (2004).

Chapter 4 - Characterization of the chlor-alkali membrane process by EIS. Part II- Kinetic analysis of two different nickel cathodes[2]

4.1 Abstract

The hydrogen evolution reaction (HER) was studied in a chlor-alkali membrane cell equipped with a commercial nickel electrode. Two electrode morphologies were studied, solid and mesh. The electrochemical kinetic properties of HER were obtained at 75 ºC using an aqueous solution of NaOH 8.9 M during operation and using the anode as a reference electrode; a negligible anode overpotential was assumed. The Tafel slopes (*b*) obtained for the solid and mesh electrodes were -171 mV dec^{-1} and -183 mV dec^{-1}, respectively. Electrochemical impedance spectroscopy (EIS) was also used to investigate the HER in the Tafel region. The mesh electrode morphology was found to affect the impedance spectra due to ac penetration through the mesh structure. Additionally, the kinetic parameters were used to estimate the *k-factor* that was compared with the *k-factor* obtained from the potential-current density curve.

---

[2]A.C. Dias, L. Brandão, F. Magalhães, A. Mendes, Journal of Electrochemical Society (2010) – Submitted.

4.2. Introduction

In part I of this work, electrochemical impedance spectroscopy (EIS) was applied *in situ* to study the effect of operating conditions on the ohmic resistance of a chlor-alkali lab cell [1]. It was observed that cell voltage was strongly affected by the presence of gas bubbles in the electrolyte. Following that work, the overall performance should be evaluated and the electrochemical reactions taking place at the anode and cathode surface studied.

High efficiency electrodes are of concern on the chlor-alkali industry, since the overpotentials are crucial in energy consumption. The main requirements for the electrodes are activity and long term stability. At the anode, where the chloride is oxidized to gaseous chlorine, a DSA® anode made of titanium coated with oxides of titanium, ruthenium and iridium is commonly used [2]. Titanium-ruthenium-iridium oxide anodes exhibit a very high electrocatalytic activity and selectivity towards the anodic chlorine evolution reaction. On the other hand, the electrochemical reaction that occurs at the cathode is the hydrogen evolution from sodium hydroxide aqueous solutions. Several different materials were investigated as a catalyst for the hydrogen evolution reaction (HER). Nickel-based cathodes are not the most electroactive but they are frequently used because of their excellent corrosion resistance under severe conditions [2,3].

There are innumerous publications concerning the kinetics of HER and chlorine evolution reactions [4-12]. A typical Tafel slope of -120 mV dec $^{-1}$ (1 mol dm^{-3} NaOH at 20 ºC and transfer coefficient $\alpha = 0.5$) is mentioned for the HER kinetics using nickel electrodes [4-9]. On the other hand, a Tafel slope of 30-40 mV dec $^{-1}$ is reported for the chlorine evolution reaction on DSA® electrodes (in 5 M NaCl at 80-90 ºC and $\alpha = 0.5$) [9-12].

Although electrode kinetics of individual electrochemical chlorine and hydrogen evolution reactions were obtained [4-13], the study of these electrodes during chlor-alkali cell operation has never been reported. Instead, the electrochemical reaction and the mass transfer kinetics at the membrane cell are usually evaluated by current-voltage characteristic curves (polarization curve) [14], where the slope of this polarization curve and corresponding interception are used in the chlor-alkali industry to characterize the overall performance of the process - *k-factor* method [14]. The use of *k-factor* is based on the assumption that overpotential follows the Tafel equation and that the electrolyte and membrane resistances follow the ohm's law [14]. The slope of the polarization curve is associated with ohmic resistance changes and the intercept is related to the electrodes performance [14].

HER is a complex reaction evolving two electrons and is generally believed to proceed according to three consecutive steps [2, 4, 6, 13]:

A. The discharge-adsorption of hydrogen (Volmer reaction),

$$M + H_2O + e^- \leftrightarrow MH + HO^- \quad (4.1)$$

B. The electrochemical desorption of hydrogen (Heyrovsky reaction),

$$MH + H_2O + e^- \leftrightarrow M + H_2 + HO^- \quad (4.2)$$

C. Recombination-chemical desorption (Tafel reaction),

$$2MH \leftrightarrow 2M + H_2 \quad (4.3)$$

HER proceeds primarily by the discharge of water molecules (proton donors) on the surface of the electrode to form adsorbed H (step A). The following step can be either the electrochemical desorption (B) or/and the chemical desorption (C) of the adsorbed intermediate. These steps can be combined in different pathways depending on the nature and sequence of the intermediate reaction steps. Recent studies privilege the mechanism that considers the initial discharge step (A) followed by the electrochemical desorption of the adsorbed hydrogen intermediate (B) [6, 13, 16-17]. For the nickel electrodes that have high bond energy, the most likely rate-determining step (rds) is the electrochemical desorption (B) [2]. N. Krstajic et al. [6] calculated the dependence of hydrogen surface coverage, θ_H, as a function of the overpotential at the nickel electrode. They found that at potentials close to the theoretical HER equilibrium potential, E_e (HER)= -0.824 V versus the standard hydrogen electrode (SHE) (at 20 ºC in 1.0 M),

the hydrogen surface coverage is almost zero but at potentials around -1.0 V (vs SHE) the nickel electrode is almost fully covered by adsorbed hydrogen, $\theta_H \rightarrow 1$.

It is proposed, in the present study, the use of electrochemical impedance spectroscopy technique (EIS) to characterize the HER during cell operation. Due to the very high catalytic activity of anode reaction compared to the HER at the cathode [6-9], the anode overpotential can be neglected [9-10]. Under such assumption, the overall impedance response of the cell should be attributed to the cathode reaction and the cathode kinetics can be estimated without the need of a reference electrode, under normal operating conditions. For this purpose, the kinetic parameters of the HER on a nickel electrode (Tafel slope (*b*), exchange current density, (j_0), and transfer coefficient (α) were obtained from polarization curves (Tafel analysis) and from EIS analysis. Two electrodes designs, solid and mesh electrodes, were investigated. The overall performance of the cell (*k-factor* and overpotential) was also evaluated and compared with the one computed from the kinetic parameters obtained.

4.3. Experimental

The detailed description of the experimental setup used can be found elsewhere [1]. Tests were performed at 75 ºC by feeding the anolyte and the

catholyte at a volumetric flow rate of 150 mL min^{-1} to the lab membrane cell. The sodium chloride solution was 5 M (anolyte) and sodium hydroxide solution was 8.9 M (catholyte). Anode and cathode chambers were separated by a Flemion (Ref. F893.4) membrane with a 250 μm thickness. Solid and mesh electrodes were used (geometric area of 1.0 x 10^{-2} m^2, with the geometric projected area of the mesh being 9.2 x 10^{-3} m^2 for the cathode and 8.1 x 10^{-3} m^2 for the anode, from ElectroCell, Denmark); the cathode was made of nickel and the anode was DSA®. The gap between electrodes was $12x10^{-3}$ m for the solid electrodes and $5.5x10^{-3}$ m for the mesh electrodes.

Polarization curves and EIS were obtained using an electrochemical workstation (Zahner-elektrik, equipped with IM6eX, and PP-240 potentiostat) under galvanostatic mode and for potentials up to 4 V. Before each experiment the cell was pre-treated applying a constant potential of 2.2 V during 30 min. The cell was then kept at a certain current density for at least 210 s in order to reach the steady state. EIS spectra were obtained by superimposing a 10 mV ac signal over the frequency range from 100 kHz to 100 mHz. Impedance spectra were fitted to an appropriate electrical analogue by means of ZView software.

Regarding the mesh electrodes, they were partially coated with a Teflon® aqueous dispersion to disable the back and lateral parts of the mesh structure. For that, both electrodes were immersed into a Teflon® aqueous

dispersion and the resin was cured by heating up to 337 ° C, following the producer recommendation.

4.4. Results

4.4.1. Comparison between solid and mesh electrodes based on the k-factor method

The polarization curves for solid and mesh electrodes are plotted in Figure 4.1.

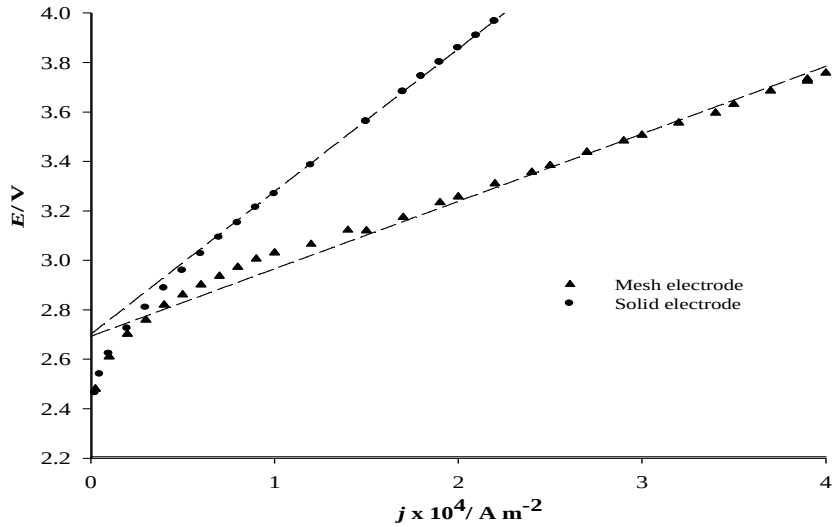

Figure 4.1– Polarization curves obtained for the solid and mesh nickel electrodes.

Figure 4.1 shows that the mesh electrode performs better than the solid electrode. The lower slope of the polarization curve associated to the mesh electrodes indicates that ohmic resistance is lower; this should be related to the smaller electrode gap used in this configuration. On the other hand, the

close intercept values for both polarization curves indicates similar electrode overpotentials.

The slope and interception values in the linear region of the polarization curves (usually observed over the current density range of 1.5 - 5 kA m^{-2}) are currently used in the chlor-alkali industry to characterize the overall performance of the process – the so-called *k-factor* method [14]; moreover, the slope is known as *k-factor*. In this region, the relationship between potential and current density is given by:

$$E = k \times j + E_0 \tag{4.4}$$

where the *k-factor* (*k*) is associated with ohmic resistances and E_0 is related to the electrode overpotential [14].

The curvilinear part of the polarization curve, observed in the lower current density region (< 1.5 kA m^{-2}) (*Q-factor* analysis), can be fitted by log relationship between potential and current density in this region [14]:

$$E = S \times \log(j) + R \times j + Q \tag{4.5}$$

where *S*, *R* and *Q* are constants related to the basic characteristics of the electrodes, membrane and electrolytes.

The fitting of equations (4) and (5) to the respective polarization curves regions are given in Table 4.1 for the solid and mesh electrodes.

Table 4.1 – Estimated parameters for solid (12 mm gap) and mesh electrodes (5.5 mm gap).

	$E = kj + E_0$ (j > 1.5 kA m^{-2})		$E = Q + S\log(j) + Rj$ (j < 1 kA m^{-2})		
Electrode	k **x 10^{-4} (Ω m^2)**	E_0 **(V)**	Q **(V)**	S **(V)**	R **x 10^{-4} (Ω m^2)**
Solid	5.770	2.701	2.757	0.189	5.156
Mesh	2.510	2.753	2.801	0.207	2.373

Table 4.1 shows that the mesh electrodes exhibit a lower ohmic resistance because of the smaller electrode gap (5.5x10^{-3} m) (k and R). This difference is more evident for the high current density region (j > 1.5 kA m^{-2}) probably due to the bubble effects. Our previous study indicated that solid electrodes probably exhibit a higher overpotential penalty than the mesh ones due to the presence of bubbles, especially in the higher current density region [1]. On the other hand, the ohmic resistances for the mesh electrodes are similar for the lower (R) and higher current density (k) regions indicating that gas void fraction could be neglected for this type of electrodes (Table 4.1). This probably happens because the gas bubbles also rise through the backside of the mesh, thus decreasing the void fraction between the electrodes. Concerning the parameters that characterize the reaction kinetics, E_o, Q and S, they are similar for both electrodes.

4.4.2. Electrode kinetics

A more rigorous analysis of the kinetic parameters of the electrochemical reactions is required to validate the previous diagnostic based on the semi-empirical *k-factor* and *Q-factor* methods.

Electrode kinetics are normally studied by using Bulter-Volmer equation or simply by the Tafel equation, which is valid for high overpotentials. Kinetic parameters for the HER (j_0, b and α) are derived from the Tafel equation [18]:

$$\eta = a + b\log(j) \tag{4.6}$$

where η (V) represents the cathode activation overpotential, j (A m^{-2}) is the current density, b (V dec^{-1}) is the Tafel slope and a (V) is the intercept.

The magnitude of the Tafel slope (b) and the intercept (a) depends on the rate determining step and is generally of the form:

$$b = -2.303\frac{RT}{\alpha nF} \text{ and } a = 2.303\frac{RT}{\alpha nF}\log(j_0) \tag{4.7}$$

where α represents the charge transfer coefficient, j_0 is the exchange current density, R is the gas constant (8.314 J $mol^{-1}K^{-1}$), T is the temperature, n is the number of exchanged electrons and F is the Faraday constant (96485 C mol^{-1}). The cathodic overpotential was ploted as a function of current density and shown in Figure 4.2. It was assumed that anode reaction rate is negligible when compared with the slower kinetics of the HER on nickel cathodes [6,9-

10]. The ohmic resistances, obtained from EIS analysis, 5.47×10^{-4} Ω m^2 and 2.83×10^{-4} Ω m^2 for mesh and solid electrodes respectively, were subtracted from potential values on Figure 4.1.

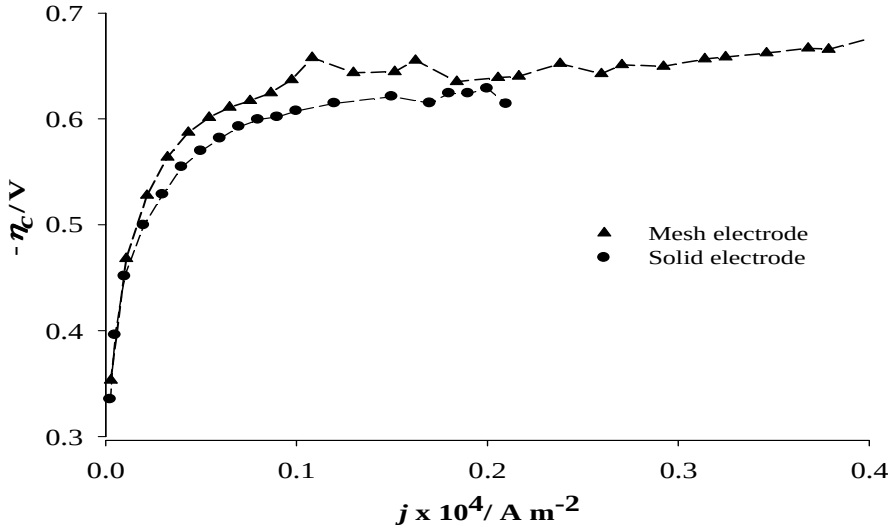

Figure 4.2 – Cathode overpotential as a function of the current density for solid and mesh electrodes - lines were introduced to improve readibility.

Figure 4.2 shows the cathode overpotential for both electrode configurations, which are in agreement with the literature for nickel substrates [9]. The overpotential at the mesh electrode is slightly higher than at the solid electrode.

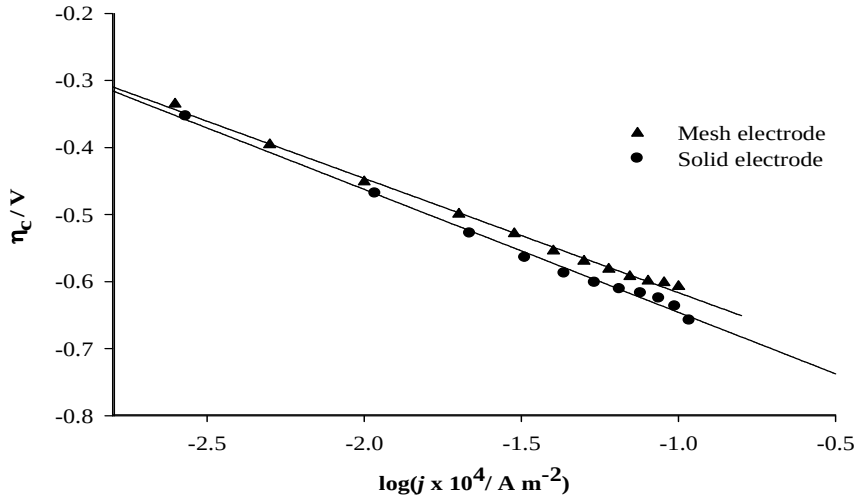

Figure 4.3 – Tafel polarization curves for solid and mesh nickel electrodes.

Figure 4.3 shows the Tafel curves obtained for the HER using nickel electrodes (solid and mesh) between -1.2 V to -1.5 V (vs DSA®). The slope value of these curves is -171 mV dec^{-1} for the solid electrode and -183 mV dec^{-1} for the mesh electrode (Table 4.2).

Table 4.2 – Tafel slopes (b), exchange current densities (j_0) and charge transfer coefficients (α) of HER at nickel solid and mesh nickel cathodes determined from the polarization curves.

Electrode	***-b*** **(V dec^{-1})**	***j_0*** **(A m^{-2})**	α
Solid	0.171	2.43 x 10^{-9}	0.405
Mesh	0.183	3.01 x 10^{-9}	0.376

The Tafel slopes (b) are lower than the values obtained by other authors, $b \approx -120$ mV dec^{-1}, NaOH 1 M at 25 ºC [6, 13, 16, 17], where the transfer coefficient (α) is normally assumed to be constant, $\alpha = 0.5$, and independent of the temperature. However, according to the Tafel relation j_0 increases with temperature and the value of b decreases (Eq. 4.7), assuming constant transfer coefficient [6, 9, 20]; this way, lower Tafel slopes are expected for higher temperatures. Additionally, Krstajic et al. [21] reported a linear relationship between the transfer coefficient and the inverse of temperature, for the HER; the transfer coefficient decreases with the temperature increase. The transfer coefficients ($\alpha = 0.40$ and 0.38, Table 2) are in agreement with this behaviour. Other authors found similar values for the transfer coefficient [13, 16]. This way, assuming that $\alpha = 0.5$ oversimplifies the problem and originates Tafel slopes that are artificially higher.

Moreover, the magnitude of the Tafel slope (b) can also give an indication about the reaction mechanism. Complex expressions for the Tafel slope were proposed considering the HER kinetics of individual reaction steps. Frequently, the Tafel slope magnitude is interpreted based on the limiting cases of complete or negligible surface coverage by adsorbed hydrogen [6, 19, 20]. As reported by Krstajic et al. (see above) the surface coverage of adsorbed hydrogen is high within the potential range where Tafel parameters were obtained (between -1.2 V and -1.5 V (vs DSA®) [6]. Under

high coverage conditions ($\theta_H \rightarrow 1$), as in this case, the Tafel slope obtained for the solid and mesh electrodes is equal to $-\frac{RT}{\alpha F}$ (T=75 ºC), indicating that the electrochemical desorption of hydrogen, Eq. (4.2), is the rate determining step [6, 19, 20].

The exchange current density, j_0 of the HER at nickel cathodes obtained based on the projected geometric area of the electrodes, is in the same order of magnitude as found elsewhere [19, 21]. It was considered that the exchange current density is almost independent of the NaOH concentration [22]. The exchange current density increases with temperature, therefore the values obtained are slightly higher than the ones reported elsewhere [19,21]. The values obtained for the exchange current density for the solid and mesh electrodes are very close to each other as expected, because the only difference between them is the surface geometry.

The kinetic parameters obtained by Tafel equation will be used to calculate the polarization curve parameters obtained on Table 4.1 for j < 1 kA m^{-2} (*Q-factor* method) in order to compare these two strategies. The overall voltage is given as a function of current density by the following equation:

$$E_{cell} = E^0 + \eta_A + \eta_C + \eta_{ohm} \quad (4.8)$$

Assuming Tafel behaviour for anode and cathode and rearranging Eq. (4.6 and 4.7) becomes:

$$\eta = b \times \log\left(\frac{j}{j_0}\right) \tag{4.9}$$

Substituting Eq. (4.9) in Eq. (4.8) and rearranging Eq. (4.5) is obtained, which was introduced before, where $\eta_{ohm} = R \times j$ and

$$Q = E^0 - b_A \log(j_{0,A}) + b_C \log(j_{0,c}) \text{ and } S = (b_A - b_C) \tag{4.10}$$

E^0 is the thermodynamic potential (2.116 V vs SHE) and subscripts A and C indicate anode and cathode, respectively.

From kinetic parameter values given in Table 4.2 and assuming b_A = 0, we can estimate Q and S. The ohmic resistance (R) is obtained directly from the EIS analysis (see below), where a value of 5.47×10^{-4} Ω m^2 was read for the solid electrode and 2.83×10^{-4} Ω m^2 for the mesh electrode. Parameters Q and S obtained from the polarization curve (*Q-factor* method) and computed from the kinetic data (for both electrodes) are shown in Table 4.3. These values are close to the ones given in Table 4.1 obtained from the polarization curve for $j < 1$ kA m^{-2}.

Table 4.3 – Parameters *Q* and *S* obtained directly from the polarization curve for $j < 1$ kA m^{-2} (*Q-factor* method) (Table 1) and calculated from the kinetic data in Table 4.2.

	From polarization curve		**From kinetic data**	
Electrode	***Q*** **(V)**	***S*** **(V)**	***Q*** **(V)**	***S*** **(V)**
Solid	2.757	0.189	2.733	0.171
Mesh	2.801	0.207	2.762	0.183

Table 4.2 shows that parameters obtained directly from the polarization curve are in agreement with the ones obtained from the kinetic data, indicating that despite being much simpler, the first method can produce comparatively accurate results.

4.4.3. EIS Analysis

Electrochemical impedance analysis was carried out for current densities within the linear region of the Tafel polarization curve in Figure 4.3, for the solid and mesh electrodes. The spectra obtained for a current density of 25 A m^{-2} are shown in Figure 4.4. One single semicircle is visible for the solid electrode. However, a second semicircle seems to be present in the case of mesh electrode, at high frequencies. The difference between the ohmic resistances of both electrodes can be seen in Figure 4.4. The mesh electrode exhibits a larger semi-circle in the Nyquist plot, suggesting a slightly slower

cathode reaction in comparison to the solid electrode and in accordance with the kinetic data observed in Table 4.2.

The impedance spectra obtained at different current densities for the solid electrode are given in Figure 4.5. Only a single semicircle is observed over the whole range of scanned frequencies, point out a charge transfer controlled process at the cathode [18].

a)

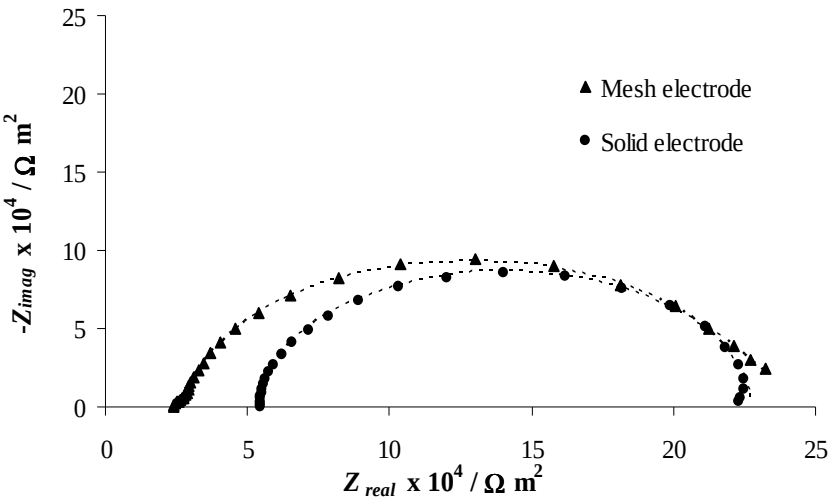

b)

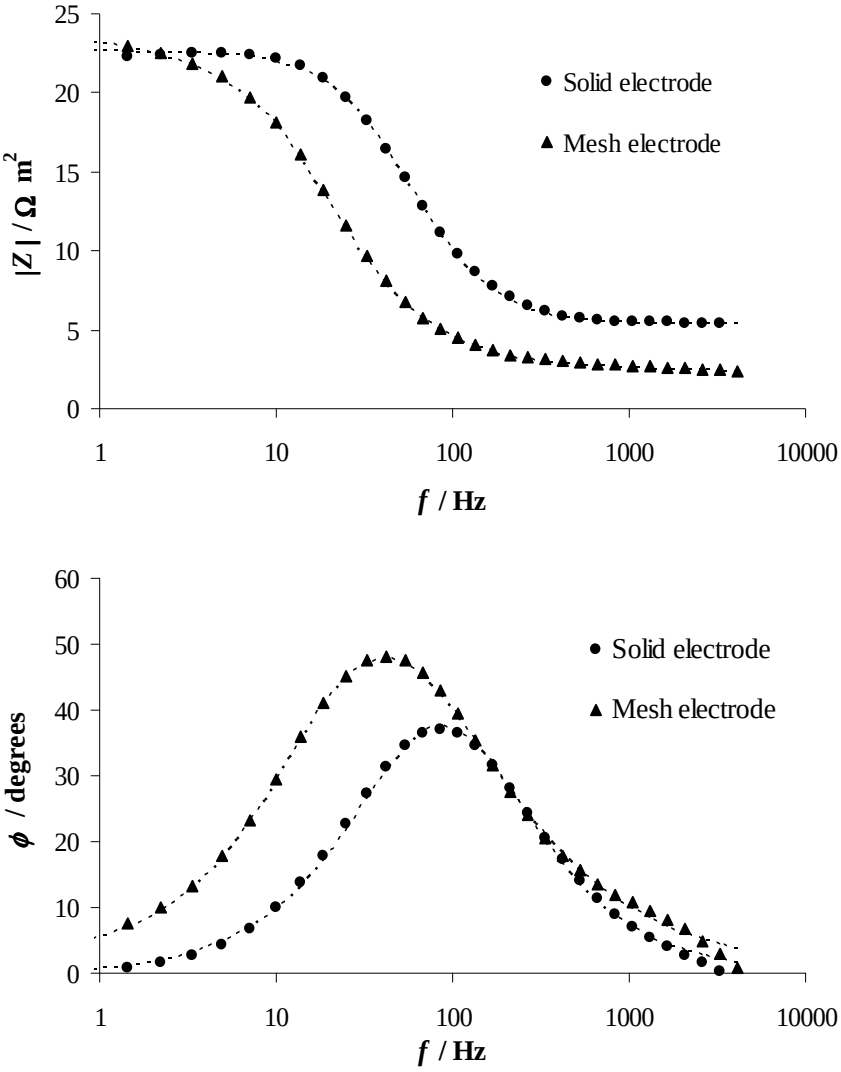

Figure 4.4 – Nyquist and bode plots (figures a) and b) respectively) for HER on the solid and mesh nickel electrodes measured at 25 A m^{-2}. Dots – experimental data; lines – fittings of the equivalent circuits.

a)

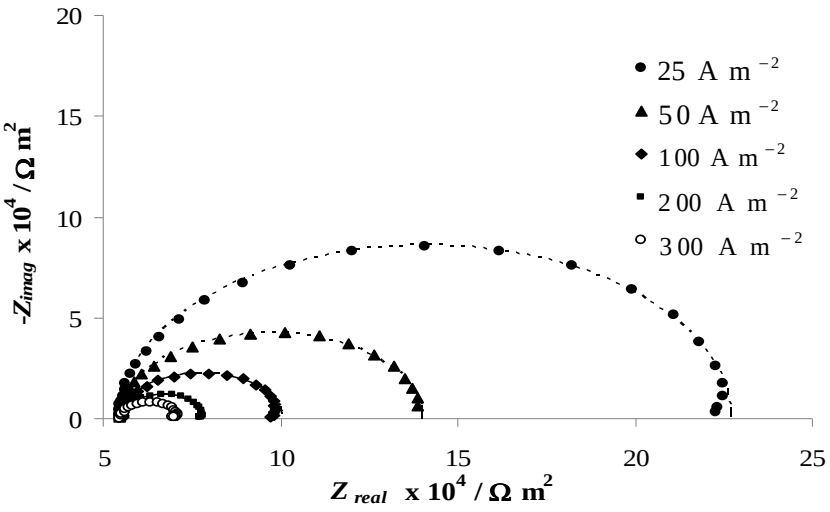
20
15
10
5
0
5
10
15
20
25
25 A m −2
50 A m −2
100 A m −2
200 A m −2
300 A m −2
-Zimag x 10^4 / Ω m^2
Z real x 10^4 / Ω m^2

b)

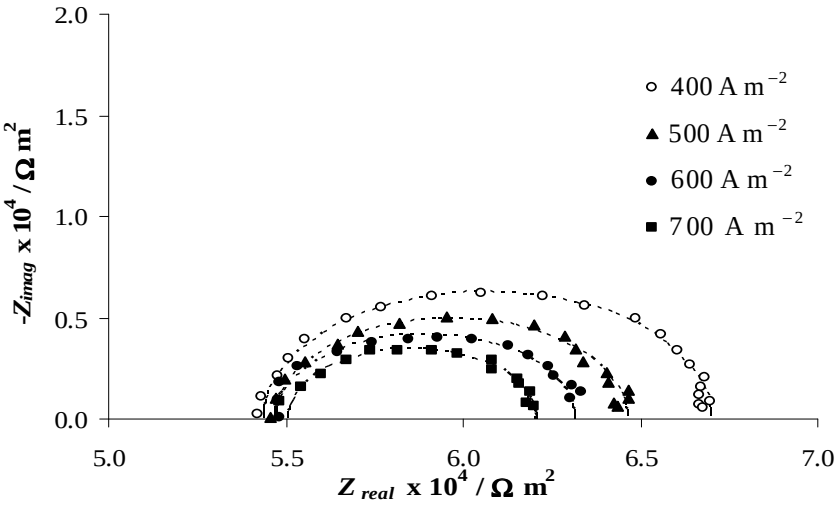
2.0
1.5
1.0
0.5
0.0
5.0
5.5
6.0
6.5
7.0
400 A m −2
500 A m −2
600 A m −2
700 A m −2
-Zimag x 10^4 / Ω m^2
Z real x 10^4 / Ω m^2

c)

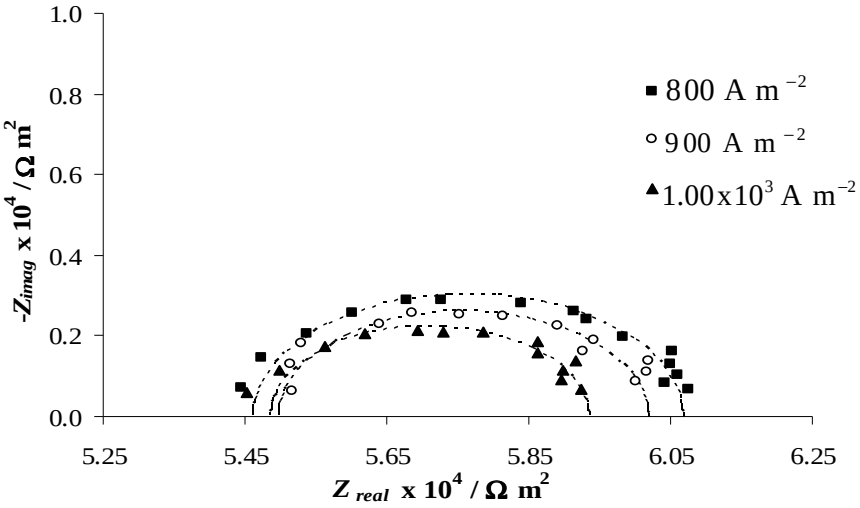

Figure 4.5 - Nyquist plots for HER on the solid nickel electrode measured at current densities between a) 25 A m^{-2} and 300 A m^{-2}; b) 400 A m^{-2} and 700 A m^{-2} and c) 800 A m^{-2} and 1.00x10^3 A m^{-2}. Dots – experimental data; lines – fittings of the equivalent circuits.

These impedance spectra were fitted to a Randles equivalent electric circuit [15, 19, 23] given in Figure 4.6. This equivalent circuit combines the electrolyte resistance in series with a charge transfer resistance (R_{ct}), in parallel with a double layer capacitance (C_{dl}). The estimated parameters are given in Table 4.4.

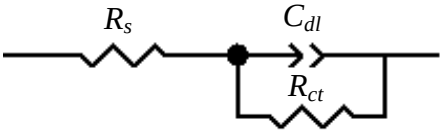

Figure 4.6 – Randles equivalent electrical circuit.

a)

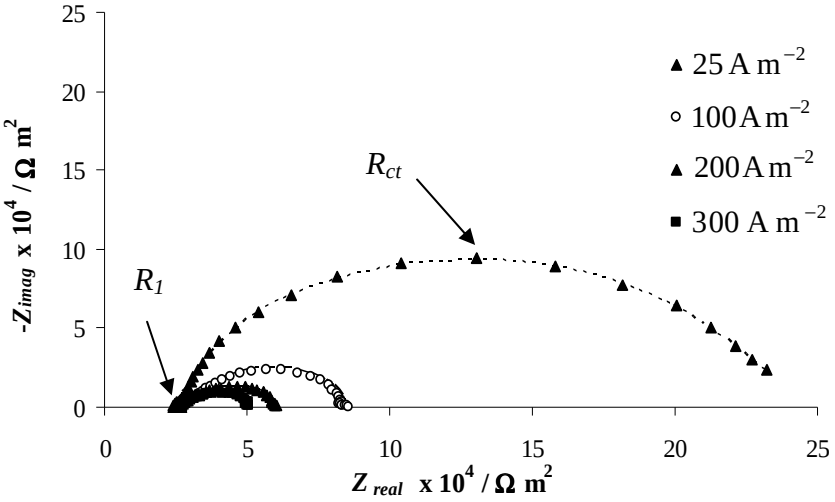

b)

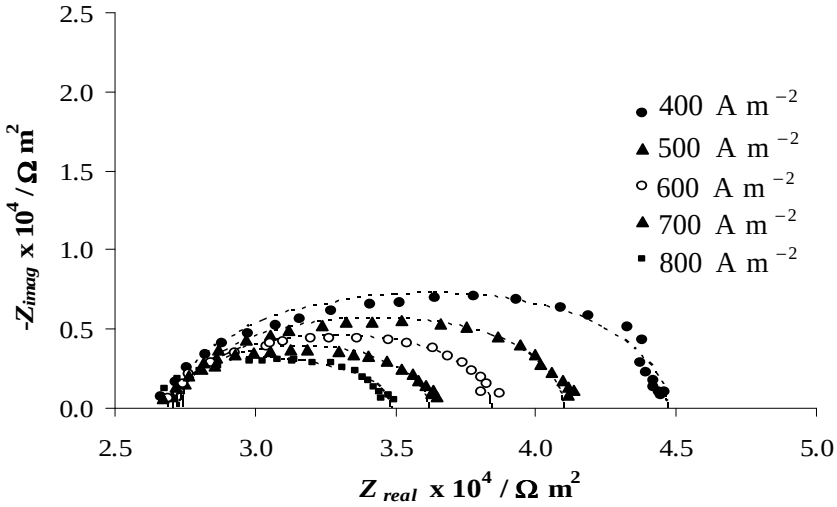

Figure 4.7 – Nyquist plots for HER on the mesh nickel electrode measured at current densities between a) 25 A m^{-2} and 300 A m^{-2} and b) 400 A m^{-2} and 800 A m^{-2}. Dots – experimental data; lines – fittings of the equivalent circuits.

Table 4.4 – Charge transfer resistance and double layer capacitance of the cathode (solid electrode) obtained by fitting the experimental results to the equivalent circuit.

η_{cat} V	R_{ct} x 10^4 (Ω m^2)	C_{dl} (F m^{-2})
-0.335	17.24	2.18
-0.396	8.52	2.01
-0.451	4.50	1.96
-0.500	2.37	2.09
-0.529	1.63	2.22
-0.555	1.26	2.47
-0.570	0.99	2.61
-0.582	0.84	2.71
-0.593	0.70	3.15
-0.599	0.60	3.47

The impedance parameters obtained by the fitting to the experimental results are shown in Table 4.4. As it can be seen the charge transfer resistance decreases as the overpotential increases. On the other hand, the double layer capacitance increases with overpotential indicating that the electrode activity is increasing. Values given in Table 4.4 are in the same order of magnitude of the ones reported elsewhere [17, 24].

Figure 4.7 shows the impedance spectra obtained for the mesh electrode. In this case, two slightly superposed semicircles can be observed mainly for lower current densities (Figure 4.7a). The equivalent electric circuit used to characterize these spectra is depicted in Figure 4.8 and combines two circuits in series that are visible in the Nyquist plot at high and

low frequencies. R_1 and C_1 are charge transfer resistance and the high frequency double layer capacitance, respectively, and are visible at high frequencies.

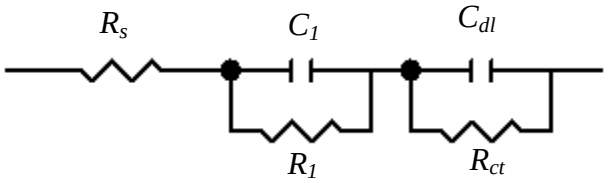

Figure 4.8 – Equivalent circuit used to fit the impedance data obtained for the cathode mesh electrode.

The high frequency region of the impedance spectra for the mesh electrodes can be related to the meshed structure; this high frequency semicircle is not obtained with the solid electrode. Hitz et al. attributed the high frequency semicircle of the impedance spectrum to geometric factors, i.e. a porous electrode [25, 26, 27]. The high frequency semicircle seems to have less significance as the overpotential increases, which can be due to a smaller ac penetration depth for higher current densities [25]. SEM images of the electrode surface were obtained to check for any porosity. Figure 4.9 shows that the cathode electrode surface is not porous.

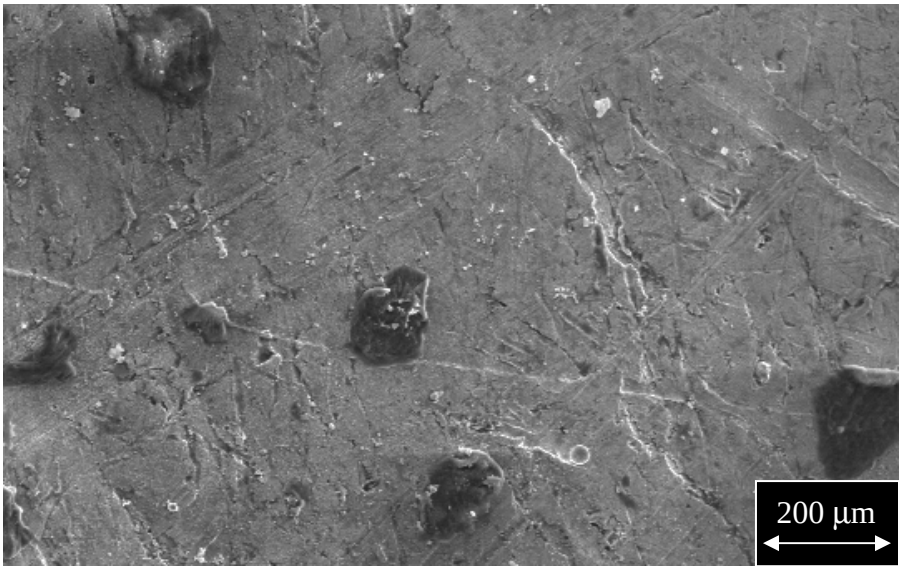

Figure 4.9 - SEM image of the surface of the cathode mesh electrode.

The impedance data were analyzed according to the equivalent circuit shown in Figure 4.8 and Table 4.5 shows the corresponding fitted parameters for the mesh electrode.

Parameters on Table 4.5 show that the low frequency charge transfer resistance (R_{ct}) decreases with the current density and the high frequency charge transfer resistance (R_1) is almost independent of the current density. The high frequency double layer capacitance is current density independent, while the low frequency capacitance increases with current density. Once the kinetic parameters of electrocatalytic reactions depend on the applied potential, it can be assumed that the high frequency skewed semicircle is not related to kinetics [26].

Table 4.5 – Charge transfer resistance and double layer capacitance of the cathode (mesh electrode) obtained by fitting experimental results.

η_{cat} (V)	R_{ct} x 10^4 (Ω m^2)	C_{dl} (F m^{-2})	R_1 x 10^4 (Ω m^2)	C_1 (F m^{-2})
-0.353	20.46	5.0	0.36	4.9
-0.468	4.96	5.3	0.69	3.2
-0.528	2.41	6.5	0.77	3.2
-0.564	1.54	8.4	0.77	3.4
-0.587	1.00	9.1	0.74	3.4
-0.601	0.74	10.4	0.61	3.7
-0.611	0.57	11.9	0.54	3.6
-0.617	0.38	17.2	0.53	3.9
-0.625	0.27	30.5	0.52	3.3

Figure 4.10 and Figure 4.11 show the potential dependence of charge transfer resistance (R_{ct}) and of the double layer capacitance (C_{dl}) for the HER reaction at solid and mesh cathodes, respectively.

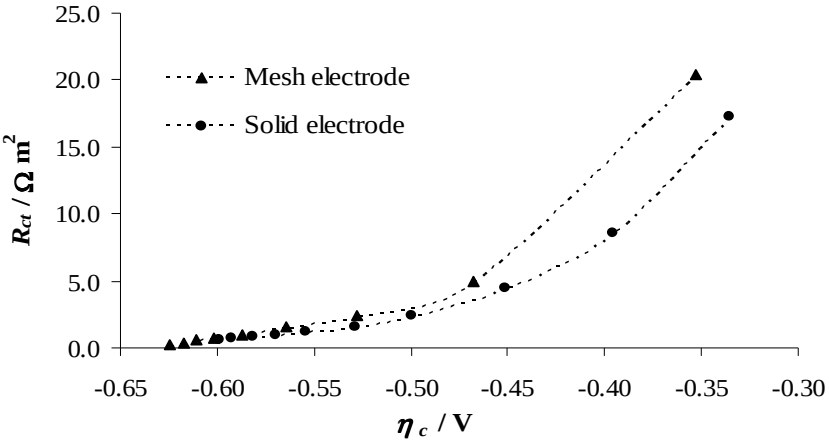

Figure 4.10 – Charge transfer resistance as a function of the applied overpotential, for HER on nickel electrodes (solid and mesh).

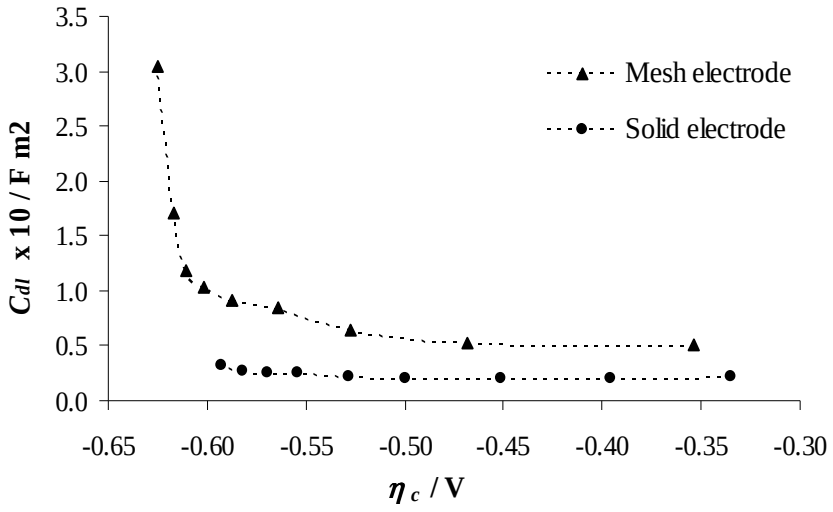

Figure 4.11 – Double layer capacitance as a function of the applied overpotential for HER on nickel electrodes (solid and mesh).

Figure 4.10 shows that the activation kinetics dominates and the charge transfer resistance (R_{ct}) is large at lower overpotentials. As the overpotential increases, R_{ct} decreases indicating faster reaction kinetics. Figure 4.11 shows that the double layer capacitance increases with the applied potential indicating an increase in the electrode activity. The electrochemical activity depends on the real surface area and electrodes with high specific surface area, with a rough surface, provide more sites for reaction than smooth electrodes. Kaninski et al. had observed a decrease of C_{dl} with the overpotential increase, which was associated to the occlusion of pores by the increasing presence of gas bubbles [20]. However, in the present work, the

bubble effects seem to be negligible at low current densities (25 A m^{-2} to $1.00x10^3$ A m^{-2}) where the Tafel lines are obtained.

A linear relationship is expected between the inverse of the charge transfer resistance (A=1/R_{ct}) and overpotential [4]:

$$\eta_c = -\frac{2.303 \times RT}{\alpha F}\left[\log\left(\frac{1}{R_{ct}}\right) + \log\left(\frac{\alpha F}{RT}\, j_0\right)\right] \qquad (4.11)$$

Figure 4.12 shows the inverse of charge transfer resistance (A) as a function of the applied overpotential (η_c) for the HER on both types of nickel cathodes. As expected from Eq. (4.11), the relationship between the inverse of charge transfer resistance and the overpotential is linear. From the slope and intercept of these plots the kinetic parameters can be determined and compared with the ones obtained from Tafel plots (Table 4.2).

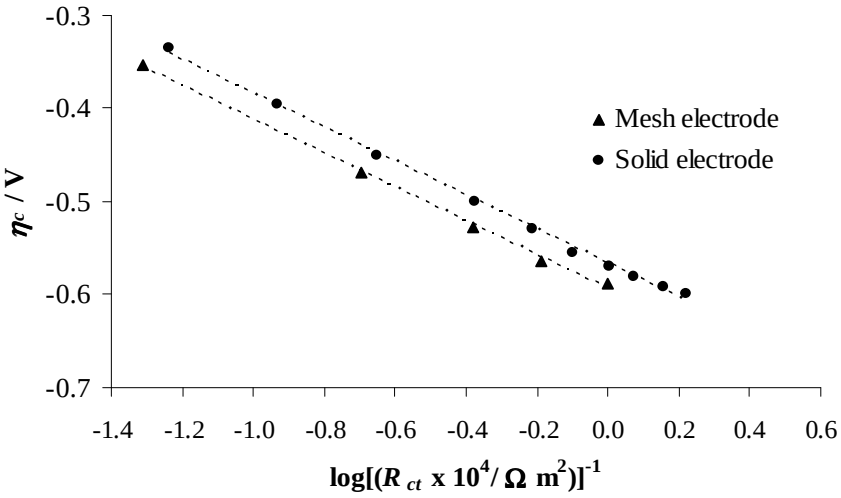

Figure 4.12 – Inverse of charge transfer resistance obtained from impedance data as a function of overpotential for the HER on nickel cathodes.

Table 4.6 – Tafel slopes, exchange current densities and charge transfer coefficients of HER at nickel solid and mesh nickel cathodes determined from the EIS analysis.

Electrode	**$-b$ (V dec^{-1})**	**α**	**j_0 (A m^{-2})**
Solid	0.183	0.377	6.34×10^{-9}
Mesh	0.182	0.379	4.32×10^{-9}

The kinetic parameters obtained from Eq. (4.11) and Figure 4.12 are given in Table 4.6. These are in agreement with the Tafel slopes obtained from the polarization curves – Table 4.2. Figure 4.13 shows the overpotential for the HER on nickel mesh cathodes a function of the logarithmic current density and the logarithmic of inverse of charge transfer resistance obtained from impedance data. The separation between these two plots should be equal to $\log\left(\frac{\alpha F}{RT}\right)$, Eq. (4.6) and Eq. (4.11). As a consequence, the exchange current density values are slightly higher when determined from the impedance analysis (Table 4.6).

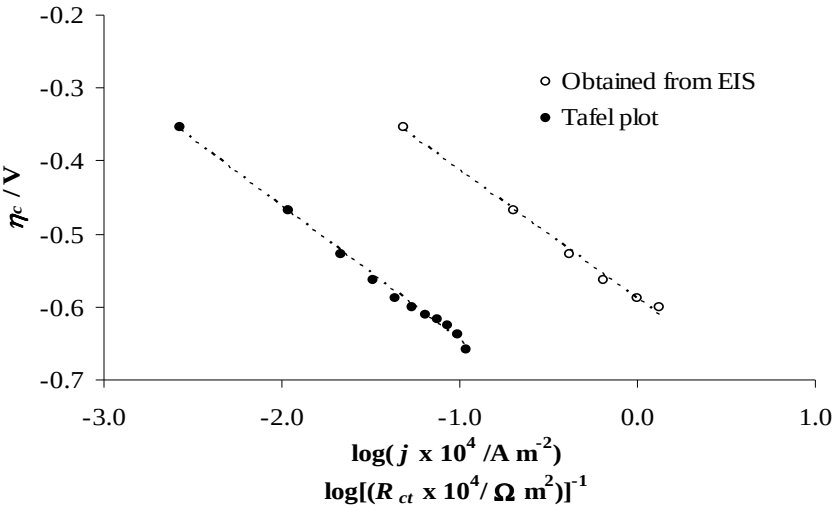

Figure 4.13 – Overpotential for the HER on nickel mesh cathode as function of the current density, and as function of the inverse of charge transfer resistance obtained from impedance data.

The comparison between the kinetic parameters of the solid and mesh electrodes shows a slightly faster reaction (better polarization characteristics) for the solid electrode – Table 4.2. Actually, the Tafel slope (*b*) for the solid electrode is higher than for the mesh electrode, which is in accordance with a lower activation polarization (Figures 4.2 and 4.4). This can be related to differences in the active surface area; where higher overpotentials are related to smaller active areas. The impedance analysis allows understanding better this difference in performance for the solid and mesh cathodes. Figure 4.10 shows a higher charge transfer resistance for the mesh electrode that can justify the slower electrochemical reaction kinetics at this electrode. For

lower applied potentials, the double layer capacitance of the mesh electrode is twice as much as compared to the solid electrode and this difference increases with the applied potential. Assuming $2.0x10^{3}$ F m^{-2} [19] as a reference value for the C_{dl}, the surface roughness for both electrodes can be obtained dividing C_{dl} by this ideal value. A surface roughness from 25 to 150 is obtained for the mesh electrode while for the solid electrode values between 10 and 15 are found. However, the electrode with higher surface roughness, i.e. the mesh electrode, is not the one with higher catalytic activity. In fact, the mesh electrode has a higher charge transfer resistance that can be due to a larger ohmic resistance in the pores of the mesh due to nickel hydride formation or related to the current distribution. From Tables 4.2 and 4.6, the values of the kinetic parameters obtained are similar and any of these two methods can be used to obtain the kinetic parameters of the HER at nickel cathodes, whenever the anode overpotential is negligible. Finally, the absence of anode related record in the impedance spectra confirms the negligible effect of the anode on the overall overpotential.

4.4.4. Impedance analysis of the mesh structure electrodes

As mentioned before, the Nyquist plot of both types of cathodes are different – Figure 4.4; namely the mesh electrode plot shows a high frequency second semi-circle. To test if this difference was related to the

mesh structure, i.e. ac penetration depth [26], the back and side areas of the electrode were coated with Teflon.

The cathodic overpotential of the partially coated mesh electrode was ploted as a function of current density and compared to the previous one, Figure 4.14.

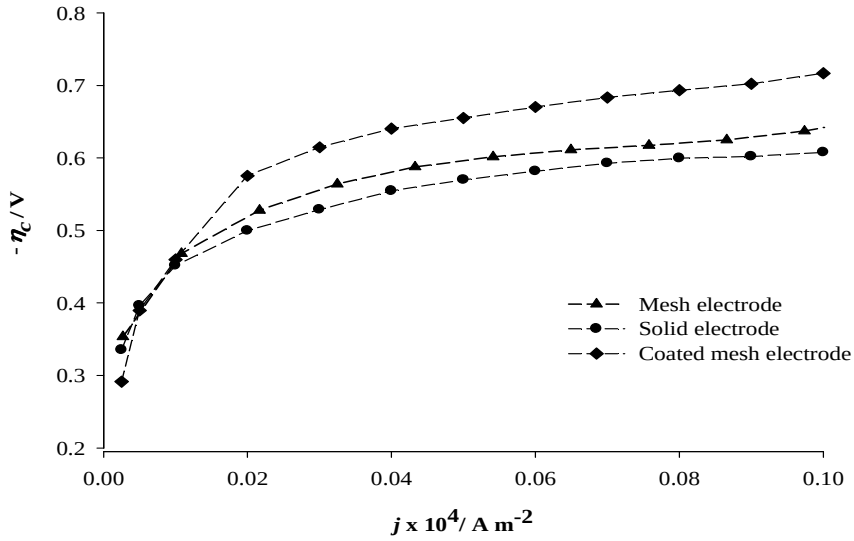

Figure 4.14 - Cathode overpotential as a function of the current density for solid, mesh and coated mesh electrodes.

As can be seen in Figure 4.14, the partially coated mesh cathode has a higher overpotential than the solid and mesh cathodes; this should be related to the lower electrode active area. The high frequency region of the impedance spectra for the partially coated mesh electrode is shown in Figure 4.15.

a)

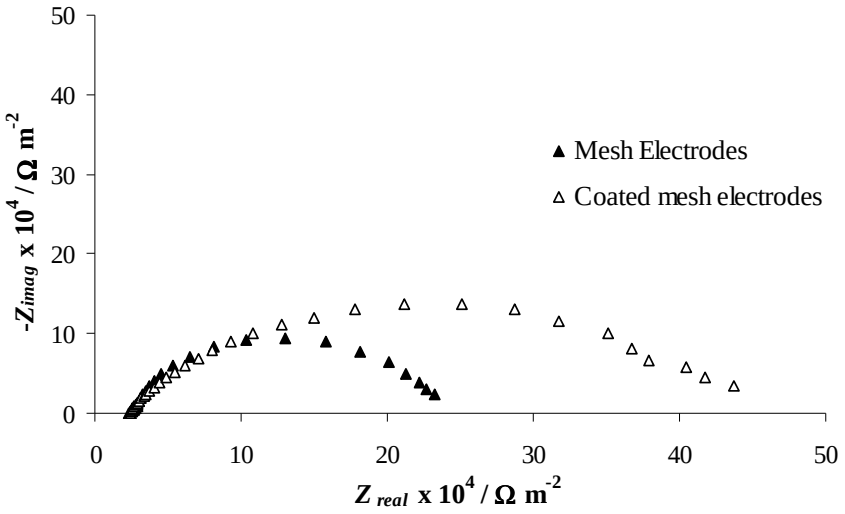

b)

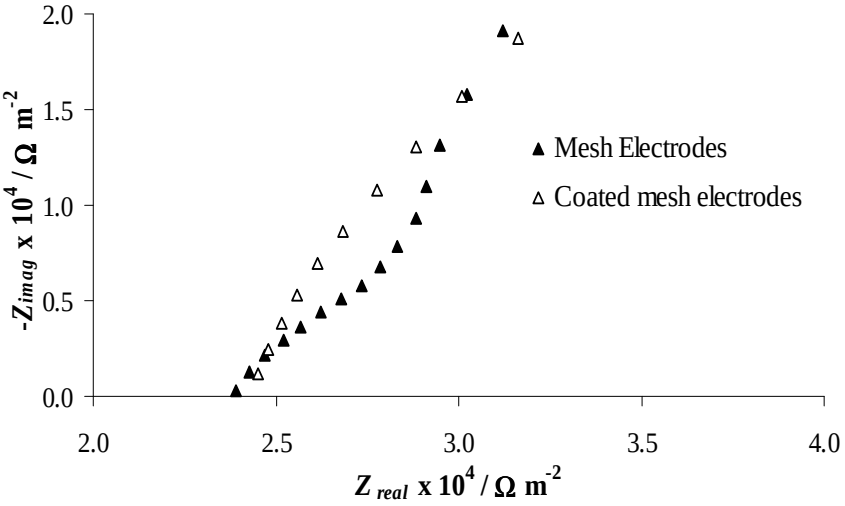

Figure 4.15 – Nyquist plots for the HER on the mesh and coated mesh nickel electrodes measured at 25 A m^{-2}: a) complete spectra and b) high frequency region.

Figure 4.15 shows that the high frequency semicircle disappeared for the coated mesh electrode. This means that the high frequency semicircle that appears on the non-coated mesh electrode should be related to the ac penetration depth in the mesh holes.

4.5. Conclusions

The so-called *k-factor* (linear approximation) and *Q-factor* (log relationship) analyses are widely used methods in the industry to assess the membrane and electrode overpotentials. Concerning the chlor-alkali process, the present study determines the hydrogen evolution reaction (HER) kinetic parameters at the cathode, under normal operation and assuming a negligible anode overpotential (much faster anode reaction). A Tafel analysis was performed to obtain the HER overpotential, exchange current density and Tafel slope. These values were compared to the ones obtained from the polarization curve (*k-factor* and *Q-factor*). Additionally, EIS analysis was also used to obtain the parameters of a chlor-alkali process electric analog.

Two different electrode morphologies were studied, solid and mesh. Mesh electrode allowed the reduction of the gap between electrodes from $12x10^{-3}$ m (solid electrode) to $5.5x10^{-3}$ m. Slightly higher electrode overpotential and significantly lower ohmic resistance were found for the mesh cathode; the lower ohmic resistance was related to the smaller electrode gap. This indicates that the electrode gap is the most relevant gain for the

process when using mesh electrodes. Moreover, a good agreement was found between the kinetic parameters for both mesh and solid electrodes and between the characterization methods used. The impedance spectra showed no record related to the anode, validating the assumption of negligible anode overpotential. The electrochemical impedance analysis of the cathode mesh electrode showed a second semicircle at high frequencies related to the mesh structure. Furthermore, it was concluded that the kinetic parameters of the cathode could be determined by EIS during operation without a reference electrode.

4.6. References

[1] - A.C. Dias, M. J. Pereira, L. Brandão, P. Araújo, A. Mendes, "Characterization of the chlor-alkali membrane process by EIS Part I- Ohmic resistance", *J. Electrochem. Soc.*, **157** (5), E75 (2010).

[2] - V.S. Bagotsky, in *Fundamentals of Electrochemistry*, 2nd edition, Chapter 15, 17 and 26, Wiley Interscience, New Jersey (2006).

[3] – B.E. Conway, B.V. Tilak, H. Angerstein-Kozlowska and M.A. Sattar, "Study of a decomposition hydride phase at nickel cathodes by measurement of open-circuit potential decay", *J. Electrochem. Soc.*, **130** (9), 1825-1836 (1983).

[4] – A. Lasia and A. Rami, "Kinetics of hydrogen evolution on nickel electrodes", J. *Electroanal. Chem.*, **294**, 123-141 (1990).

[5] – J.M. Jaksic, M.V. Vojnovic, N.V. Krstajic, "Kinetic analysis of hydrogen evolution at Ni–Mo alloy electrodes", *Electrochim. Acta*, **45**, 4151–4158 (2000).

[6] – N. Krstajic, M. Popovic, B. Grgur, M. Vojnovic, D. Sepa, "On the kinetics of the hydrogen evolution reaction on nickel in alkaline solution, Part I. the mechanism", *J. Electroanal. Chem.,* **512,** 16-26 (2001).

[7] – P. Elumalai, H.N. Vasan, N. Munichandraiah and S.A. Shivashankar, "Kinetics of hydrogen evolution on submicron size Co, Ni, Pd and Co- Ni

alloy powder electrodes by d.c. polarization and a.c. impedance studies", *J. Appl. Electrochem.*, **32**, 1005-1010 (2002).

[8] – N. V. Krstajic, V.D. Jovic, Lj. Gajic-Krstajic, B.M. Jovic, A.L. Antozzi, G.N. Martelli, "Electrodeposition of Ni- Mo alloy coatings and their characterization as cathodes for hydrogen evolution in sodium hydroxide solution", *International Journal of Hydrogen Energy*, **33**, 3676-3687 (2008).

[9] - T. F. O'Brien, T.V. Bommaraju and F.Hine, in *Handbook of Chlor-Alkali Technology – Volume I*, chapter 4, Springer, New York (2005).

[10] – B.V. Tilak, V.I. Birss, J. Wang, C.-P. Chen and S.K. Rangarajan, "Deactivation of thermally formed Ru/Ti Oxide Electrodes", *J. Electrochem. Soc.*, **148** (9), D112-D120 (2001).

[11] – Brian E. Conway and Gu Ping, "Surface Electrochemistry of the anodic Cl_2 evolution reaction at Pt" J. *Chem. Soc. Faraday Trans*, **86** (6), 923-930 (1990).

[12] – M. Thomassen, C. Karlsen, B. Borresen, R. Tunold, "Kinetic investigation of the chlorine reduction reaction on electrochemically oxidised ruthenium", *Electrochim. Acta*, **51**, 2909-2918 (2006).

[13] – P. Elumalai, H.N. Vasan, N. Munichandraiah and S.A. Shivashankar, "Kinetics of hydrogen evolution on submicron size Co, Ni, Pd and Co- Ni alloy powder electrodes by d.c. polarization and a.c. impedance studies", *J.Appl. Electrochem.*, **32**, 1005-1010 (2002).

[14] – K.L. Hardee, "A Simple procedure for evaluating membrane electrolyzer performance", *Modern Chlor-Alkali Technology*, **6**, 235-242 (1995).

[15] – R. O' Hayre, Suk- Won Cha, W. Colella and F. B. Prinz, in *Fuel Cell Fundamentals*, Chapter 7, Wiley, New York (2006).

[16] - Shalini Rodrigues, N. Munichandraiah and A. K. Shukla, "Kinetics of hydrogen evolution reaction on $Zr_{0.5}Ti_{0.5}V_{0.6}Cr_{0.2}Ni_{1.2}$ alloy in KOH electrolyte", Bulletin of Material Science, **23** (5), 383-391 (2000).

[17] – N. V. Krstajic, V.D. Jovic, Lj. Gajic-Krstajic, B.M. Jovic, A.L. Antozzi, G.N. Martelli, "Electrodeposition of Ni- Mo alloy coatings and their characterization as cathodes for hydrogen evolution in sodium hydroxide solution", *International Journal of Hydrogen Energy*, **33**, 3676-3687 (2008).

[18] - C.H. Hamann, A. Hamnett, W. Vielstich, in *Electrochemistry*, 2nd edition, Chapter 4 and 5, Wiley-VCH (2007).

[19] - T. F. O'Brien, T.V. Bommaraju and F.Hine, in *Handbook of Chlor-Alkali Technology – Volume I*, chapter 4, Springer, New York (2005).

[20] – B. V. Tilak, C.-P. Chen, "Generalized analytical expressions for Tafel slope, reaction rate and a.c. impedance for the hydrogen evolution reaction (HER): mechanism of HER on platinum in alkaline media", *J. Appl. Electrochem.*, **23**, 631-640 (1993).

[21] – N. Krstajic, M. Popovic, B. Grgur, M. Vojnovic, D. Sepa, "On the kinetics of the hydrogen evolution reaction on nickel in alkaline solution, Part II. Effect of temperature", *J. Electroanal. Chem.*, **512,** 27-35 (2001).

[22] - Y. Ogata, H. Hori, M. Yasuda, and F. Hine, "On the cathode behaviour and the cell voltage in NaOH solutions under elevated temperatures", *J. Electrochem. Soc.*, **135** (1), 76-83 (1988).

[23] - R.K. Shervedani, A. H. Alinoori and A. R. Madram, "Electrocatalytic activities of nickel-phosphorous composite coating reinforced with codeposited graphite carbon for hydrogen evolution reaction in alkaline solution", *Journal of New Materials Electrochemical Systems*, **11**, 259-265 (2008).

[24] – R.M. Abouatallah, D. W. Kirk and J.W. Graydon, "Impedance study of nickel cathode reactivation by vanadium during hydrogen evolution in alkaline water", *Electrochemical and Solid-State Letters*, **5**, E9-E12 (2002).

[25] – A. Lasia, "Impedance of porous electrodes", *J. of Electroanal. Chem.*, **397,** 27-33 (1995).

[26] - L. Birry and A. Lasia, "Studies of the hydrogen evolution reaction on Raney nickel–molybdenum electrodes", *J.Appl. Electrochem.*, **34**, 735–749 (2004).

[27] – C. Hitz, A. Lasia, "Experimental study and modeling of impedance of the her on porous Ni electrodes", *J. Electroanal. Chem.*, **500**, 213-222 (2001).

Chapter 5 - Benchmarking methodology for Ion-Exchange Membranes used in the Chlor-Alkali Process[3]

5.1. Abstract

As one of the most energy intense electrochemical processes, the chlor-alkali industry is been made many efforts to reduce the specific energy consumption. Nowadays, great energy savings can be obtained by using high performance membranes. However, in a plant where the operational upsets are common the performance and durability of these membranes can be severely affected. It was developed a benchmarking methodology based on the average cost history of the chlorine produced. This methodology also permits to decide when it is the right moment for membrane replacement.

Three types of membranes, from two major suppliers, were installed in three electrolyzers. The overall performance of the plant was evaluated monthly and the total process costs per ton of chlorine calculated for each electrolyzer. The energy cost was shown to be the major factor affecting the total process cost, representing more than 90 % of this cost. Regarding the durability, maintenance, energy and fixed costs the membrane with the

lowest average cost per ton of chlorine produced was a high voltage and high strength membrane.

[3]A.C. Dias, P. Araújo and A. Mendes, Journal of Applied Electrochemistry (2010) – Submitted.

5.2. Introduction

The chlor-alkali process involves the electrolysis of a sodium chloride solution (brine) to produce chlorine, hydrogen and caustic soda. The chlor-alkali industry is one of the largest electrochemical industries in the world. Chlorine and caustic soda are key raw materials in the manufacturing of polymers and as intermediates in other chemical, pharmaceutical (85 % of medicines use chlorine) and crop protection industries [1]. The world chlorine production capacity was 62.8 million metric tons per year in 2008, where Europe represents ca. 20 % [2].

There are three different chlor-alkali processes: the mercury cell, the diaphragm cell and the membrane cell. However, over the last thirty years remarkable improvements have been made on the membrane cell process and better performing ion-exchange membranes were developed [3,4].

The membrane cell process uses an ion-exchange membrane as a permselective barrier between anode and cathode compartments. A saturated brine solution is fed to the anode where chlorine gas is produced. The sodium ions migrate through the membrane to the cathode compartment and combine with the hydroxyl ions produced from the water reduction that happens with the generation of molecular hydrogen. The ion exchange membranes are generally composed by a tetrafluoroethylene matrix containing fixed ionic groups [3-5]. The fixed sites must prevent the transport of anions (i.e. OH^-,

Cl^-) through the membrane and so cation exchange groups are used. Carboxylic and sulfonic groups are used as fixed sites on the anode and cathode sides of the membrane, respectively. A high performance ion-exchange membrane must have the following characteristics: high transport selectivity, high conductivity, high mechanical strength and good chemical stability [4, 5].

During operation, these ion exchange membranes are subject to tentering stresses that can originate physical damages such as tears, pinholes, and blisters [6]. Handling and installation, conditions during operation (e.g. stable voltage), frequency of shutdowns, electrolyzer design and robustness of the electrode coatings have a great importance on the membrane performance and durability [4-6]. Excellent brine quality is also required to avoid the accumulation of impurities in the membrane that can disrupt its structure and chemical integrity and that can ultimately cause mechanical damages. Mechanical damages or physical relaxation of the membrane structure leads to the degradation of the permselectivity (back migration of sodium hydroxide ions) and the loss of current efficiency.

Nowadays, there are three main suppliers of ion-exchange membranes for the chlor alkali industry: Asahi Glass Company (Flemion™), Dupont (Nafion®) and Asahi Kasei Corporation (Aciplex™) [4]. They have been developing cation-exchange membranes with improved energy savings and

tolerance to operational upsets and impurities [3-4]. Two classes of membranes can be found considering their main characteristics and application, named low voltage and high strength membranes.

The membrane cell performance is affected by the current and potential efficiencies [4]. The potential efficiency depends mainly on the membrane ohmic resistance and on the electrodes activity (overpotential). While the potential efficiency is characterized and evaluated from the polarization curve, the current efficiency is a more complex parameter that relies on the material balance of the chemical species involved in the electrolysis [4].

The major cost component in the chlor-alkali industry is the energy consumption that depends upon the electrolyzer design, the type of membrane used, brine quality, and operating conditions. This way, the selection of the adequate membrane to install in an electrolyzer is a complex and high relevant decision that should balance operating and fixed costs. A low voltage membrane can be a good choice for a plant with high brine quality or for a plant with high electrical energy costs. On the other hand, high strength membranes should be considered in a plant where the operational upsets are more frequent.

This work studies the performance history of three types of ion exchange membranes and estimates the corresponding average cost history of

chlorine produced. The contribution of energy, maintenance and fixed costs were determined monthly as well as the average cost history per ton of chorine produced. It is proposed a membrane benchmarking methodology and a methodology for determining the best instant for replacing a given set of membranes.

5.3. Experimental section

An electrolyzer is formed by a set of several individual membrane cells. Two types of electrode arrangements can be used in the chlor-alkali industry to connect electrically the individual electrolytic cells; monopolar and bipolar [4]. In a bipolar cell arrangement the individual cells, which are called elements, are electrically in series and the electrolyzers are connected in parallel. In a monopolar cell arrangement the elements are connected in parallel and the electrolyzers in series [4]. The studied plant has a bipolar arrangement and the evaluation of electrolyzer performance can be done individually. This way, the three different sets of membranes (M_1, M_2 and M_3) were installed in three electrolyzers (E_1, E_2 and E_3) as shown schematically in Figure 5.1.

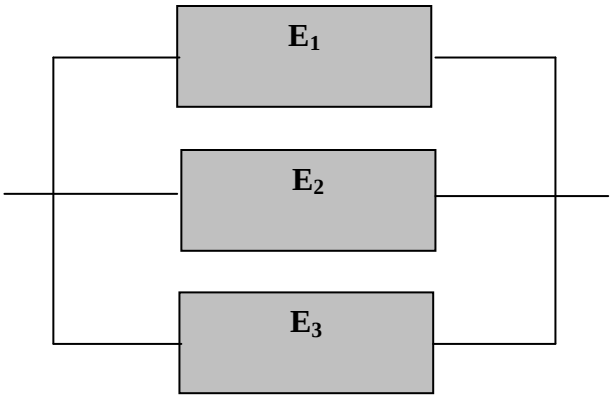

Figure 5.1 - Schematic representation of a bipolar plant where three types of membranes (M_1, M_2 and M_3) were installed in three different electrolyzers.

The set of membranes installed in electrolyzer E_3 have higher mechanical strength than the ones installed in electrolyzers E_1 and E_2 The comparative voltage and mechanical strength of the membranes used, provided by the producers, are schematically represented in Figure 5.2 [4, 6, 7].

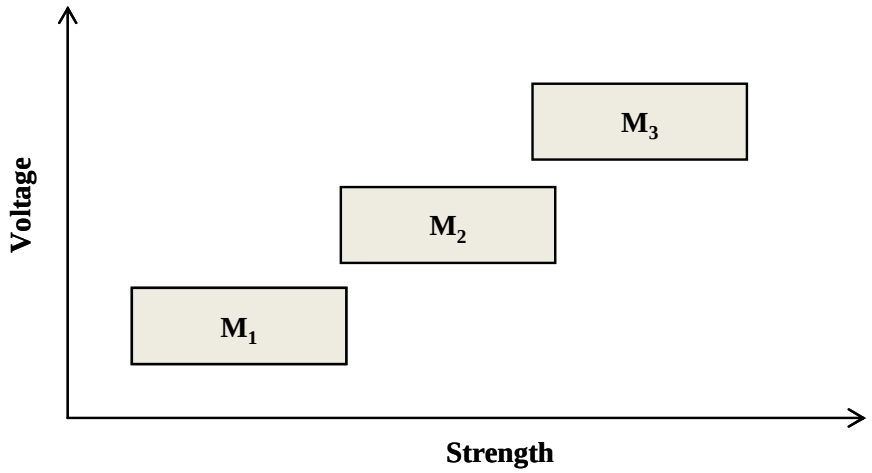

Figure 5.2 - Schematic representation of the comparative voltage and mechanical strength of membranes M_1, M_2 and M_3.

The supplier defines M_1 and M_2 as high performance membranes with low voltage. M_2 has higher tensile strength than M_1 indicating that this last should have a higher mechanical strength. In these membranes the type of reinforcement is different; M_1 uses a cloth with sacrificial fibres while M_2 uses a stronger cloth without sacrificial fibres [4, 6, 7]. The type of construction and reinforcement of M_3 is different from membranes M_1 and M_2. It is expected that membranes M_3 operate with higher voltage and have higher mechanical strength than membranes M_1 and M_2 (Figure 5.2).

The performance of a membrane cell is related to the current and potential efficiencies. The current efficiency is the ratio of the amount of chlorine produced to the expected amount of chlorine produced that is obtained from the Faraday's law of electrolysis [4]. The flow rate of chlorine produced was obtained from the material balance to the chemical species (Cl^-, Cl_2, Na^+ and HO^-) in the anode compartment, since it is very difficult to determine directly the chlorine gas molar flow rate [4]. The molar flow rates of sodium chloride, dissolved chlorine and byproducts present in the feed and exit solutions (NaCl, Na_2CO_3, NaHO, Na_2SO_4, $NaClO_3$) as well as the gas phase oxygen (electrochemically and chemically produced) and chlorine concentrations were then routinely recorded. The chlorine current efficiency was computed according to the method described elsewhere [4].

The potential efficiency was evaluated based on the *j-V* curves (polarization curve) obtained during the normal operation of the electrolyzers. Since the operating voltage depends on the outlet electrolytes concentration and temperature, these variables were also recorded daily. The overall efficiency, which is the product between the current and potential efficiencies, was obtained and used to calculate the specific energy consumption (energy consumption per ton of chlorine produced). The average cost per ton of chlorine was assessed based on the energy, fixed and maintenance costs after filtering the databases from irrelevant measurements.

5.4. Results and discussion

The choice of the most adequate membrane for a particular plant should be done considering the history of each factor affecting the total process costs. As mentioned before, two classes of membranes can be considered; low voltage and high strength. The low voltage membranes are more suitable for zero gap cells [4] and they are more sensitive to damage. In a plant where the operating upsets are frequent and the brine quality is beneath more robust membranes should be considered.

Electrolyzer overall performance

The potential efficiency of the chlor-alkali process is often

characterized by the *k-factor* method that involves the fitting of current density and voltage data. This method allows the differentiation between changes in electrodes overvoltage and in the membrane resistance; i.e. the slope of the polarization curve (k) is associated to the membrane resistance and the intercept voltage (V_0) is related to the electrodes performance [4, 8]:

$$V = k \times j + V_0 \tag{5.1}$$

where j is the operating current density and V is the cell voltage. The *k-factor* method can be used to assess membrane and electrodes problems [8]. Figure 5.3 shows the polarization curves for electrolyzer E_1 (M_1 membranes) obtained over two years of operation.

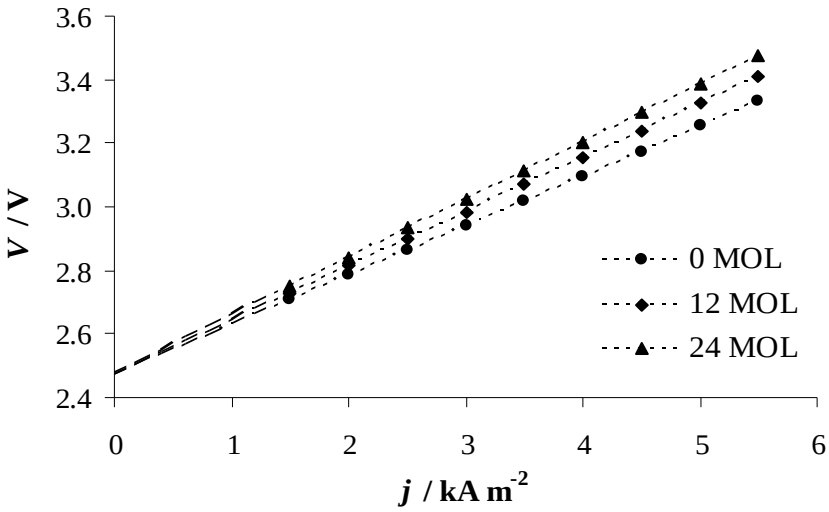

Figure 5.3 - Polarization curves obtained at 0, 12 and 24 months online (MOL) for the membrane M_1, electrolyzer E_1 – lines were introduced to improve readability.

Figure 5.3 shows that the voltage intercept changes little over time whereas the slope changes significantly. As the voltage intercept is nearly constant, the slope can be computed from the cell current density and voltage. This value can provide an early indication of membrane problems in the plant. However, V_0 must be determined frequently to check for any deviation or electrodes problems.

Table 5.1 shows the dimensionless slope of the *j-V* curves of the membranes studied at the beginning of operation. Due to confidentiality reasons all the values presented below are dimensionless. The dimensionless slope was defined as:

$$k^* = \frac{k - k_{ref}}{k_{ref}} \tag{5.2}$$

where k_{ref} is the reference slope took as the initial k value for membrane M_1.

Table 5.1 – Dimensionless slope of the polarization curve (k^*) for each type of membrane at the beginning of operation (month 0).

M_1	0.000
M_2	0.039
M_3	0.089

The dimensionless slope of the polarization curves follows $M_1 < M_2 < M_3$ and indicates the contribution of the membrane to the process voltage. This

sequence is in agreement to the producer's information, Figure 5.2. In an industrial plant the dimensionless slope (k^*) tends to increase with time and the rate of the slope variation depends on the type of membrane. Figure 5.4 shows the dimensionless slope history for each type of membrane.

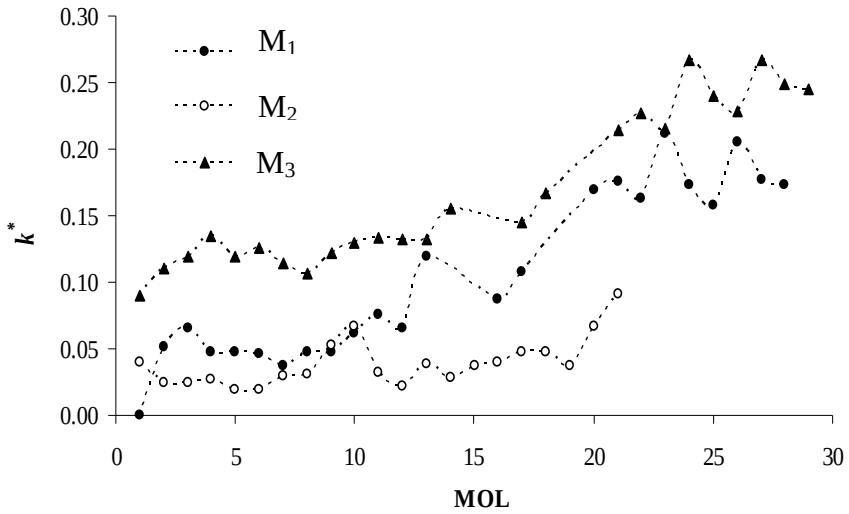

Figure 5.4 – Dimensionless slope of polarization curves as a function of months online for each type of membrane – lines were introduced to improve readability.

Figure 5.4 shows a higher dimensionless slope (k^*) rate increase after 16 MOL (months online) for membrane M_1 and after 17 MOL for membrane M_3, which corresponds to the same moment in real time. On the other hand, the electrolyzer corresponding to membrane M_2 began operating 6 month earlier than membranes M_1. These membranes were then replaced at the same moment as membranes M_1 and M_3 started experiencing a higher polarization

slope. Since the polarization slope increase happened simultaneously for the two electrolyzers this should be assigned to a brine quality change or to operational upsets. Unexpectedly, membrane M_2 supposedly with a higher mechanical strength than M_1 failed after 21 months online. As expected, a higher dimensionless slope (k^*) of the polarization curve is observed for the high strength membrane M_3.

In a parallel electrolyzer configuration (bipolar cell) the operating current density is distributed through each electrolyzer depending on its electrical resistance – see Figure 5.1. Since we are operating in a parallel configuration, to be able to compare the potential efficiency of different electrolyzers it is a normal procedure to consider a standard current density (j_{ref}) – 5 kA m^{-2} [4]. Based on this current density value it is possible to compute the corresponding corrected voltage from the *j*-*V* curve for each electrolyzer. The temperature and caustic concentration have a significant effect on the cell voltage. In practice these parameters can vary over time and between electrolyzers and therefore correction factors are often applied. The corrected voltage (V_{norm}) is given by [4]:

$$V_{norm} = V_0 + (V - V_0)\frac{j_{ref}}{j} + \frac{j}{j_{ref}}\left\{F_T(T - T_{ref}) - F_{[NaOH]}([NaOH] - [NaOH]_{ref})\right\} \quad (5.3)$$

where $F_{[NaHO]}$ and F_T are the correction factors for the caustic concentration ([NaHO]) and temperature (T), respectively. $[NaOH]_{ref}$ and T_{ref} are the

reference caustic concentration and temperature, respectively. These correction factors are 10 mV K^{-1} for temperature and 17 mV $wt.\%^{-1}$ for caustic concentration [4]. Temperature usually varies between 85 ºC - 90 ºC and the caustic concentration may vary around 0.5 wt.% among electrolyzers and as a function of time [4]. The brine concentration has normally a non significant effect on the cell voltage and was not taken into consideration [4]. Figure 5.5 illustrates the dimensionless corrected voltage for each type of membrane as a function of month online. The dimensionless corrected voltage was defined as:

$$V_{norm}{}^{*} = \frac{V_{norm} - V_{norm,ref}}{V_{norm,ref}} \tag{5.4}$$

where $V_{norm,ref}$ is the reference corrected voltage took as the initial V_{norm} value for membrane M_1.

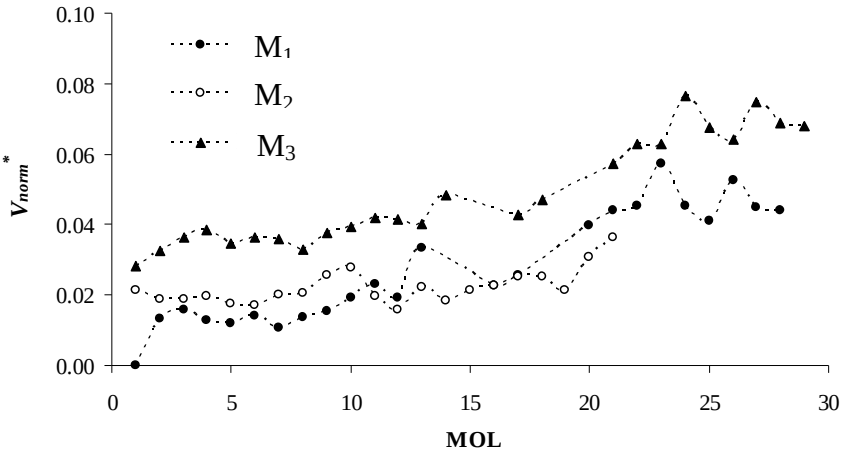

Figure 5.5 – Dimensionless corrected voltage as a function of the month online – lines were introduced to improve readability.

As shown in Figure 5.5, membrane M_1 exhibits lower dimensionless corrected voltage than M_2 and M_3. This was expected since the corresponding polarization curves exhibit a voltage intercept (related to the electrodes overpotential) that is almost constant as a function of time for each electrolyzer; this way, the voltage history for each electrolyzer has the same trend as the polarization slope history (related to the membrane ohmic resistance). The dimensionless corrected voltage increases as a function of time due to physical damage of the membranes and impurities accumulation [4-5]. In terms of potential efficiency, M_1 membrane proved to be the best membrane, exhibiting the lowest voltage over time – Figure 5.5.

In chlor-alkali industry the specific energy consumption is one of the most relevant parameters to the total process cost. The specific energy consumption is related to the cell voltage and to the current efficiency. The main reason for the loss of current efficiency is the back migration of sodium hydroxide ions from the cathode to the anode compartment through the permselective membrane [4-5]. As mentioned before, the current efficiency degradation is often related to the accumulation of impurities in the carboxylic layer of the membrane and depends on the structure (e.g. the type of reinforcement, membrane thickness) and on the physicochemical properties of the membrane. The current efficiency data can give information on the process performance as well as it gives an indication about the physical condition of the membranes. Figure 5.6 plots the dimensionless chlorine current efficiency as a function of time; the dimensionless chlorine current efficiency was defined as:

$$\xi^{*}_{Cl_2} = \frac{\xi_{Cl_2} - \xi_{Cl_2,ref}}{\xi_{Cl_2,ref}} \tag{5.5}$$

where $\xi_{Cl_2,ref}$ is the reference chlorine current efficiency, equal to the initial ξ_{Cl_2} value for membrane M_1.

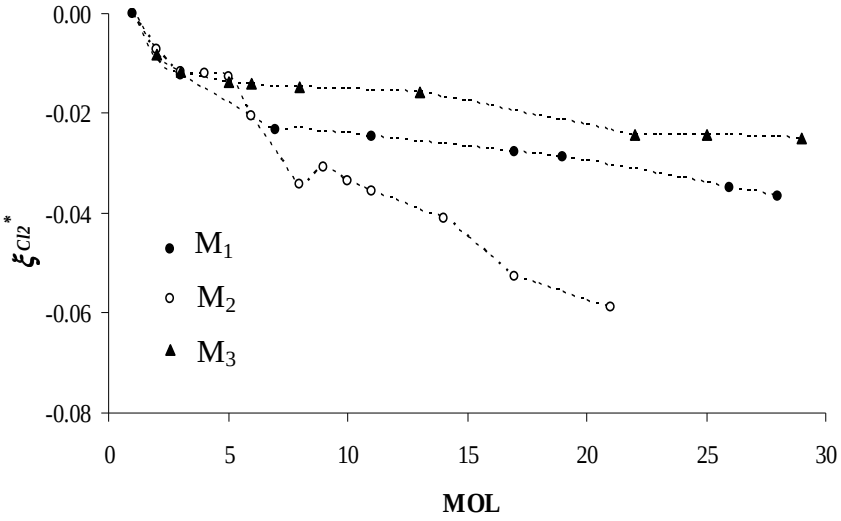

Figure 5.6 – Dimensionless chlorine current efficiency ($\xi^*_{Cl_2}$) as a function of months online (MOL) – lines were introduced for improving the readability.

The decline of the dimensionless chlorine current efficiency ($\xi^*_{Cl_2}$) depends on the type of membrane (Figure 5.6). In the present work the operating conditions were the same for all electrolyzers and so the relative current efficiency changes should be related to the tolerance of each type of membrane to operational upsets. A premature and quick current efficiency loss was observed for membrane M_2 (electrolyzer E_2) that showed mechanical damages (holes) after two years online. M_3 membrane, which is the membrane with the highest strength, also showed the highest current efficiency (the lowest $\xi^*_{Cl_2}$ slope – Figure 5.6); membranes with high mechanical strength tend to be more resistant to operational upsets.

Economic analysis

The total process cost, T_c, is the sum of the fixed costs, F_c, and the operating costs, O_c and must be determined for each electrolyzer:

$$T_c = F_c + O_c \tag{5.6}$$

The fixed cost (F_c) comprehends the membranes and other fixed costs and is given by:

$$F_c = n \times F_m + F_k \tag{5.7}$$

where n is the number of membranes in an electrolyzer and F_m the cost of each membrane; F_k is other fixed costs. The operating costs comprise the maintenance, raw materials and energy consumption. As the main goal of the present work is to compare the total process cost for each electrolyzer as a function of time, and since it is assumed that raw materials costs are approximately the same for all electrolyzers, these costs will not be taken into account. The specific energy consumption (P_c) is the main operating cost (O_c) of a chlor-alkali plant and is given by [4]:

$$P_c = E_q \frac{V}{\xi_{Cl_2}} \tag{5.8}$$

where E_q is the electrochemical equivalent of chlorine, ξ_{Cl_2} is the chlorine current efficiency and V the voltage across the electrolyzer. The dimensionless specific energy consumption was estimated for each electrolyzer taking into consideration the dimensionless corrected voltage

shown in Figure 5.5 and the dimensionless chlorine current efficiency data presented in Figure 5.6. Figure 5.7 shows the dimensionless specific energy consumption of each electrolyzer as a function of months online; the dimensionless specific energy consumption was defined as:

$$P_c^* = \frac{P_c - P_{c,ref}}{P_{c,ref}} \tag{5.9}$$

where $P_{c,ref}$ is the reference specific energy consumption, equal to the initial P_c value for membrane M_1.

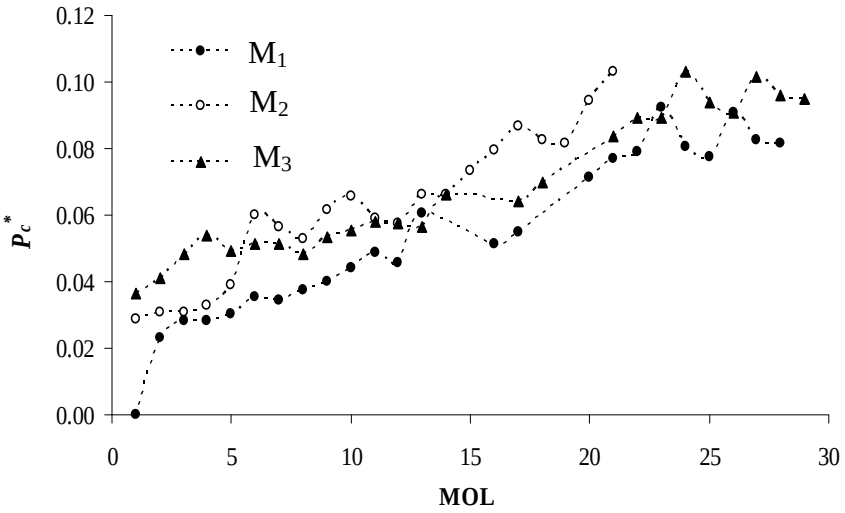

Figure 5.7 – Dimensionless specific energy consumption per ton of chlorine (corrected for 5 kA m^{-2}, 32 % NaOH and 90 ºC) for each electrolyzer as a function of months online (MOL) - lines were introduced for improving the readability.

Depending on the physicochemical properties of each type of membrane its current and potential efficiency deterioration is different and so the specific energy consumption history. The specific energy consumption increases 0.3 % per 10 mV of potential increase whereas it is directly affected by the current efficiency degradation – Eq. (5.8).

Over the operating lifetime, to keep the electrolyzers running properly some maintenance work is needed to substitute damaged membranes and electrodes. The damaged cells are detected from the individual cell voltage system analysis. A physical damaged membrane must be replaced as soon as possible in order to avoid electrodes corrosion. Figure 5.8 shows the dimensionless maintenance cost per month of operation for each electrolyzer that was defined as:

$$M_c^* = \frac{M_c}{M_{c,ref}} \tag{5.10}$$

where M_c is the specific maintenance cost and $M_{c,ref}$ is the reference specific maintenance cost, equal to M_c value for electrolyzer E_1.

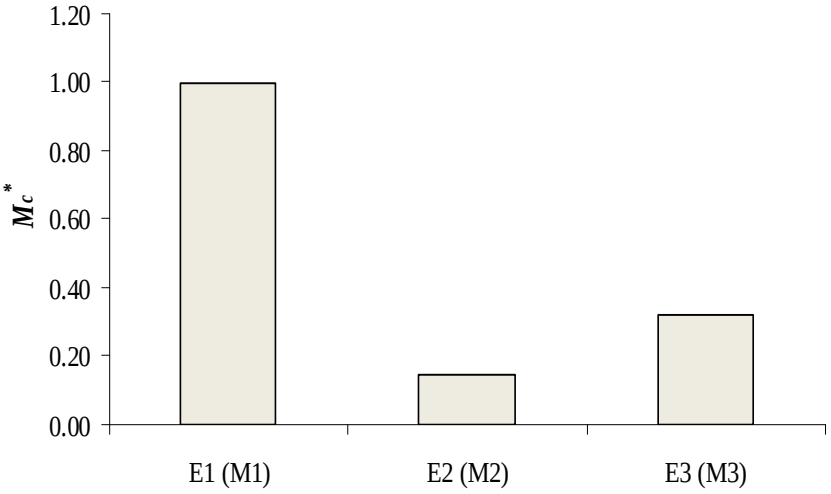

Figure 5.8 – Dimensionless average maintenance costs per month of operation for each electrolyzer.

Figure 5.8 shows that there is a significant difference between the dimensionless specific maintenance cost of electrolyzers E_1 (membrane M_1) and E_3 (membrane M_3); the more robust membrane (higher strength, M_3) shows low dimensionless specific maintenance costs.

The operating cost (O_c) during the lifetime of the membranes was estimated taking into account the energy (E_c) and the maintenance costs (M_c).

$$O_c = \sum_{t=0}^{MOL} E_c \; + M_c \tag{5.11}$$

$$E_c = P_c \times m_{Cl_2} \times \frac{e}{\xi_{rectifier}} \tag{5.12}$$

where *MOL* is the lifetime in months online, m_{Cl_2} the mass of chlorine produced, *e* the price of electricity (AC) and $\xi_{rectifier}$ the rectifier efficiency.

Figure 5.9 shows the dimensionless average energy cost per ton of chlorine produced for each type of membrane as a function of months online. The dimensionless average specific energy cost was defined as:

$$E_c^{\,*} = \frac{E_c - E_{c,ref}}{E_{c,ref}} \tag{5.13}$$

where $E_{c,ref}$ is the reference average specific energy cost, equal to the initial E_c value for membrane M_1.

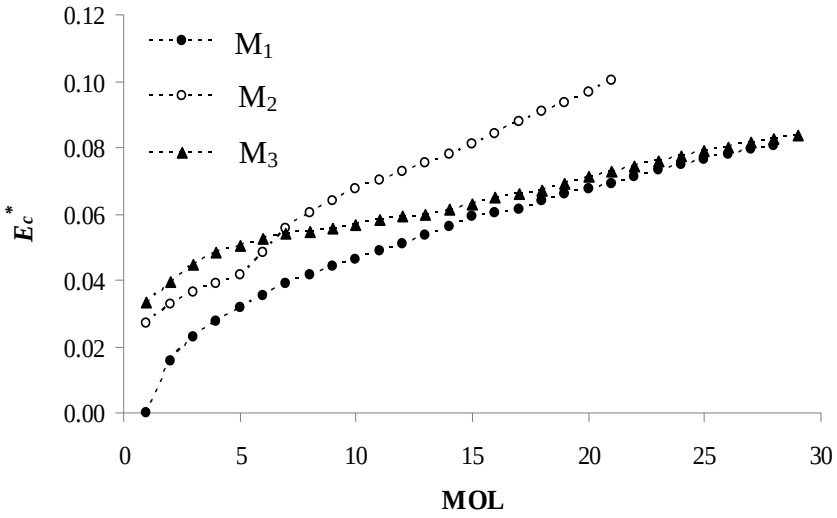

Figure 5.9 – Dimensionless average energy cost per ton of chlorine produced for membranes M_1, M_2, M_3 as a function of months online (MOL).

As expected, the lowest voltage membrane (M_1) has the lowest dimensionless average specific energy cost and the more robust membrane (higher strength, M_3) has less maintenance cost, Figure 5.8 and Figure 5.9. The interaction between these two values determines the total process cost.

The average total process cost per ton of chlorine produced (T_c) was obtained dividing the accumulated total process costs (operating plus fixed costs) by the accumulated mass of chlorine produced, within the lifetime of a set of membranes. The best instant to replace a set of membranes can now be easily obtained when the history of T_c reaches a minimum. Figure 5.10 shows the dimensionless T_c history for the studied membranes. The steps in the curves (cf. Figure 5.10b) are related to the maintenance costs, which are assigned to a given month. The dimensionless T_c history was defined as:

$$T_c^* = \frac{T_c - T_{c,ref}}{T_{c,ref}} \tag{5.14}$$

where $T_{c,ref}$ is the reference average specific total process cost, equal to the initial T_c value for membrane M_1.

a)

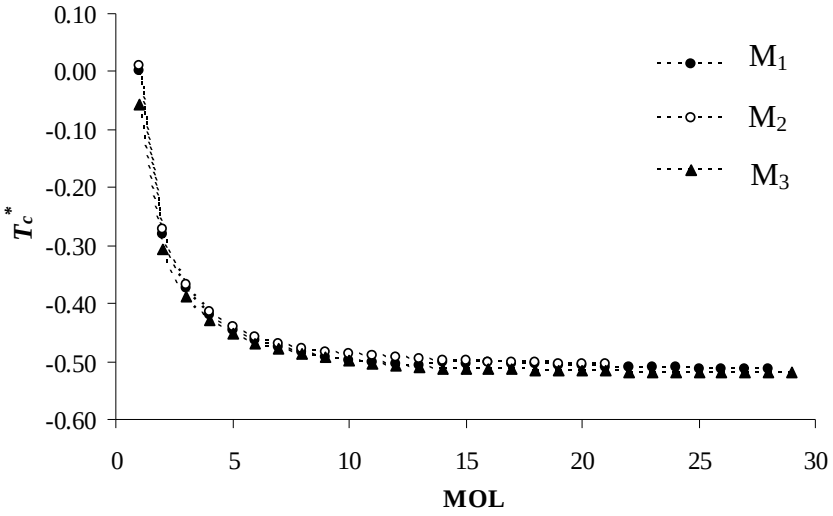

b)

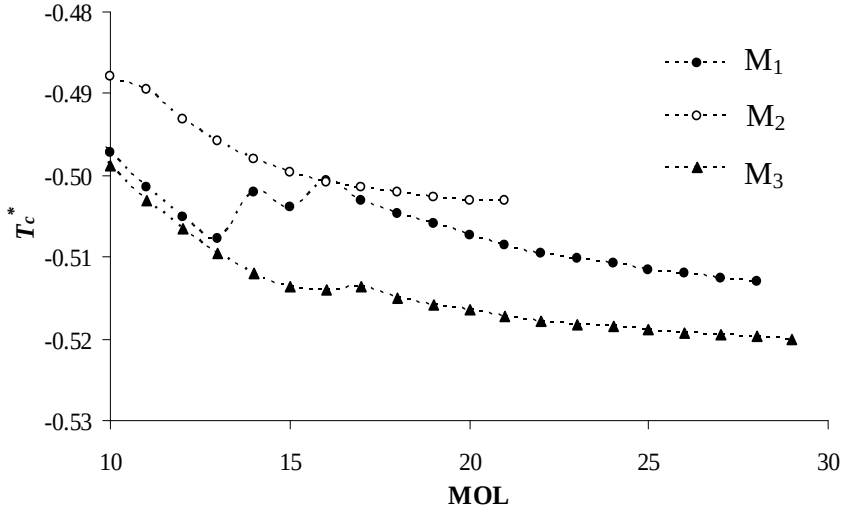

Figure 5.10 –Dimensionless total process costs per ton of chlorine as a function of months online (MOL): a) complete plot and b) zoom in for the last months of operation. - lines were introduced for improving readability.

From Figure 5.10 it can be seen that T_c * tends to a minimum, since the initial membrane cost (fixed costs) is being amortized and the operating costs increase. The average energy cost represents more than 90 % of the total process cost after 10 months online. Membranes M_3 have the lowest fixed and maintenance costs but they need higher operating voltage. Despite, these membranes proved to produce the lowest average chlorine cost. On the other hand, M_1 membrane have the highest fixed and maintenance costs but they need the lowest operating voltage. Membranes M_2 failed prematurely showing then the highest dimensionless average chlorine cost, Figure 5.11. As a result, M_2 membrane is not adequate to this plant because it is more susceptible to physical and impurity damages. As membranes M_1 and M_3 are still running, the evolution of T_c was simulated up to 48 months of operation - Figure 5.11; it is normally expected that a membrane last 48 months. This simulation was made assuming a linear increase on the specific energy consumption accordingly to Figure 5.7.

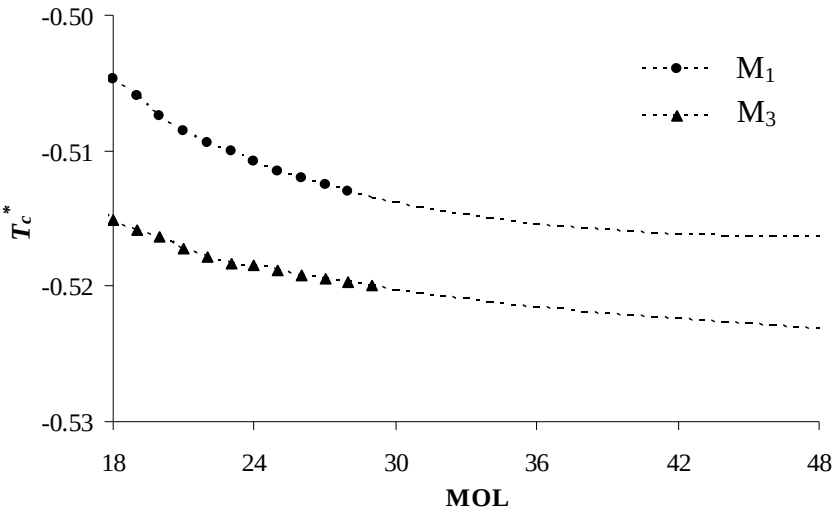

Figure 5.11 – Dimensionless average total process costs per ton of chlorine as a function of months online (MOL) for membranes M_1 and M_3.

Figure 5.11 shows that the dimensionless total process costs levels out after 40 MOL for membrane M_1 and after 44 MOL for M_3 membranes, whereas a minimum would be achieved for more than 48 MOL. This simulation assumes that no extra planned maintenance work is needed; a decision concerning membranes replacement must be taken whenever an intervention is needed. The historic record of membrane M_1 indicates that it should be replaced in average after 35 months of operation. In this case, membranes M_3 have the lowest average total process cost per ton of chlorine, being 1.5 % cheaper than for membrane M_1.

5.5. Conclusions

A benchmarking methodology of ion exchange membranes for the chlor-alkali industry was presented. This methodology was based on the history of the average total process cost per ton of chlorine produced and it was applied to three different types of membranes. The methodology revealed to be powerful for comparing membranes as well as for finding when a given membrane set should be replaced due to progressive deterioration.

The chlorine average cost calculation was based on the current and the potential efficiencies. Two classes of membranes were considered, namely low voltage and high strength membranes. Despite its higher voltage, the high strength membrane M_3 was found to originate the lowest chlorine specific cost, about 1.5 % lower than membrane M_1, a low voltage type membrane; this was mainly related to the higher maintenance cost.

5.6. References

[1] - www.eurochlor.org/chlorine-industry-facts-2007, accessed in May 2010.

[2] - worldchlorine.com/, accessed in July 2010.

[3] - T. Navin, "Membrane Cell Technology - State of the art industry", Eltech Systems Corporation, 2002.

[4] - T. F. O'Brien, T.V. Bommaraju and F.Hine, in *Handbook of Chlor-Alkali Technology – Volume I and IV*, Springer, New York (2005).

[5] - H. Strathmann, in *Ion-Exchange Membrane Separation Processes*, Chapter 3, Membrane Science and Technology Series, 9, Hungary (2004).

[6] - R. Theobald, "Mechanical aspects of membrane operation", Paper presented at the Eltech Seminar, October, Cleveland, Ohio (2000).

[7] - Technical information, Introduction of Flemion Membranes, Asahi Glass Co., Ltd (Flemion Seminar 2002).

[8] - K.L. Hardee, "A Simple procedure for evaluating membrane electrolyzer performance", *OxyTech Systems, Inc*.

Chapter 6 – General Conclusions and Future Work

6.1. General Conclusions

The research described in this thesis concerns a better understanding of the chlor-alkali membrane process. This aims to develop strategic knowledge at CUF-QI and enhance its negotiation capabilities.

A membrane characterization experimental setup and an electrochemical membrane reactor setup were developed and tested. The former unit was used to measure the membrane permselectivity and proved to perform well when compared with values obtained in a well - known laboratory. Some of the critical parameters of the membrane reactor were compared with reference values to determine its performance. Good agreement was found for the cell temperature, *j-V* curves and membrane conductivity. A malfunction was detected in the hydrogen flowmeter. Additionally, it was possible to reproduce one of the most important damages occurring in the industrial process - blistering. It was concluded that membrane blistering causes the ohmic resistance to increase significantly.

The impedance spectroscopy technique was applied *in situ* to the experimental membrane reactor to investigate the contribution of each component on the cell performance. The effect of the most important parameters on the ohmic resistances was discussed. It was concluded that the

main factors affecting the cell potential are the outlet temperature and brine concentration. The cell potential (at constant current density) was minimized at high temperatures and at high brine concentrations. However, it was found that the membrane conductivity was more affected by the caustic concentration (2.1 mS cm^{-1} /wt.% NaOH) than by the brine concentration (1.7 mS cm^{-1}/wt.% NaCl). In the present work, the electrolyte resistance accounted for 45 % of the overall ohmic resistance. This way, the effect of brine concentration on the electrolyte resistance (overpotential) was found to be the major contribution to the cell potential. Gas bubble revealed to have a significant effect on the ohmic resistance of the cell, especially at the anode side, representing a potential increase of 110 mV (for a gas void fraction of 12 % at 2.0 kA m^{-2}). The gas bubble effect showed to be minimized by high feed flow rates.

The kinetic parameters of the hydrogen evolution reaction (HER) at nickel cathodes were obtained under normal operating conditions by electrochemical impedance spectroscopy and were discussed. As the anode reaction was much faster than the cathode reaction, which was verified experimentally, the anode was used as a reference electrode. The Tafel slopes, the exchange current densities and the electrode overpotentials were obtained for solid and mesh plate cathodes. The main advantage of using mesh electrodes was found to be the ohmic resistance reduction. They

allowed operating at higher current densities at the same cell potential. Good agreement was found between the kinetic parameters of both electrodes and literature values.

A benchmarking methodology was developed for comparing ion exchange membranes. It was applied to three different types of membranes, two low voltage membranes and one high strength membrane, used in the chlor-alkali industry. This methodology was based on the history of the average total process cost per ton of chlorine produced. The potential and current efficiencies of the process were obtained monthly and used to compute the specific energy consumption. The average total specific process cost was then obtained from the sum of the operating and the fixed cost. It was concluded, that the high strength membrane (higher voltage) was the one with the lowest average total specific cost, originating savings of around 1.5 % compared to the second best membrane. This methodology proved to be an accurate tool to determine the appropriate moment for membrane replacement.

6.2. Future Work

During the development of the present work many difficulties were encountered mainly due to the scarce scientific information available. The design and assembly of the laboratory electrochemical membrane reactor unit

was a great challenge especially in which concerns attaining the corresponding industrial performances. It was concluded that the experimental setups can be used to determine the relevant performance parameters of a given membrane. This thesis was just the beginning of the research on this topic and should serve as a support for future developments.

One of the critical experimental shortcomings was the continuous monitoring of relevant parameters of the experimental reactor. The on-line read of chlorine and hydrogen flow rates must be improved. This would allow a further investigation of the membrane reactor current efficiency. Furthermore, a complete performance assessment should include the following aspects:

- Visual membrane inspection;
- Determination of the thickness and of the tensile properties (tensile strength, elongation at yield and tear strength) of the membranes;
- Determination of the cell voltage, membrane conductivity, current efficiency and power consumption;
- Impurity analysis on the membranes used (by ICP mass spectrometry and colorimetry);
- Detailed information about the physical condition of the used membranes (SEM images).

It is suggested to study the effect of aging as a function of the operating and design conditions and the influence of the impurities on tensile properties, cell voltage, membrane conductivity, current efficiency and power consumption. It is suggested namely to study the effect of the unsteady operation on membrane and electrodes aging and on the electrolyzer productivity. Additionally, Electrochemical Impedance Spectroscopy (EIS) analysis can be used to study the cell components deactivation as well as to investigate the effect of impurities on the membrane and electrodes. For example, the DSA anodes experience an exponential voltage increase when deactivating due to the growth of a non-electrical conductive layer of titanium oxide, or due to formation of contaminant deposits. EIS can be used to determine the development of a passivation layer and is able to assess the threatening of this situation.

It would also be interesting to investigate the electrodes *in situ* reactivation.

It was shown that the gas bubble effect has a great impact on the cell performance. Thus, further elucidation of gas release and gas flow motion in electrochemical cells is required.